

Aus dem Institut für Klinische Neuroimmunologie  
der Ludwig-Maximilians-Universität München  
Direktion: Prof. Dr. med. Reinhard Hohlfeld,  
Prof. Dr. med. Martin Kerschensteiner

**The role of calcium in axonal degeneration  
in an animal model of multiple sclerosis**

Dissertation  
zum Erwerb des Doktorgrades der Medizin  
an der Medizinischen Fakultät der  
Ludwig-Maximilians-Universität zu München

vorgelegt  
von Adrian Minh Schumacher  
aus Donaueschingen

2016

Mit Genehmigung der Medizinischen Fakultät  
der Universität München

Berichterstatter: Prof. Dr. Martin Kerschensteiner

Mitberichterstatter: Prof. Dr. Stephan Kröger

Prof. Dr. Nikolaus Plesnila

Prof. Dr. Dr. Markus Kipp

Dekan: Prof. Dr. med. dent. Reinhard Hickel

Tag der mündlichen Prüfung: 28.04.2016

## **Table of Contents**

<b>Table of Contents</b> .....	
<b>List of Figures</b> .....	<b>III</b>
<b>List of Tables</b> .....	<b>III</b>
<b>List of Abbreviations</b> .....	<b>IV</b>
<b>Zusammenfassung</b> .....	<b>VI</b>
<b>Summary</b> .....	<b>VIII</b>
<b>1. Introduction</b> .....	<b>1</b>
1.1 Multiple Sclerosis .....	1
1.1.1 Definition .....	1
1.1.2 Diagnosis and clinical course.....	2
1.1.3 Pathology and pathogenesis.....	4
1.1.4 Animal Models .....	7
1.2 Axon degeneration.....	9
1.2.1 Axon degeneration programs .....	9
1.2.2 Molecular mechanisms of axon degeneration .....	12
1.3 In vivo visualization of neuronal calcium levels .....	14
1.3.1 Intravital 2-photon microscopy of the nervous system.....	14
1.3.2 Genetically encoded calcium indicators.....	17

---

<b>2.</b>	<b>Objectives .....</b>	<b>22</b>
<b>3.</b>	<b>Material and Methods.....</b>	<b>23</b>
3.1	Material list.....	23
3.2	Experimental animals.....	29
3.3	Methods.....	29
3.3.1	Experimental autoimmune encephalomyelitis (EAE).....	29
3.3.2	Tissue processing and immunohistochemistry .....	30
3.3.3	Confocal microscopy .....	31
3.3.4	Surgery procedures.....	31
3.3.5	2-Photon in vivo imaging.....	33
3.3.6	Data analysis .....	34
<b>4.</b>	<b>Results.....</b>	<b>37</b>
4.1	Characterization of GECI transgenic animals.....	37
4.2	Interpretation of ratiometric calcium indicator signals.....	39
4.2.1	Imaging settings and bleedthrough correction.....	39
4.2.2	Baseline ratiometric signal and positive controls.....	40
4.3	Axonal calcium levels in acute EAE.....	42
4.4	Axonal calcium levels in EAE remission.....	46
4.5	Fate mapping of affected axonal populations over time .....	47
4.6.	Additional Figures .....	50

---

<b>5. Discussion.....</b>	<b>53</b>
5.1 In vivo calcium imaging: pitfalls and potentials .....	53
5.1.1 Detection of calcium signals .....	53
5.1.2 Interpretation of the measured signals.....	55
5.1.3 Potential improvements in signal detection .....	56
5.2 Calcium predicts the fate of degenerating axons in inflammatory lesions.....	58
5.2.1 Calcium in focal axonal degeneration .....	58
5.2.2 Assessing the predictive value of increased calcium.....	59
5.3 Sources and mechanisms of calcium overload.....	60
5.3.1 Correlation with other mediators of inflammatory axon degeneration.....	60
5.3.2 Mediators of calcium influx.....	64
5.3.3 Effects of Ca <sup>2+</sup> overload.....	71
5.4 Future therapeutic strategies .....	72
5.5 Concluding remarks .....	76
<b>6. References.....</b>	<b>79</b>
<b>7. Acknowledgements .....</b>	<b>90</b>

## List of Figures

Figure 1	Disease course of multiple sclerosis.....	3
Figure 2	Persistence of a “black hole” in the brain MRI of a multiple sclerosis patient.....	6
Figure 3	Focal axonal degeneration .....	12
Figure 4	Basic principles of 1 and 2-photon excitation .....	15
Figure 5	Structure of a FRET based genetically encoded calcium indicator.....	20
Figure 6	Measuring regions of interest (ROIs) for single axons and nearby background .	34
Figure 7	<i>In vivo</i> signal of thy1-CerTN-L15 and thy1-TN-XXL.....	37
Figure 8	Analysis of axon populations of the GECI lines.....	38
Figure 9	Signal-to-noise plot for different excitation detection parameters.....	40
Figure 10	Baseline signal and ratios after spinal cord cut. ....	42
Figure 11	Axonal calcium levels in acute EAE .....	44
Figure 12	Effects of pH on fluorophores in acute EAE .....	45
Figure 13	Axonal calcium levels in EAE remission.....	46
Figure 14	Control timelapse imaging .....	47
Figure 15	Assessment of axonal cohort over time.....	49
Figure 16	Effects of H <sub>2</sub> O <sub>2</sub> on healthy spinal cord axons.....	51
Figure 17	Effects of intrathecal treatment with bepridil in EAE .....	52
Figure 18	Ca <sup>2+</sup> conducting structures of the axonal and organelle membranes.....	66

## List of Tables

Table 1	Selected Troponin C based calcium sensors .....	21
Table 2	EAE clinical scoring scale.....	30
Table 3	Staining protocol Myelin Basic Protein (MBP) .....	31
Table 4	Determined optimal imaging settings for constant application.....	40

## **List of Abbreviations**

Å	ångström, $10^{-10}$ m
AAD	Acute axonal degeneration
A.U.	Arbitrary units
aCSF	Artificial cerebrospinal fluid
aEAE, pEAE	Actively induced EAE, passively induced EAE
ALS	Amyotrophic lateral sclerosis
AMPA	$\alpha$ -amino-3-hydroxy-5-methyl-4-isoxazolepropionic acid
AOM	Acousto-optic modulator
AOTF	Acousto-optic transmission filter
APP	Amyloid precursor protein
ASIC1	Acid-sensing ion channel-1
ATP	Adenosine triphosphate
BF	Bleedthrough factor
BFP	Blue fluorescent protein
BKGND	Background
Ca <sup>2+</sup>	Calcium
CerTN	CerTN-L15 calcium sensor protein
CFP	Cyan fluorescent protein
CIS	Clinically isolated syndrome
CNS	Central nervous system
csTnC	Chicken skeletal troponin C
CyPD	Cyclophilin D
DMF	Dimethyl fumarate
DMSO	Dimethylsulfoxide
DNA	Deoxyribonucleic acid
EAE	Experimental autoimmune (allergic) encephalomyelitis
EGTA	Ethylene glycol tetraacetic acid
FAD	Focal axonal degeneration
FIJI	FIJI is just ImageJ
FRET	Fluorescence (Förster's) resonance energy transfer
FRET	Försters (Fluorescence) resonance energy transfer
GaAsP	Gallium arsenide phosphide
GECI	Genetically encoded calcium indicator
GFP	Green fluorescent protein
H <sub>2</sub> O <sub>2</sub>	Hydrogen peroxide
Int	Intensity
K <sub>d</sub>	Dissociation constant
LUT	Look-up table
MBP	Myelin basic protein
MOG	Myelin oligodendroglial glycoprotein
mPTP	Mitochondrial permeability transition pore
MRI	Magnetic resonance imaging

---

MRS	Magnetic resonance spectroscopy
MS	Multiple sclerosis, dt. Multiple Sklerose
NA	Numerical aperture
Na <sup>+</sup>	Sodium
NAA	N-acetyl-aspartate
NADH	Nicotinamide adenine dinucleotide
NADPH	Nicotinamide adenine dinucleotide phosphate
Na <sub>v</sub>	Voltage gated sodium channel
NCX	Sodium (Natrium) - calcium exchanger
NDD	Non-descanned detectors
nm	Nanometer
NMDA	N-Methyl-D-aspartic acid
NMNAT	Nicotine mononucleotide adenylyltransferase
NO	Nitric oxide
OCT	Optical coherence tomography
PFA	Paraformaldehyde
PLP	Proteolipid protein
PMT	Photomultiplier tube
PP-(MS)	Primary progressive (MS)
PUFA	Poly-unsaturated fatty acid
RNFL	Retinal nerve fibre layer
RNS	Reactive nitrogen species
ROS	Reactive oxygen species
RR-(MS)	Relapsing-remitting (MS)
RT	Room temperature
S/N	Signal to noise
SD	Standard deviation
SEM	Standard error of the mean
SP-(MS)	Secondary progressive (MS)
T <sub>H</sub>	T-helper cell
TNF- $\alpha$	Tumor necrosis factor alpha
TRP	Transient receptor potential
TRPM4	Transient receptor potential cation channel subfamily M4
VGCC	Voltage gated calcium channel
WD	Wallerian degeneration
WLD <sub>s</sub>	Slow Wallerian degeneration phenotype
Wld <sub>s</sub>	Slow Wallerian degeneration gene
WT	Wildtype
XFP	Variants of fluorescent protein
YFP	Yellow fluorescent protein
$\Delta R/R$	Fractional ratio change

## **Zusammenfassung**

Die Multiple Sklerose (MS) ist eine entzündliche Erkrankung des zentralen Nervensystems, die mit Demyelinisierung sowie persistierendem Verlust von Axonen einhergeht. Remyelinisierung kann zu einem Teil den Verlust von Myelin kompensieren, während axonale Schäden irreversibel und potenziell dafür verantwortlich sind, dass Patienten progressive klinische Einschränkungen erfahren. Mit der fokalen axonalen Degeneration (FAD) wurde vor kurzem in einem Tiermodell der MS ein neuer, zellulärer Mechanismus der axonalen Schädigung beschrieben, welcher sequentiell Stadien durchläuft und schließlich zu irreversibler Fragmentierung des Axons führt. Erstaunlicherweise sind frühe Stadien dieses Prozesses noch reversibel. Um einen besseren Einblick in die molekularen Mechanismen zu bekommen, welche der fokalen axonalen Degeneration zugrunde liegen, habe ich in dieser Arbeit in einem Mausmodell der MS, der Experimentellen Autoimmunen Enzephalomyelitis (EAE), die intra-axonalen Kalziumkonzentrationen in entzündlichen Läsionen des Rückenmarks gemessen. Dafür setzte ich *in vivo* Multi-Photonen Mikroskopie ein, um Axone im intakten Rückenmark der lebenden Maus zu verfolgen. Zur Messung der Kalziumkonzentration verwendete ich transgene Mauslinien, die ein ratiometrisches, genetisch enkodiertes Kalzium-Sensorprotein unter dem neuronalen Thy1 Promoter exprimieren. Zuerst analysierte ich die Expressionsmuster des Sensorproteins in spinalen Axonen, optimierte daraufhin den Bildgebungsansatz und etablierte die Messbasis in gesunden Kontrolltieren. Danach charakterisierte ich Morphologie und Kalziumkonzentrationen von Axonen in akuten und chronischen EAE-Herden. Während die Basiswerte in gesunden Tieren nur eine geringe Variabilität aufweisen, zeigen viele Axone in Tieren mit EAE deutlich erhöhte Konzentrationen von intrazellulärem Kalzium. Interessanterweise finden sich erhöhte Kalziumwerte nicht nur in den fortgeschrittenen Stadien von FAD, sondern auch in Axonen mit intakter Morphologie. Um zu bestimmen, inwiefern erhöhte Kalziumkonzentrationen für Axone die Wahrscheinlichkeit erhöhen, zu

---

degenerieren, verfolgte ich Kalziumkonzentration und Morphologie in einer Kohorte von über 300 Axonen über mehrere Stunden. Diese Experimente zeigen, dass Kalzium ein wichtiger prädiktiver Faktor für die anschließende, irreversible Degeneration ist. In Nachfolgestudien versuchen wir nun die Mechanismen zu bestimmen, die zur intra-axonalen Akkumulation von Kalzium führen. Dafür analysieren wir die Einflüsse von u.a. Glutamat Exzitotoxizität, Azidose, reaktiven Sauerstoff- und Stickstoffspezies (ROS/RNS) und der Funktionsumkehrung des Natrium/Kalzium Austauscher (NCX). Zusätzlich bewerten wir die Effekte von erhöhtem Kalzium, z.B. die Aktivierung von  $\text{Ca}^{2+}$ -abhängigen Proteasen wie Calpain. Unser Ziel ist es, durch gezielte Manipulation dieser Mechanismen neue Therapiekonzepte zu entwickeln, welche in der Lage sind, die Progredienz der klinischen Einschränkung bei MS Patienten zu verhindern.

---

## **Summary**

Multiple sclerosis (MS) is a common inflammatory disease of the central nervous system that features demyelination as well as persistent axonal loss. While demyelination can be partially compensated by remyelination, damage to axons is irreversible and thought to be responsible for the progressive disability seen in MS patients. How axons are damaged in MS remains unclear. Recently, our lab has identified a new cellular mechanisms of axon loss in an animal model of MS, that we termed “focal axonal degeneration” (FAD). FAD is characterized by a progression through sequential stages that ultimately leads to axon fragmentation. Surprisingly, axons in the early stages of FAD can still recover. To better understand the molecular mechanisms that determine the balance between degeneration or recovery, I have now investigated how intra-axonal levels of calcium, a prominent mediator of cellular degeneration and death, drive FAD. To obtain a readout of intra-axonal calcium levels *in vivo*, I used multi-photon microscopy to image axons in the lumbar spinal cord of transgenic mice expressing a ratiometric, genetically encoded calcium indicator protein under the neuronal Thy-1 promoter. First, I assessed the expression of the sensor protein in spinal axons, optimized the signal detection and characterized baseline calcium levels in healthy animals. Afterwards, I performed single time-point measurements of axons during the formation and remission of neuroinflammatory lesions in a commonly used animal model of MS (experimental autoimmune encephalomyelitis, EAE). My results show that whereas axonal calcium levels are tightly controlled in healthy animals, many axons in EAE mice show elevated levels of intracellular calcium. Interestingly, levels are not only increased in the more advanced stages of the degeneration process but also in a subset of axons that exhibit intact morphology. To address to what extent calcium levels predict the subsequent fate of axons, I followed changes in axonal morphology and calcium levels in a cohort of over 300 axons over several hours. These experiments indicate that calcium levels are a crucial predictor of axonal fate, with elevated levels indicating a high risk of subsequent degeneration. In follow-up studies we are now trying to identify the mechanisms that lead to intra-axonal calcium accumulation, and to evaluate, amongst other things, the effect of glutamate excitotoxicity,

acidosis, reactive oxygen and nitrogen species (ROS/RNS) and the reversed function of the  $\text{Na}^+/\text{Ca}^{2+}$  exchanger (NCX). In addition, we analyse the downstream effects of elevated calcium, e.g. the activation of  $\text{Ca}^{2+}$ -dependent proteases like calpain. The aim of these studies is to identify the key mechanisms that induce calcium influx in axons and represent new targets for strategies to limit progressive clinical disability in MS patients.

## **1. Introduction**

### **1.1 Multiple Sclerosis**

“We are constantly accepting, adapting and moving forward, together toward new normals” N. Lemelle, multiple sclerosis patient (Lemelle, 2011).

It is hard to overestimate the impact that the diagnosis of multiple sclerosis has on an affected person’s daily life and attitudes. Since its description in the 19<sup>th</sup> century, this enigmatic disease has troubled many researchers because of its poorly understood cause, the variable mechanisms and the lack of long-term efficient medication. Of great importance is also the effect on society, where it remains the number one neurological disease of young adults and a major cause of early disability (Sospedra and Martin, 2005). Patients and their families, physicians and researchers share the strong wish to gain more insight into this complex phenomenon. The pace of discoveries that have dismantled some long-established dogmas about the disease has increased over the last two decades. The finding of shared mechanisms with other CNS diseases might even allow the transfer of some therapeutic principles.

#### **1.1.1 Definition**

Multiple Sclerosis is a chronic inflammatory disease of the human central nervous system. It features disseminated demyelinated plaques and focal lymphocytic infiltration in brain and spinal cord as well as progressive neuro-axonal degeneration (Compston and Coles, 2008; Compston et al., 2005; Friese et al., 2014). Since in principle the entire CNS can be affected, possible clinical signs include a large variety of neurological deficits, which comprise for the most part motor, sensory, visual and autonomic systems. However, many other symptoms can occur, e.g. cognitive impairment, fatigue, vertigo and tremor (Compston and Coles, 2008).

### **1.1.2 Diagnosis and clinical course**

The entity of the clinically isolated syndrome (CIS) describes the affection of one site at one timepoint (e.g. optic neuritis). It forms the presenting symptom for 80% of the patients (Compston and Coles, 2008) and will remain the diagnosis until the so-called temporal and spatial dissemination have settled the final diagnosis of MS. This concept requires multiple lesions that affect different areas (and therefore neurological systems) at multiple timepoints. It has been implemented in the by now twice-revised McDonald criteria for MS diagnosis (McDonald et al., 2001; Polman et al., 2005; 2011). Even though clinical evidence still plays the greatest role in the establishment of the diagnosis, paraclinical findings have become increasingly important: These include MR Imaging, biomarkers in the cerebrospinal fluid and retinal optical coherence tomography (OCT). For instance, a lesion-positive brain MRI at presentation with a CIS is highly predictive of a long-term MS diagnosis, with over 80% suffering MS after 10 years (O’Riordan et al., 1998). The use of gadolinium enhancement allows distinguishing of inactive and active lesions, which renders an early diagnosis possible and therefore speeds up treatment planning.

The course of the disease in an individual patient is often unpredictable and can unfold in strikingly manifold ways. In principle, one must distinguish between two clinical entities: either a disease modality where symptoms flare up (relapse) and then eventually disappear without any remnants (remission), or a constant worsening of symptoms referred to as progressive MS. Patients can have one of these manifestations from the onset of disease, which allocates them to the groups of relapsing-remitting (RR)-MS or primary-progressive (PP)-MS, respectively. However, it is the combination of these two different types – meaning a RR-MS that is secondarily followed by a progressive phase (SP) – that represents, with around 70% of patients, the most frequent type of disease (Weinshenker et al., 1989).

Remarkably, no matter if the progressive phase occurs secondarily to RR-MS or if it started a priori, it leads around a similar median age to the appearance of irreversible disability (e.g. limited walking without aid at a median age of around 44 years). Many of the

individuals that do show an earlier onset of irreversible disability were also diagnosed at a younger age. This renders the age of diagnosis a much stronger factor in predicting the start of irreversible disability than the entity (RR-MS vs. PP-MS) or inflammatory activity of the disease (Confavreux and Vukusic, 2006). In addition, there is also a form of benign MS in about 10% of patients that will do well for more than 20 years (Noseworthy et al., 2000). Taken together, this variability in the disease course suggests not only one, but several underlying pathomechanisms that might act partially independently of each other.

Even though in most cases physical impairment becomes severe with increasing age, over all life expectancy is shortened only slightly in multiple sclerosis. One should note however that there are rare cases reported, where a fulminant disease leads to patients deceasing just a few months after the diagnosis. Further, suicide rates among MS patients show a more than sevenfold increase compared to age-matched control groups (Sadovnick et al., 1991)

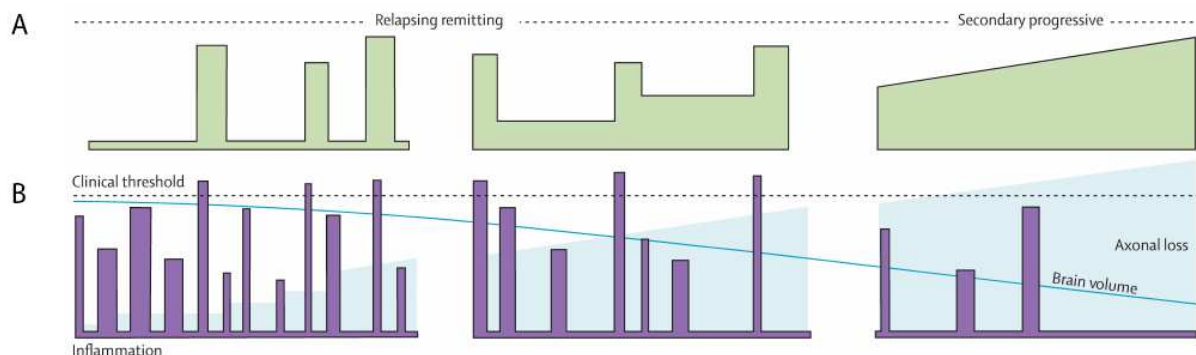


**Figure 1** Disease course of multiple sclerosis

(A) Schematic representing the different clinical courses of multiple sclerosis. The green graph depicts waxing and waning of clinical symptoms that manifest in patients in the relapsing-remitting form (RR-MS, left) and the slow progression to progressive disease (SP-MS, right), where symptoms persist. Primary progressive (PP-MS) form skips a preceding phase of relapse and remission and resembles SP-MS. (B) Assumed underlying pathological processes: The violet bars propose frequent flaring of inflammatory activity that mostly does not reach clinical relevance. Neuroaxonal loss and resulting brain atrophy occur simultaneously, and seem to be a better correlate of progressive symptoms. Adapted from Compston and Coles, 2008.

### **1.1.3 Pathology and pathogenesis**

The characteristic pathological feature of multiple sclerosis is the demyelinated plaque, an initially hypercellular and later hypocellular area, characterized by the loss of myelin and the formation of astrocytic scars. Besides the common assumption that the responsible mechanism is a primary inflammatory process caused by an autoimmune reaction against a myelin component, current pathogenesis models suggest a dualism of two interconnected arms: inflammation and neurodegeneration. Which of these comes first, or if one causes the other, is not known.

#### **1.1.3.1 Immunopathogenesis**

One main component that initiates the inflammatory part of the disease process is the migration of autoreactive lymphocytes across the blood-brain barrier. This is probably due to the failure of regulatory T-cells to suppress these effector cells (Viglietta et al., 2004) and/or the overexpression of survival factors (e.g.  $\beta$ -arrestin1) that makes the apoptosis of autoreactive cells go awry (Shi et al., 2007). The target antigen has so far been proven not to be one single CNS protein, like the myelin-specific proteins used in MS animal models or Aquaporin-4 in the sister-disease neuromyelitis optica (Lennon et al., 2005). It is proposed to be either a rather nonspecific, polyclonal activation of T and B cells by bacterial or viral antigens, or a result of structural homology between a self-protein and a pathogen-protein, a phenomenon commonly known as molecular mimicry (Sospedra and Martin, 2006; Steinman et al., 2002).

Inflammatory, demyelinating plaques cluster around the lateral ventricles and corpus callosum, in the cortex and subcortical white matter, the optic nerves, in the brainstem and throughout the spinal cord (Compston and Coles, 2008). In addition to T-lymphocytes, mainly macrophages but also B-cells, plasma cells and NK-cells can be found in the affected CNS. Whereas B-cells have been detected in the brain parenchyma, it is assumed that differentiation, maturation and the secretion of antibodies happens in the meningeal spaces

and the Virchow-Robin spaces, leading to a compartmentalised humoral immune response with intrathecal antibody production that is assumed to contribute to cortical pathology in the later stages of the disease (Magliozzi et al., 2007). Diagnostically relevant evidence comes from the appearance of so-called ‘oligoclonal bands’ on protein electrophoresis gels of lumbar puncture fluid obtained from MS patients. They are the correlate of the autoantibodies present in the subarachnoid compartment.

### **1.1.3.2 Demyelination**

A major hallmark of MS is the formation of multiple demyelinating lesions throughout the CNS. Historically, researchers have assumed that the demyelination is a primary process where the immune system has been tricked into seeing CNS myelin as foreign and therefore attacks and removes it. By now, four different types of demyelinating lesions have been described. They could potentially appear in different subpopulations of MS patients and for each has been suggested a distinct underlying mechanism (Lassmann et al., 2001). Demyelination may be induced by macrophages, which have been activated by Th1 cells and secrete toxic factors (including TNF- $\alpha$  and ROS/RNS), resulting in pattern I. In pattern II, specific demyelinating antibodies and complement is described as the main factor - similar to animal models that include immunization with myelin-specific proteins. The so-called “distal oligodendroglialopathy” of pattern III supposedly leads to degenerative changes in the distal processes of the oligodendrocytes that surround axons and is followed by apoptosis. In this case, a demyelination occurs that appears similar to white matter viral infections or ischemia. The presumed mechanism for pattern IV is a primary oligodendrocyte degeneration but it seems to be less frequent than the other patterns.

### **1.1.3.3 Neuroaxonal damage**

Axonal injury and loss has been described since the very first publications about MS and is considered to be a major feature in inflammatory lesions. However, for a long time it had been thought to be a secondary process to the inflammatory, demyelinating attacks and therefore therapies have focused mainly on reducing inflammatory activity and lesion load. A change of

paradigm is now taking place, attributing the irreversible neuroaxonal loss a major role in the pathogenesis of the disease and depicting it as the main correlate for cumulative neurological disability (Bjartmar et al., 2000).

MRI studies have detected hypointense T1 ‘black holes’, cortical lesions and atrophy of the brain and spinal cord early in the disease course (Barkhof et al., 2009; Chard et al., 2002). Magnetic resonance spectroscopy (MRS) studies showed a reduction of N-acetyl-aspartate (NAA, a marker of axonal integrity) in the white matter of MS patients that correlates with the extent of their neurological deficits (Stefano et al., 1998; 2005).

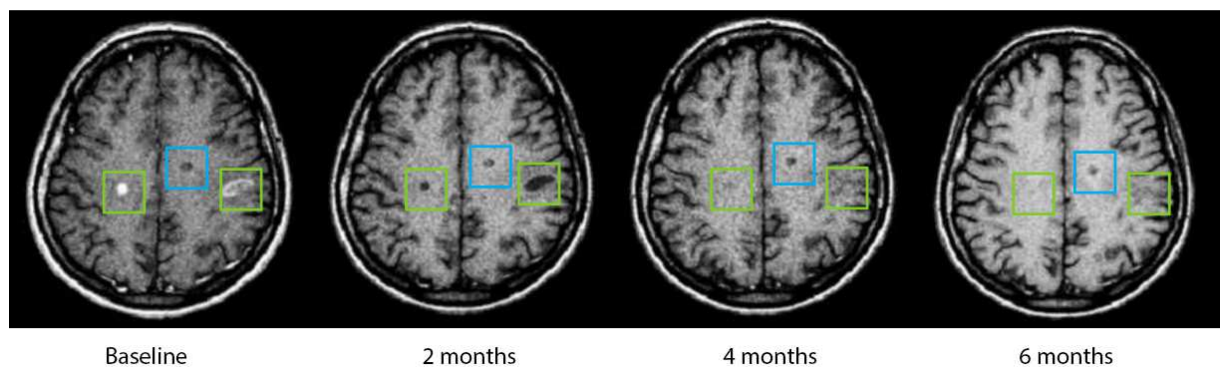


**Figure 2** Persistence of a “black hole” in the brain MRI of a multiple sclerosis patient

T1-weighted spin-echo MRI of a multiple sclerosis patient, first image contrast-enhanced. Two gadolinium-enhancing lesions (green boxes) that appear hypointense without contrast (not shown) subsequently become isointense on follow-up, consistent with remyelination. An old lesion, presenting as a hypointense “black hole” (blue box) remains the same, correlating with a chronic lesion showing axonal loss. Adapted from (Barkhof et al., 2009)

Axon loss has also been detected in the retina. The easy optical access to unmyelinated CNS axons in the retinal nerve fibre layer (RNFL) allows for unprecedented measurement of axons at micrometre resolution *in vivo*, using the technology of optical coherence tomography (OCT). With this tool, RNFL neurodegeneration in patients with MS who had no prior

clinical history of optic neuritis was found to be increased tenfold compared to disease-free controls (Petzold et al., 2010).

In histopathology, immunohistochemistry has been used to detect axonal pathology. Amyloid precursor protein (APP) is a protein that is transported along the axon and, when the cytoskeleton breaks down, accumulates to a degree that it becomes detectable. Stainings for APP have shown early axon loss in lesions and at the border of active lesions (Ferguson et al., 1997; Kuhlmann et al., 2002). Another staining, called SMI-32, shows non-phosphorylated neurofilament that is also known to accumulate in the process of axon injury. Studies using SMI-32 immunohistochemistry also revealed axon loss in active lesions and at the border of chronic lesions (Trapp et al., 1998).

A positive correlation of axonal injury and inflammation (characterized by the infiltration density of macrophages and T-cells) has been shown in multiple sclerosis lesions (Bitsch et al., 2000). This suggests that immune-initiated mechanisms directly lead to axon damage. However, Kornek et al. correlated axon damage with lesional stages, assigned by the presence and antigenic composition of myelin debris in macrophages, and found that acute axon loss was found even in inactive lesions. This renders the pathogenesis even more intriguing: it suggests processes, that will damage axons not only in a setting with nearby immune cells, but also an ongoing process in the “burnt-out” lesions that slowly contributes to the total axonal loss and therefore increasing disability (Kornek et al., 2000; Lassmann, 2003). If the mechanisms that underlie these different settings of axonal damage are related or distinct remains elusive.

#### **1.1.4 Animal Models**

“One of the most enduring models of human disease” (Steinman, 2003), Experimental Autoimmune Encephalomyelitis (or Experimental Allergic Encephalomyelitis, EAE), has been used for more than 80 years to study autoimmune-mediated damage to CNS structures. EAE is an inflammatory, demyelinating disease of the CNS that has many clinical and pathological

---

similarities with MS. It was originally inspired by the “paralytic accidents” that arose from vaccination with rabies-infected rabbit spinal cord by Louis Pasteur in 1885. Rivers and colleagues immunized rhesus monkeys with rabbit brain emulsion to trigger a demyelinating, sterile encephalomyelitis (Rivers and Schwentker, 1935; Rivers et al., 1933). The intention of the original experiment was to understand acute disseminated encephalomyelitis after viral infections, not MS. Complete Freund’s adjuvants, a solution containing inactivated mycobacteria tuberculosis and mineral oil that triggers a strong immune response, were implemented to produce a highly reproducible model of paralysis and white matter inflammation (Kabat et al., 1947). Since then, a lot of effort has been put into refining this model disease to resemble the MS disease course, its immunopathology, and to make it a suitable paradigm for preclinical therapy studies. In simple terms, two main methods of EAE induction have been used: an actively-induced EAE (aEAE) versus a passively-transferred variant (pEAE). The basic protocol for aEAE is the immunization with self or foreign proteins that find themselves in the white matter of the CNS, such as myelin basic protein (MBP), myelin oligodendroglial glycoprotein (MOG) or proteolipid protein (PLP) (Steinman, 1999). There are many experimental permutations concerning the mouse strains used, as well as the peptides or proteins taken as antigens (that by now include several more myelin, neuronal and glial antigens). Actively-induced EAE mostly follow a similar disease course that evolves acutely and eventually wanes to different degrees of residual disease. To include clinical events such as relapsing and remitting episodes of paralysis, more suitable EAE models have been developed (Brown and McFarlin, 1981; Lublin et al., 1981). Problematic aspects of aEAE include the obligatory active induction. Also, there are rather inelegant side effects like the large deposits of adjuvants that may interfere with the global immune reactivity of the immunized animal.

In another approach, EAE is passively transferred (pEAE) by *in vitro* activated autoimmune T-cell lines. This “adoptive transfer model” has been useful in drug screening, functional gene characterization (Krishnamoorthy and Wekerle, 2009) and to elucidate the specific roles and capability of T-cell subtypes to induce a CNS inflammation. However, bulk

infusions of immune cells, which have been activated to their maximum in vitro, do not necessarily resemble the situation in MS. Current EAE development focuses also on the creation of spontaneous models, achieved by transgenic mice that carried T-cells and B-cells with myelin-specific receptors (Krishnamoorthy et al., 2007).

To improve the relevance of EAE studies to MS, efforts have further been undertaken to humanize the critical parts of disease initiation: mice that are transgenic for human MHC-class II and a T-cell receptor from a MS patient's myelin-specific T<sub>H</sub> clone (Gregersen et al., 2004) are beginning to reproduce some of the various clinical manifestations and corresponding CNS lesions of multiple sclerosis. It is therefore postulated that these spontaneous models will develop into a more valid model for translational research than the traditional ones (Friese et al., 2006).

## **1.2 Axon degeneration**

*When considering the molecular mechanisms of axonal damage, two different phases of axonal disintegration have to be distinguished: the trigger of axonal damage and the downstream pathways of axonal dissolution. Although the triggers of axonal injury seem to be specific for inflammatory conditions, such as MS, the downstream mechanisms of axonal dissolution appear similar in a variety of different pathological conditions of the nervous system, including inflammation, ischemia, or trauma (Lassmann, 2003).*

### **1.2.1 Axon degeneration programs**

Many neurological disorders have been found to include axon degeneration. A range of insults can trigger a dismantling of axons, including not only CNS injury, genetic defects and toxins, but also a milieu that is a result of metabolic disturbance, myelin disorders, ischemia or inflammation. Downstream axonal dissolution shows a certain diversity, but retains, however, many common features. Several different degeneration phenotypes have been described that will be discussed below.

---

One such type of axonal degeneration that has been heavily focussed on is Wallerian degeneration (WD). This is an axon degeneration program that occurs after axonal transection, where the axon region distal to the site of injury starts degenerating about 1.5 days after the lesion. The axonal skeleton first disintegrates to form axonal swellings, forming a “beads-on-a-string” like appearance, with the axonal membrane subsequently breaking apart. This is followed by degradation of the myelin sheath and infiltration by phagocytic cells. Even though August Waller described his observations over 150 years ago, in recent decades the topic has been resurrected by attempts to decipher the mechanism behind the effect of *Wld<sub>s</sub>*, a mutant gene whose overexpression leads to the phenotype of a tenfold-delayed axon dismantling compared to wildtype Wallerian degeneration (Lunn et al., 1989; Perry et al., 1990). To this day, several other mutations have been found to delay the same process for 10 days or more (Babetto et al., 2013; Mack et al., 2001; Osterloh et al., 2012) and great effort has been put into delineating the specific roles these factors have in a putative post-injury signalling pathway. One prominent enzyme family that slows Wallerian degeneration when overexpressed within axons are the nicotinamide mononucleotide adenylyltransferases (NMNATs), also comprising *WLD<sub>s</sub>* which contains NMNAT1.

The importance of this is twofold: firstly, these findings show that axonal degeneration is more than plain atrophy of axons that lack nutrition supply when transected, but is rather an active signalling process that can be elicited by various conditions and that involves many different molecular factors. Secondly, components of the pathways can be a shared hallmark of a variety of conditions where axons are disassembling. Attempts to classify observed degeneration processes have been focussed to a large extent on changes in morphology. Axon degeneration seen in peripheral neuropathies, ALS and other disorders have been assigned the term “Wallerian-like degeneration” due to the presence of ovoids of degenerating myelin, fragmentation of distal axons and, in the CNS, large axonal swellings. Many different diseases and animal models have in the meantime been assessed regarding their susceptibility to the effect of *WLD<sub>s</sub>* and overexpressed NMNAT isoforms. One can therefore also distinguish between conditions where these factors play an important role: “*WLD<sub>s</sub>*-sensitive

degeneration” (e.g. models of traumatic nerve injury, glaucoma, toxic neuropathy or Parkinson’s disease) and conditions where there has been no or only little effect, e.g. ALS, spinal muscular atrophy or hereditary spastic paraplegia (Conforti et al., 2014). In EAE, a moderate effect of WLDs is presumed (Kaneko et al., 2006).

With the technological advancement in bioimaging approaches, other processes of axonal degeneration have also been identified that are different in both temporal progression and morphological changes compared to WD. Acute axonal degeneration (AAD) describes a sudden dieback of proximal and distal ends of a transected axon in the first few hours after lesion, that lasts less than five minutes and that is strongly affected by the WLDs mutation (Kerschensteiner et al., 2005). Even though many morphological characteristics of AAD seem comparable to WD, it presents itself as an independent entity that temporally precedes characteristic WD in a spinal cord injury model.

Recently, another entity of axonal degeneration was characterized under the neuroinflammatory conditions seen in EAE. Focal axonal degeneration (FAD) describes the spontaneous formation of semi-stable focal axonal swellings inside inflammatory foci that can persist for days. Interestingly, they can progress to either fragmentation or morphological recovery. The axon fragmentation spreads slowly from the sites of disruption ( $3.5 \mu\text{m min}^{-1}$ ) in both directions and stops with the formation of terminal bulbs on both stumps. It often appears to start at the nodes of Ranvier and can occur almost synchronously at several sites at the same time. FAD can be detected both in demyelinated as well as myelinated axons, hence weakening the general belief that damage to myelin is a prerequisite for axon damage. It also tends to affect small calibre more than large calibre axons. The same morphological features of degeneration could be detected in actively demyelinating multiple sclerosis lesions and many axons that appeared swollen or fragmented were shown to be still wrapped in myelin (Nikić et al., 2011).

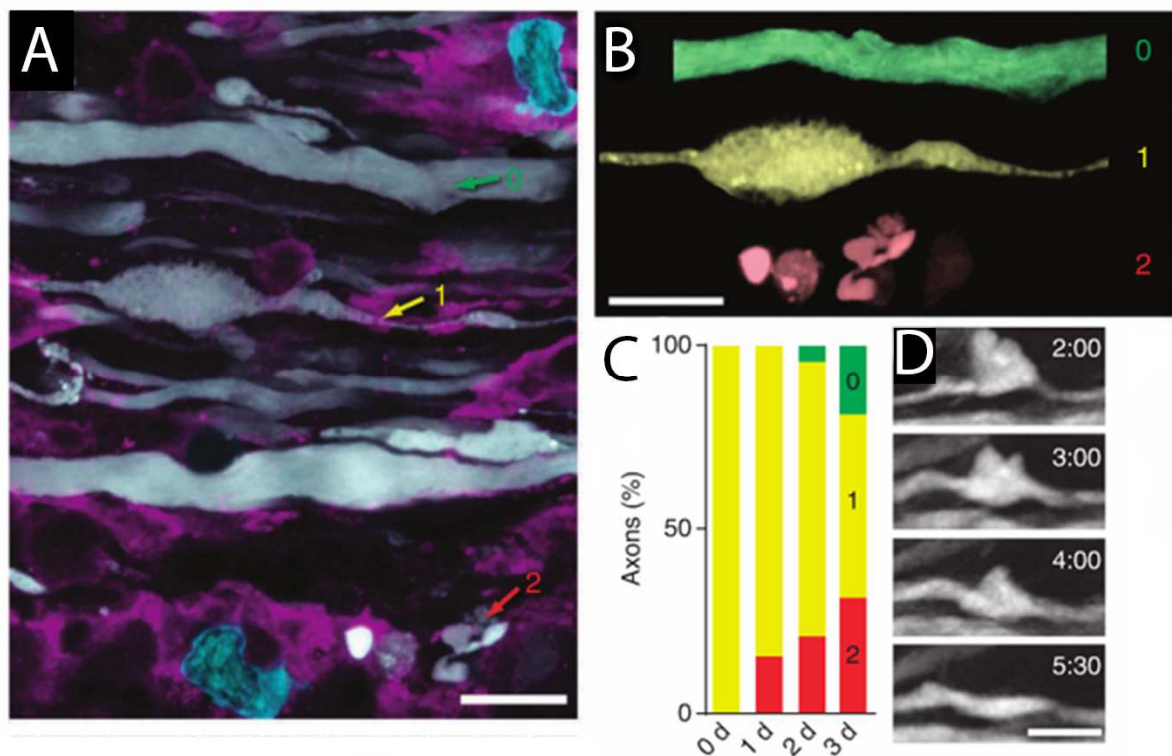


**Figure 3 Focal axonal degeneration**

(A) Confocal projection image showing fluorescently labelled axon (white), activated macrophages/microglia (magenta) and T-cells (cyan) in an acute spinal cord lesion in EAE. (B) Selected axons taken from (A) showing different stages of focal axonal degeneration: intact morphology (stage 0, green), focal swellings (stage 1, yellow) and fragmentation (stage 2, red). (C) Fate of axons originally presenting with stage 1 morphology over the timecourse of 4 days, stages of degeneration color-coded as in B. (D) *In vivo* 2-photon time-lapse images of an axon showing recovery from stage 1 to stage 0. Scale bars: 10  $\mu$ m. Adapted from (Nikić et al., 2011)

### **1.2.2 Molecular mechanisms of axon degeneration**

There are multiple elements in the puzzle of a putative degeneration sequence that all have been proven to be important factors, but their order and grade of importance has yet to be sorted out. Reactive oxygen species (ROS), reactive nitrogen species (RNS) and mitochondrial failure have been proposed to play a crucial role in axon damage, especially under inflammatory conditions (Dutta et al., 2006; Kapoor et al., 2003; Smith et al., 2001). In the setting of FAD, subcellular changes can be observed in axons within lesion sites: in swellings

---

as well as in normal appearing axons, mitochondria present a swollen and shortened dysmorphic shape accompanied by a decrease in membrane potential. These alterations could be reproduced by applying ROS or RNS to the healthy spinal cord. Mononuclear phagocytes have been suggested to be a major source of ROS/RNS. They can be found spatially close to degenerating axons for prolonged periods of time (Nikić et al., 2011). This is in line with the assumption that oxidative damage to mitochondria plays an important role in MS (Haider et al., 2014; Lin and Beal, 2006). The subsequent effects of mitochondrial malfunction can be manifold: lowered ATP levels, generation of ROS, impaired calcium buffering leading to an imbalance of cellular homeostasis, activation of the mitochondrial permeability transition pore (mPTP), as well as the release of pro-apoptotic signals and other cell death mechanisms (Court and Coleman, 2012). However, the exact sequence of these events and a potential interplay among them remain unknown.

Mitochondrial damage is closely related to another player in the process of degeneration: Increased intracellular calcium concentrations have been shown to play a fundamental role in different models of axon degeneration. For example, in Wallerian degeneration, an influx of extracellular calcium was proposed to be necessary and sufficient for induction, probably triggering activation of calpains that degrade the cytoskeleton (Schlaepfer, 1974). In a parallel study to this work, an *in vivo* study of spinal cord contusion, we have found a calcium rise in a large population of axons that drives axon loss in a calpain-dependent fashion (Williams et al., 2014). Under the inflammatory conditions of MS, EAE and Acute Optic Neuritis (AON), an altered expression of  $\text{Ca}^{2+}$  channels and the  $\text{Na}^+/\text{Ca}^{2+}$  antiporter has been shown and suggested to play a role in mediating calcium overload of the cells (Craner et al., 2004a; 2004b; Friese et al., 2007; Gadjanski et al., 2009; Rossi et al., 2010). The question of whether axonal calcium is a crucial factor for axon degeneration in EAE, and what the main effectors and sources of intra-axonal calcium changes are, remains elusive. Finding the answer to these questions motivated the development of the approach described in this work here.

### **1.3 *In vivo* visualization of neuronal calcium levels**

Imaging cellular, subcellular and even molecular processes over time in the intact tissue of rodents has recently become possible with the great advances in light microscopy techniques. The ability of fluorescence microscopy to probe non-translucent tissues and advances in transgenic technology that allow to specifically label different cell types and structures makes a wide variety of imaging paradigms possible. However, a comprehensive understanding of the tools used is essential to interpret the data that is being generated by these novel techniques.

#### **1.3.1 *Intravital 2-photon microscopy of the nervous system***

The desire of scientists to study structure, function and dysfunction in the complex structure of the CNS has always been great. However, to achieve this, easy access to the organ to be imaged had to be established, often resulting in *ex-vivo* explant models or slice cultures. If an organ like the spinal cord is exposed by sophisticated surgery techniques (Misgeld et al., 2007), the rays of a conventional light microscope would only be able to resolve signals on the very surface. This is due to strong scattering of the light, resulting in an image that appears blurred and with suboptimal resolution. Even though the poor z-resolution of an epifluorescent excitation can be overcome by introducing a pinhole to achieve confocality (to exclude light that comes from above and below the focus), tissue penetration of visible, confocal laser lines is too poor to allow for well-resolved imaging in greater depth. To move fluorescent microscopy into the field of non-linearity was an ingenious step by the pioneers of the early 1990s that developed the two-photon microscope (Denk and Svoboda, 1997; Denk et al., 1990; 1995; Helmchen and Denk, 2005; Zipfel et al., 2003).

Two-photon laser-scanning microscopy combined with in-vivo fluorescent labelling techniques is the dominant method that has evolved out of the non-linear microscopy field. It made non-invasive imaging of intact tissue possible with an improved resolution in XY and Z, managing imaging depths up to almost 1 mm with an unprecedented signal-to-noise ratio compared to other fluorescence microscopy methods. The principle behind the method is that of a “higher-order” interaction between a defined wavelength of excitation light and the

corresponding fluorophore. In conventional fluorescent microscopy, a single photon excites a fluorophore to move its electrons to a higher energy state, rendering it a linear process that is directly proportional to the light intensity. In nonlinear microscopy, multiple photons of higher wavelength and therefore lower energy can be used to generate contrast in matter. However, they need to be highly concentrated in space and time to allow for sufficient excitation of the fluorophores. High spatial densities can be generated by using a high numerical aperture (NA) objective to focus the laser beam. Concentration in time requires the use of sophisticated lasers that emit ultrashort pulses, which last only femtoseconds but show correspondingly high peak intensities (Helmchen and Denk, 2005).

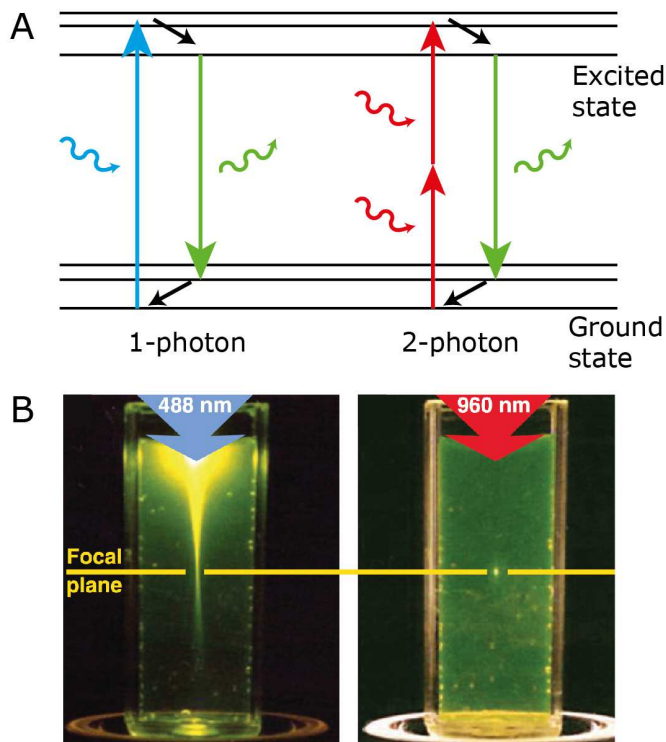


Figure 4 Basic principles of 1 and 2-photon excitation

(A) Jablonski diagram depicting one-photon and two-photon absorption. The emission of a photon of a “green” wavelength (e.g. 520 nm) can be evoked by the excitation with “blue” (e.g. 488 nm) or a high density of near-infrared photons (e.g. 960 nm). (B) In linear, single-photon microscopy, an entire cone of fluorescence light is generated (left), whereas in multi-photon, nonlinear excitation, the signal is localized in the point spread function of the focal spot (right) (B Modified from Zipfel et al., 2003).

---

The advantages of the technique are twofold: First, in contrast to linear fluorescent microscopy, the photons used for excitation are of a longer wavelength (near-infrared) than the emitted photons of the sample. This facilitates tissue penetration of the excitation light-beam strongly, since biological samples scatter shorter wavelengths more and present a variety of endogenous absorbers that will render the light energy to heat and result in tissue damage. Second, the high spatial and temporal photon density needed will in theory only be reached in the actual focus of the laser beam – neither below nor above. This results in an automatic selection for the perifocal z-volume without the application of a pinhole that decreases signal intensity. As there is little to no excitation of out-of-focus volumes this leads to less photobleaching and toxicity in the biological sample. The signal can be detected by “external” detectors, also referred to as non-descanned detectors (NDDs), which bypass the excitation lightpath including the scanning mirrors. Thereby they detect all the photons falling into the large opening angle of the high-NA objective. This again leads to a stronger in-focus signal without harming the rest of the specimen.

When it comes to *in vivo* observations in the CNS, the development of new molecular biological tools to label the structures of interest have proved equally important as the invention of new imaging modalities. The generation of transgenic mice that show a strong labelling of neurons and their processes with fluorescent proteins was of particular importance (Misgeld and Kerschensteiner, 2006). To be able to follow a single neuronal cell or its neurites in space and time, a Golgi-like staining pattern is needed in living animals. This was achieved by expressing different spectral variants of fluorescent proteins (XFPs) under the control of a modified Thy1-promoter element (Feng et al., 2000). In addition to transgenic mouse lines that display sparse patterns of neuronal labelling, other lines are available that have dense or almost full labelling, which enables the researcher to analyse large populations of neurons in a single experiment. Glial cells such as astrocytes, oligodendrocytes, microglia

and immune cells can also be specifically studied *in vivo* using a similar approach (Pfrieger and Slezak, 2012).

The tools available for fluorescent *in vivo* microscopy even allow imaging on the level of subcellular structures and can give a functional readout of various intracellular molecules and ions in the CNS. The possibilities include, for example, the assessment of mitochondrial transport (Misgeld et al., 2007a), microtubule dynamics (Kleele et al., 2014), indicators of intracellular metabolic state like ATP or NADH (Berg et al., 2009; Zhao and Yang, 2014), pH and redox state (Breckwoldt et al., 2014; Gutscher et al., 2008; Tantama et al., 2011).

One cellular measurement that has traditionally been of outstanding interest to neurophysiologists is intracellular calcium, as it not only is a key player in cellular signalling and pathology, but is also a reliable readout of activity, rising concomitantly with increasing numbers of action potentials during cellular firing. Calcium can be monitored *in vivo* using synthetic or genetically encoded calcium sensors, and therefore provide insight into physiological activation states or pathological mechanisms of cells and, particularly for this study, neurons.

### **1.3.2 Genetically encoded calcium indicators**

Calcium is a crucial and versatile intracellular player responsible for a multitude of functions in a variety of cell types in biological organisms. Processes that include  $\text{Ca}^{2+}$  operate over a wide time range (from neurotransmitter release happening at the microsecond scale to gene transcription, which lasts for minutes and hours) and involve concentrations that span several orders of magnitude. Whereas nanomolar quantities trigger synaptic vesicle release, the influx of micromolar concentrations of  $\text{Ca}^{2+}$  is seen in cell death. The appropriate kinetics, binding capacity and signal response of  $\text{Ca}^{2+}$  sensors are therefore of paramount importance if one wishes to assess  $\text{Ca}^{2+}$  signals *in vivo* (Grienberger and Konnerth, 2012). Many different indicators have been produced or bioengineered in the last decades to match this variety of applications in research.

---

To be able to study  $\text{Ca}^{2+}$  signals in the rodent CNS under pathological conditions, a suitable sensor would need to generate a decent signal for robust  $\text{Ca}^{2+}$  transients, a stable baseline and should interfere neither with intracellular ion homeostasis nor with the cell's endogenous  $\text{Ca}^{2+}$  signalling. A non- or minimally invasive way to deliver the indicator to the tissue volume of interest would allow the distinction between experiment-induced damage and the actual disease paradigm. A major advance towards this ideal was the generation of genetically encoded calcium indicator proteins (GECI). These sensors are based on a stretch of DNA and allow engineering by any technique that the recombinant DNA toolbox offers. The sequence coding for the sensor can be delivered by direct insertion into the genome by fertilized egg manipulation leading to transgenic mouse production, or with the appropriate viral vector into cells of postnatal animals. The sensor protein is then formed within the cell *in situ* (Mank and Griesbeck, 2008). Stable cellular expression can be achieved in all kinds of organisms including rodents.

The GECIs are fluorescent protein complexes with calcium binding properties that change their emission and/or excitation behaviour according to the concentration of  $\text{Ca}^{2+}$  around them. Two distinct pathways of sensor development have been followed (Griesbeck, 2004; Miyawaki et al., 1997): In one, a single fluorophore is used as the basis to form an indicator that changes the signal intensity upon binding. These sensors have become very popular because of the high dynamic range they exhibit. They have turned out to be ideal to monitor, for example, the activity of single neurons and networks in response to external stimuli. However, as only changes in  $\text{Ca}^{2+}$  can be detected without a reference baseline, it appears difficult to use these single fluorophore indicators in disease models. In the second approach, a dual wavelength sensor works by means of fluorescence resonance energy transfer (FRET) between two different fluorescent proteins, providing a ratiometric measurement that can be used to directly quantify intracellular  $\text{Ca}^{2+}$  levels (Garaschuk et al., 2007).

---

Fluorescence (also referred to as Försters) Resonance Energy Transfer is a physical phenomenon that occurs when two neighbouring fluorescent molecules change their distance, orientation or conformation. At a distance of 100 Å and below, the so-called “donor” molecule will transfer energy non-radiatively to the “acceptor” molecule, leading to the emission of a photon by the acceptor. A prerequisite for this to occur is that the emission spectrum of the shorter-wavelength donor has to overlap with the excitation spectrum of the acceptor, which exhibits a longer wavelength (spectral overlap). The relative orientation of the donor absorption and acceptor transitions moments and the refractive index are also factors that influence the transfer rate of the process (Jares-Erijman and Jovin, 2003).

This phenomenon enables the creation of a “nanoscale ruler”, which in turn allows the visualization of conformational changes of single molecules, simply by attaching fluorescent reporters to its different domains. Indeed, when the  $\text{Ca}^{2+}$  binding domains of proteins are bound by  $\text{Ca}^{2+}$ , conformational changes in the structure occur. Different teams of researchers have therefore taken proteins (or some of their domains) known to bind calcium, attached enhanced spectral variants of green fluorescent protein (GFP) and created a protein that is able to report calcium levels. The read-out is the ratio of the two fluorophores’ signal that changes when FRET occurs. In one approach, calmodulin and its binding peptide M13 from myosin light chain kinase were inserted between BFP and GFP (Miyawaki et al., 1997). This sensor and its enhanced versions are referred to collectively as the family of “Cameleons”. As there is a variety of endogenous functions, interactions of the Cameleons with some of the many calmodulin-binding proteins in the cell are difficult to rule out. Thus, a better solution was the complete replacement of the highly regulated calmodulin with another  $\text{Ca}^{2+}$ -binding protein that is less likely to interfere in the signal transduction networks of rodent neurons.

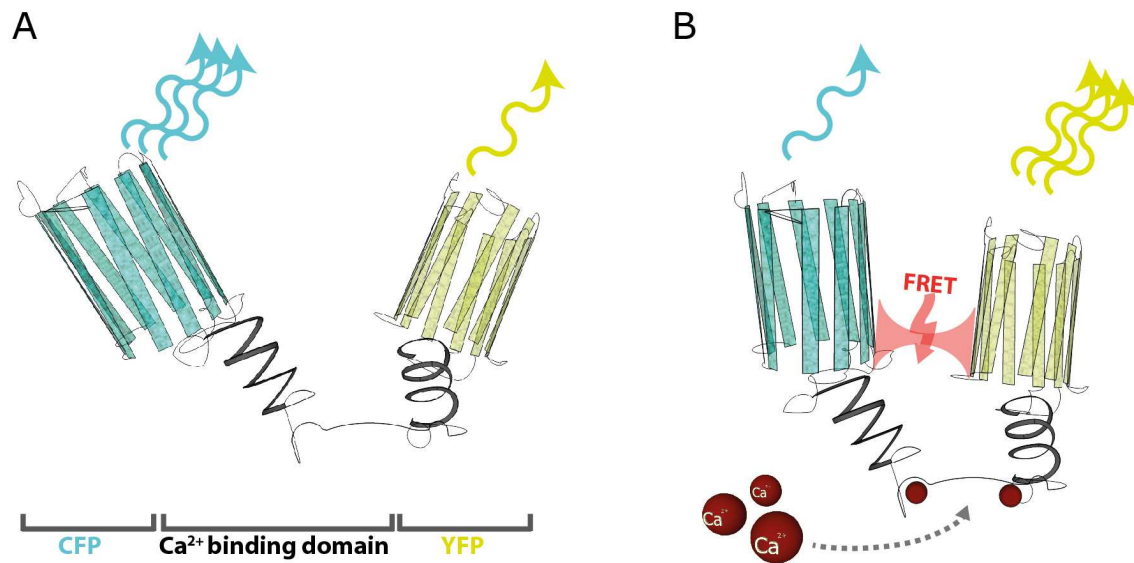


**Figure 5 Structure of a FRET based genetically encoded calcium indicator**

(A) The basal structure of the sensor contains a calcium binding domain and two fluorescent reporter proteins with overlapping wavelengths, in this case CFP and YFP. (B) Upon binding of Ca<sup>2+</sup> ions, the lower-wavelength (donor) fluorophore transfers energy to its higher-wavelength neighbouring (acceptor) fluorophore, leading to an increased emission of photons by the acceptor.

Troponin C (TnC) from skeletal and cardiac muscle appears to be a decent compromise: whereas it is a protein that folds and works at 37 °C - and hence in the rodent brain - it does not show any other functions other than to induce muscle contraction. In all of the animal kingdom, it can be found in many different variants showing diverse binding properties. Deriving it from a phylogenetically distinct species could even better rule out any undesirable interactions in the target organisms (Mank and Griesbeck, 2008). Griesbeck and colleagues have created an entire new family of GECIs by fusing variants and parts of skeletal and cardiac muscle Troponin C (TnC) with bioengineered variants of GFP (Garaschuk et al., 2007; Heim et al., 2007; Mank et al., 2006; 2008). The first sensor constructs were based on chicken skeletal muscle TnC (TN-L15) and human cardiac muscle TnC (TN-humTnC). To yield a brighter and better sensor, further engineering work produced CerTN-L15 and the intermediate

affinity sensor TN-XL. The  $\text{Ca}^{2+}$  binding domain mainly influences the sensor's binding affinity and kinetics, whereas the signal intensity and the ratio change are strongly dependent on the fluorophore variants used. The dissociation constant ( $K_d$ ) is an affinity measure and represents the concentration where 50% of the sensor protein is  $\text{Ca}^{2+}$  bound. It therefore provides a clue about the range of calcium concentrations it is able to detect. The maximal fractional ratio change ( $\Delta R/R$ ) is a measure of the amplitude of the calcium signal, dividing the maximal change in ratio ( $\Delta R$ ) by the baseline ratio. Table 1 compares selected TnC based biosensors with the specifications mentioned above.

Indicator	Binding moiety	Donor fluorophore	Acceptor fluorophore	$\text{max } \Delta R/R$	$K_d$	Reference
TN-L15	csTnC $\Delta 14$	eCFP	Citrine	140 %	1.2 $\mu\text{M}$	(Heim and Griesbeck, 2004)
CerTN-L15	csTnC $\Delta 14$	Cerulean	Citrine	95 %	1.2 $\mu\text{M}$	(Heim et al., 2007)
TN-XL	csTnC $\Delta 14$	eCFP	Citrine cp174	400 %	2.5 $\mu\text{M}$	(Mank et al., 2006)
TN-XXL	C-csTnC / C-csTnC	eCFP	Citrine cp174	230 %	0.8 $\mu\text{M}$	(Mank et al., 2008)

**Table 1 Selected Troponin C based calcium sensors**

**Selection of Troponin C based calcium sensors and their composition. csTnC: chicken skeletal Troponin C,  $\Delta R/R$  max: maximum fractional Ratio change in experiments,  $K_d$ : dissociation constant.**

The combination of the genetic tools used to label neuronal subsets (as described in 1.3.1) and the bioengineered construction of a GECI yielded the creation of the Thy1-CerTN-L15 and Thy1-TN-XXL mouse lines. These transgenic strains strongly express the fluorescent indicator protein in neurons and their processes in many regions of the brain and spinal cord, making it possible to image axonal calcium dynamics *in vivo*, as performed in this study.

## 2. Objectives

Axonal degeneration appears in a focal manner in inflammatory CNS lesions. The exact mechanisms of axon damage and its relation to infiltrating immune cells has so far remained elusive. Amongst potential mediators of this process,  $\text{Ca}^{2+}$  has been proposed to be a major player. However, so far no study has provided an in-depth analysis of axonal  $\text{Ca}^{2+}$  in actively induced models of EAE and characterized its impact on the pathway leading to focal axonal degeneration. This study aims to characterize axonal  $\text{Ca}^{2+}$  concentrations in neuroinflammatory lesions of the spinal cord and assess the influence of  $\text{Ca}^{2+}$  on the fate of the axon. Specifically, this work aims to answer the following questions:

- Is there a modality to measure intracellular  $\text{Ca}^{2+}$  of single axons *in vivo* in the spinal cord?
- Which imaging settings are needed to provide a valid and reliable readout of  $\text{Ca}^{2+}$  concentrations?
- What is the baseline level of  $\text{Ca}^{2+}$  in healthy axons and can  $\text{Ca}^{2+}$  elevations be detected under control conditions?
- Can changes in intra-axonal  $\text{Ca}^{2+}$  be detected in lesions of acute EAE and at later timepoints (remission)?
- If there appears to be a population of axons with elevated  $\text{Ca}^{2+}$ , how does this influence their fate to subsequently undergo a process of degeneration?

### 3. Material and Methods

#### 3.1 Material list

Reagents	
<b>Surgery</b>	
Agarose	Sigma-Aldrich® Chemie GmbH, 82024 Taufkirchen, Germany
Bepanthen Augen- und Nasensalbe 5 g (eye ointment)	Bayer Vital GmbH, Leverkusen, Germany
Cutasept F Lösung 250 ml (disinfectant spray)	Bode Chemie GmbH & Co, Hamburg, Germany
Ethanol 70%	CLN GmbH, 85416 Niederhummel, Germany
Forene (Isoflurane)	Abbott AG, Baar, Switzerland
Hydrogen Peroxide Solution (H <sub>2</sub> O <sub>2</sub> )	Sigma-Aldrich® Chemie GmbH, 82024 Taufkirchen, Germany
Ketamine hydrochloride 10% (Ketamine)	Bremer Pharma GmbH, Warburg, Germany
Ringerlösung Fresenius KabiPac (Ringer's solution)	Fresenius KaBI Dtl., Bad Homburg, Germany
Sterile artificial mouse cerebrospinal fluid (aCSF)	<p>Solution A:            8,66 g NaCl (Merck)            0,224 g KCl (Merck)            0,206 g CaCl<sub>2</sub> · 2H<sub>2</sub>O (Sigma-Aldrich)            0,163 g MgCl<sub>2</sub> · 6H<sub>2</sub>O (Sigma-Aldrich)</p> <p>Solution B:            0,214 g Na<sub>2</sub>HPO<sub>4</sub> · 7H<sub>2</sub>O (Merck)            0,027 g NaH<sub>2</sub>PO<sub>4</sub> · H<sub>2</sub>O (Merck)            dH<sub>2</sub>O ad 500 ml</p> <p>Mixture of solutions A and B in a 1:1 ratio</p>
Xylarium 20 mg (Xylazine)	Riemser Arzneimittel AG, Greifswald-Insel Riems, Germany

**Tissue processing/ immunohistochemistry**

Phosphate Buffer (PB) 0,2 M	27,598 g NaH <sub>2</sub> PO <sub>4</sub> · H <sub>2</sub> O, 35,598 g Na <sub>2</sub> HPO <sub>4</sub> · 2H <sub>2</sub> O dH <sub>2</sub> O ad 1l
Gibco Goat Serum	Invitrogen GmbH, Darmstadt, Germany
Goat-anti-rabbit 594 antibody	Jackson ImmunoResearch Laboratories, West Grove (Pennsylvania), USA
PFA (paraformaldehyde) 4%	8% PFA (Sigma-Aldrich) in dH <sub>2</sub> O, heated up to 55 °C and stirred additional 10 min, filtrated and mixed in a 1:1 ratio with 0,2 M PB (Phosphate buffer), pH adjusted to 7,2- 7,8
Phosphate Buffered Saline (PBS), 10x	103,23 mg Na <sub>2</sub> HPO <sub>4</sub> · H <sub>2</sub> O 26,52g Na <sub>2</sub> HPO <sub>4</sub> · 2H <sub>2</sub> O 40g NaCl H <sub>2</sub> O bidest. added to 1l Prepared in house.
Polyclonal Rabbit Anti-Human Myelin Basic Protein	Dako/Agilent Technologies, Santa Clara , California, USA
Sucrose	Sigma-Aldrich® Chemie GmbH, 82024 Taufkirchen, Germany
TBS 10x (Tris buffered saline), pH=7,6	61 g Tris base (121,14 g/mol), (Sigma- Aldrich) 90 g NaCl dH <sub>2</sub> O ad 1l
Tissue Tek optimal cutting temperature (O.C.T.)	Sakura Finetek Europe B.V. , Alphen aan den Rijn, The Netherlands
Triton X-100	Sigma-Aldrich® Chemie GmbH, 82024 Taufkirchen, Germany
Vectashield Mounting Medium, Fluorescence H-1000	Vector Labs, Burlingame, CA 94010, USA

**Immunization**

Myelin Oligodendrocyte Glycoprotein (MOG)	Stock solution, produced by laboratory of Doron Merkler (Universität Göttingen, University of Geneva)
M. tuberculosis H37 RA	Sigma-Aldrich® Chemie GmbH, 82024 Taufkirchen, Germany
Incomplete Freund Adjuvans (IFA)	Sigma-Aldrich® Chemie GmbH, 82024

	Taufkirchen, Germany
Pertussistoxin (Ptx) from Bordetella pertussis, inactivated	Sigma-Aldrich® Chemie GmbH, 82024 Taufkirchen, Germany

### Tools and materials

#### Surgical tools and materials

Wella contura W7807 (Hair clipper)	Wella, Darmstadt, Germany
Syringe 3pc 5 ml Omnifix™ luer slip (syringe for injection of Ringer's solution)	B. Braun Melsungen AG, Melsungen, Germany
BD Plastipak Hypodermic luer slip syringe 1 ml (syringe for Ketamine/Xylazine and Ptx injection )	Becton, Dickinson and Company, Franklin Lakes (New Jersey), USA
Feather stainless steel blade (surgical blade)	pfm medical ag, Cologne, Germany
Noyes Spring Scissors (Large spring scissors)	Fine Science Tools GmbH, Heidelberg, Germany
Vannas-Tübingen Spring Scissors (Small angled spring scissors)	Fine Science Tools GmbH, Heidelberg, Germany
Dumont Mini Forceps – Inox Style 3 (Small forceps)	Fine Science Tools GmbH, Heidelberg, Germany
Dumont Mini Forceps – Inox Style 5 (Small forceps, smaller tip than Inox style 3)	Fine Science Tools GmbH, Heidelberg, Germany
Hypodermic Needles BD Microlance 30 Gauge (0,3 mm, yellow) for subcutaneous injection of Ringer's solution and anesthesia	Becton, Dickinson and Company, Franklin Lakes (New Jersey), USA
Hypodermic Needles BD Microlance 3 23 Gauge (0,6 mm, blue) for subcutaneous emulsion immunization	Becton, Dickinson and Company, Franklin Lakes (New Jersey), USA
Ethicon Ethilon monofil 6-0 size, 667H (skin suture)	Johnson & Johnson Medical GmbH, Norderstedt, Germany
Ethicon Vicryl 4-0 size, MIC101H (intracorporal suture)	Johnson & Johnson Medical GmbH, Norderstedt, Germany
Sugi (absorbent triangles)	Kettenbach GmbH & Co. KG, Eschenburg, Germany

Metal plate	Custom-made
Cast Alnico Button Magnets	Eclipse Magnetics Ltd, Sheffield, UK
Rubber bands	
Support cushion	Custom-made
Osmotic minipump (Model 1007B)	Alzet, Cupertino (California), USA
Intrathecal catheter (Model 7743)	Alzet, Cupertino (California), USA

### Tools and materials for histology

Microscope slides 76x26 mm	Gerhard Menzel Glasbearbeitungswerk GmbH & Co. KG, Braunschweig, Germany
Microscope cover slips 24x60 mm	Gerhard Menzel Glasbearbeitungswerk GmbH & Co. KG, Braunschweig, Germany
Parafilm	Brand GmbH & Co. KG, Wertheim Germany
Pipettes, pipette tips and tubes (2ml and 1,5 ml)	Eppendorf AG, Hamburg, Germany
12-well cell culture plates	Becton, Dickinson and Company, Franklin Lakes (New Jersey), USA
Tissue Tek Cryomold Standard, 25x20x5 mm	Sakura Finetek Europe B.V. , Alphen aan den Rijn, The Netherlands
Tissue Tek Cryomold Biopsy, 10x10x5 mm	Sakura Finetek Europe B.V. , Alphen aan den Rijn, The Netherlands
Paper filters (185 mm Ø circles)	Whatman Schleicher & Schuell GmbH, Dassel, Germany
50 ml centrifuge tubes	Greiner Bio-One GmbH, Frickenhausen, Germany

### Technical devices

#### Surgery

Olympus KL 1500 LCD (cold light source for stereomicroscopy)	Olympus Deutschland GmbH, Hamburg, Germany
Olympus Stereo Microscope SZ51	Olympus Deutschland GmbH, Hamburg, Germany
FST 250 Hot Bead Sterilizer (sterilizer for surgical instruments)	Fine Science Tools GmbH, Heidelberg, Germany
T/Pump (Heating pad)	Gaymar Industries, Orchard Park (New York), USA

**Histology**

Leica CM1850 cryostat	Leica Microsystems GmbH, Wetzlar, Germany
Vibratome 1000Plus	Intracel LTD, Shepreth, Royston, Great Britain
Vortex-Genie 2	Scientific Industries, Inc., Bohemia (New York), USA
KERN EW 150-3M (scales)	Kern & Sohn GmbH, Balingen-Frommern, Germany
Laboratory pH meter inoLAB	WTW Wissenschaftlich-Technische Werkstätten, Weilheim, Germany
Magnetic stirring hotplate MR 3001K and stirring bars	Heidolph Instruments GmbH & Co. KG, Schwabach, Germany
Ismatec IP high precision multichannel pump (pump for perfusions)	ISMATEC SA, Labortechnik - Analytik, Glattbrugg, Switzerland
Olympus IX71 inverted fluorescence microscope (evaluation of immunohistochemistry)	Olympus GmbH, Hamburg, Germany

**Microscopy**

FV1000 confocal system mounted on an upright BX61 microscope, equipped with an x10/0.4 water immersion objective and x20/0.85 and x60/1.42 oil immersion objectives (confocal microscopy)	Olympus GmbH, Hamburg, Germany
Olympus FV1000 MPE multiphoton Microscope x25/1.05 water immersion objective	Olympus GmbH, Hamburg, Germany
MaiTai eHP/HP Titanium:sapphire laser	Newport/ Spectraphysics, Irvine, California, USA
Manual XY translation stage	Custom build, parts by Thorlabs Inc Newton (New Jersey), USA

**Data analysis/ Software**

Adobe Creative Suite (Photoshop, Illustrator)	Adobe Systems, Inc., San Jose, California, USA
ImageJ/ FIJI	General Public License <a href="http://rsbweb.nih.gov/ij/download.html">http://rsbweb.nih.gov/ij/download.html</a>

---

Graphpad Prism	GraphPad Software, La Jolla, California, USA
Microsoft Office (Powerpoint, Excel, Word)	Microsoft Corporation, Redmond, Washington, USA

### **3.2 Experimental animals**

All experimental mice were kept and bred in the animal facilities of the institution under standard conditions. Animals were held in Eurostandard Type II long cages 365x207x140 mmH (Tecniplast, Hohenpreißenberg, Germany) stored in an IVC rack system with a maximum of five mice per cage. Autoclaved food (regular food “Maus” from Ssniff, Soest, Germany) and water were supplied *ad libitum*. Mice were held at a 12 h light/12 h dark cycle. The lines used included the transgene Thy1-CeTN-L15 as well as Thy1-TN-XXL, provided by O. Griesbeck (MPI for Neurobiology, Martinsried). Both lines were created on a FVB or a FVB: C57BL/6 background and express the corresponding GECI protein CerTN-L15 (Heim et al., 2007) and TN-XXL (Mank et al., 2008) under the neuronal expression cassette Thy-1.2. To assess fluorescence bleedthrough during imaging of these sensors, we used thy1-CFP23 and thy1-YFP-H lines, and a cross of both lines for the pH effect experiments. All animal work conformed to institutional guidelines and was approved by the Animal Study Committee of the Regierung von Oberbayern, reference 55.2-1-54-2532-9-10.

### **3.3 Methods**

#### **3.3.1 Experimental autoimmune encephalomyelitis (EAE)**

Experimental autoimmune encephalomyelitis was induced according to a standard protocol (Abdul-Majid et al., 2000). Adult mice were immunized (p42-p98) with 250 µl of an emulsion containing 200 µg purified recombinant myelin oligodendrocyte protein (MOG, N1-125, produced in E-coli) in complete Freund's adjuvant containing 625 µg Mycobacterium tuberculosis H37 Ra. Each anesthetized animal (i.p. Ketamine 87 µg/g body weight, Xylazine 13 µg/g body weight) received 3 subcutaneous injections of the emulsion: 100 µl each on both flanks and 50 µl at the base of the tail. On the day of immunization and 2 days later, 250 ng of

Pertussistoxin (Ptx) in 100 µl of sterile Saline was injected intraperitoneally. All immunized mice were weighed and scored daily according to a standardized clinical EAE scale reflecting neuronal deficits (see Table 2).

Score	Clinical signs
0	No signs of disease
0.5	Distal tail weakness
1	Complete paralysis of the tail
1.5	Minor hind limb weakness, gait ataxia
2	Paresis of the hind limbs
2.5	Paresis of the hind limbs, partial dragging of the feet
3	Complete paralysis of the hind limbs
3.5	Complete hind limb paralysis with weakness of the forelimbs
4	Complete paralysis of the hind limbs and forelimbs
5	Moribund

**Table 2** EAE clinical scoring scale

### **3.3.2 Tissue processing and immunohistochemistry**

After lethal anaesthesia with isoflurane, animals were perfused transcardially with 10 ml of saline solution followed by 30 ml of 4% paraformaldehyde (PFA) in 0.1 M phosphate buffer. The vertebral column was coarsely dissected and the tissue post-fixed in 4% PFA at 4 °C for 24 h. After this, the tissue was transferred for storage to PBS, until the lumbar spinal cord was dissected under the stereomicroscope. For consecutive immunofluorescence analysis, spinal cords were cryoprotected in 30% sucrose for at least 24 h at 4 °C until the tissue density equilibrated with that of the sucrose solution. To prepare cutting the specimen was embedded in Tissue-Tek optimal cutting temperature (O.C.T.) compound and frozen at -20 °C. 40-60 µm thick transversal sections were cut on a freezing microtome, collected in well plates containing PBS and subsequently processed for immunohistochemistry. Myelin Basic

Protein (MBP) staining was done using the protocol outlined in Table 3. Neurotrace staining was performed as step 7, in a 1:500 dilution.

Step	Temperature	Time	Medium
1	Room temperature (RT)	3 x 10 min	PBS
2	-20 °C	15 min	Methanol
3	RT	3 x 15 min	PBS
4	RT	60 min	10 % goat serum (GS) in 0.5 % TrisPBS
5	4 °C	12 – 24 h	Rabbit-anti-human MBP 1:200 in 1 % GS in TrisPBS
6	RT	3 x 15 min	PBS
7	4 °C	12 – 24 h	AlexaFluor 594 goat-anti-rabbit 1:500 in 1 % GS + TrisPBS
8	RT	3 x 30 min	PBS

**Table 3 Staining protocol Myelin Basic Protein (MBP)**

After staining, tissue sections were mounted on glass slides with vectashield and coverslipped using a magnifying glass or stereomicroscope.

### **3.3.3 Confocal microscopy**

Fixed tissue samples were scanned on a FV1000 confocal system mounted on an upright BX61 microscope stand (Olympus). The system was equipped with a 10x/0.4 water immersion objective, 20x/0.85 and 60x/1.42 oil immersion objectives. Recorded 12-bit image stacks were subsequently processed using ImageJ (<http://rsbweb.nih.gov/ij>) or Adobe Photoshop software.

### **3.3.4 Surgery procedures**

#### **3.3.4.1 In-vivo imaging preparation**

All surgery procedures were done according to previously established protocols (Kerschensteiner et al., 2005; Misgeld et al., 2007a). Mice were intraperitoneally anaesthetized with ketamine-xylazine (ketamine 87 µg per g body weight, xylazine 13 µg per g body weight) and transferred to a heating pad for approximately 15-30 min to ensure deep anaesthesia. The fur above the lumbar spinal cord was shaved. To achieve good access to the intervertebral space, animals were positioned on a metal plate with limbs outstretched, with the head and

neck supported using a cushion. 70 % ethanol was used to wipe the exposed skin 4-5 times for cleaning and disinfection. A median incision of the skin above the lumbar vertebrae was performed using a scalp blade and the subcutaneous space was prepared with spring scissors. Lateral to the vertebral column, an incision of the muscle on both sides was made and the intervertebral space was opened by applying tension to the median muscular string and carefully cutting through the musculature. Any bleeding that occurred was staunched with sterile cotton swabs (Sugi). Once the spinal cord, covered by the dura mater, became visible, two vertebral laminae, along with the attached muscular tissue were removed by laminectomy with 14mm angled-blade spring scissors. The preparation was occasionally rinsed with aCSF to keep it clean and moist. To immobilize the spinal cord and reduce breathing artefacts, the vertebrae adjacent to the opening were clamped with a specifically engineered clamping device (Narishige STS-A) and equally fixed the tail of the animal. To keep the exposed area continuously moist, and to achieve a stable level of the immersion liquid, an imaging well with 2% Agarose was created that fitted the geometry of the objective, and filled it with an aCSF bath. For long-term experiments, the solution was preheated (37 °C) and superfused across the well.

#### **3.3.4.2 Implantation of osmotic mini pumps**

For bepridil treatment experiments, animals were implanted with an osmotic mini pump (Alzet) delivering 0.41mM bepridil in 0.5 % DMSO containing saline or vehicle (0.5 % DMSO in saline) through an intraspinal catheter. Pumps yielded a total capacity of approximately 100  $\mu$ l and an average output of 12  $\mu$ l per day. Each pump was weighed before and after filling to validate proper loading and only filled on the day of surgery. Implantation was scheduled for the clinical onset of disease, with a score-matched distribution of vehicle and treatment groups. Surgery was performed with the guidance and assistance of I. Nikic. The intervertebral space was accessed and opened in the caudal lumbar vertebral column. The intraspinal catheter was attached to the pre-incubated pump and inserted into the intrathecal space, pointing caudally to rule out trauma to the spinal cord. For fixation, we sutured the catheter to the vertebral muscles and attached the pump in such a way that it rested in the

subcutaneous space and therefore kept its working temperature. The skin was sutured and the mouse was rehydrated with 1 ml of s.c. injected Ringer's solution before placement into the heated wake-up station. After 3 days of treatment, animals were perfused as described in 3.3.2 and the residual volume and weight of the pumps was assessed to evaluate the success of delivery.

### **3.3.5 2-Photon *in vivo* imaging**

For *in vivo* microscopy, a FV1000MPE system was used (Olympus), consisting of a FV1000MPE scan unit with a spectrally tuneable Titanium:sapphire laser (Spectra Physics/Newport) emitting femtosecond pulses of near-infrared light. Coupling of the lightpath and IR-laser modulation was achieved via an acousto-optic modulator or a transmission filter (AOM, AOTF) and beam size was adjusted via a keplerian beam expander. The microscope stand was a BX61WI (Olympus) upright microscope with motorized nosepiece focusdrive, together with a custom built, manual stage (using parts from Thor Labs) or a motorized InVivo bridge (Luigs-Neumann). For all experiments including CerTN-L15 mice an excitation wavelength of 840 nm was used together with emission filter systems collecting 460-510 nm for the Cerulean channel and 515-560 for eYFP or FRET channel. The two corresponding detectors were non-descanned detector photomultiplier tubes (PMTs, Hamamatsu) or gallium arsenide phosphide (GaAsP) detectors. All experiments were done with a 25x/1.05w dipping cone objective (Olympus) immersed in aCSF. Images were acquired using Olympus Fluoview 1000 software. Animals were kept under constant anaesthesia with checks for breathing and reflexes at 30 min intervals. During periods when animals were not being imaged, their body temperature was regulated by radiation with an infrared lamp.

The timecontroller function of the Fluoview software enabled repeated acquisition of high-resolution overviews of the spinal cord by imaging a predefined matrix of regions using a zoom of 2-3x over a timecourse of several hours, yielding a 400-500  $\mu\text{m}$  imaging field with a pixel size of  $\approx 400$  nm. If movement-induced drift in the z-plane of the image was detected

during the experiment, the centre of the image stack was adjusted uninterruptedly to the correct position.

### 3.3.6 Data analysis

Data was processed and analysed using FIJI, a version of ImageJ optimized for life science applications (<http://fiji.sc/Fiji>), and Adobe Photoshop. Recorded images were loaded into the FIJI software using the Bioformats Importer plugin. For the evaluation of ratiometric images, the two separate channels that constituted each complete image were opened. Three regions of interest (ROI) were then drawn in the axons and background areas respectively of the first image, and then identically copied onto the second channel. The integrated fluorescence intensities within the corresponding ROIs were then measured from each channel (see Figure 6).

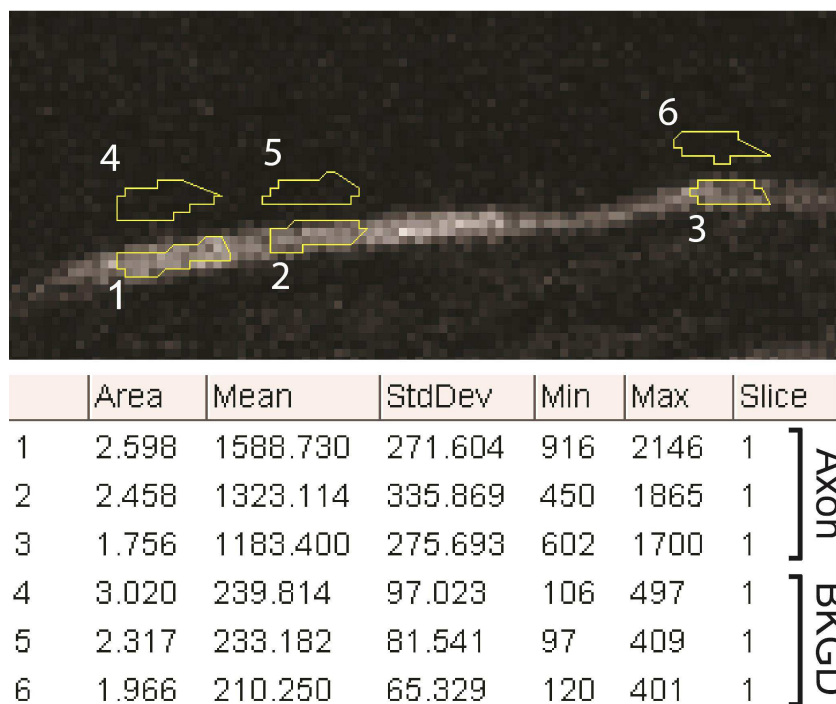


Figure 6 Measuring regions of interest (ROIs) for single axons and nearby background

Clipped part of YFP channel in raw image data stack. ROI 1-3 (yellow selections) were selected in the axoplasm, ROI 4-6 in nearby background. The measurements include area of ROIs (in  $\mu\text{m}^2$ ), mean grey value and SD (StdDev), Minimal (Min) and Maximal (Max) grey values and position in Z-stack (Slice).

The formulas applied to the measurements are depicted below. Note: To simplify terminology, CFP refers to blue fluorescent proteins in general and YFP for yellow fluorescent proteins. The abbreviations therefore include fluorophore variants like Cerulean or circularly permuted (cp) modifications.

$$\text{RATIO} = (\text{FRET}_{\text{Int}} - \text{FRET}_{\text{BKGND}}) / (\text{CFP}_{\text{Int}} - \text{CFP}_{\text{BKGND}})$$

$$\text{FRET}_{\text{Int}} = \text{YFP}_{\text{Int}} - \text{BF} \times \text{CFP}_{\text{Int}} ; \text{FRET}_{\text{BKGND}} = \text{YFP}_{\text{BKGND}} - \text{BF} \times \text{CFP}_{\text{BKGND}}$$

**Formula 1 FRET Ratio calculated from the signal and background of the two channels**

$\text{FRET}_{\text{Int}}$  and  $\text{CFP}_{\text{Int}}$  represent the intensity of the FRET and CFP channels in the ROI, and  $\text{FRET}_{\text{BKGND}}$  and  $\text{CFP}_{\text{BKGND}}$  represent the intensity of FRET and CFP in the background ROI. The original data from the YFP channel ( $\text{YFP}_{\text{Int}}$ ,  $\text{YFP}_{\text{BKGND}}$ ) was before corrected for spectral bleedthrough with an experimentally derived bleedthrough factor (BF), as shown in chapter 4.2. All grey values presented as an arbitrary unit in 12-bit images, with values ranging from 0-4095 ( $=2^{12}$ ).

To get a coarse impression of the ratiometric state, and therefore  $\text{Ca}^{2+}$  level of an axon, the CFP channel represented by a red look-up-table (LUT), and the FRET channel coded in a green LUT, were merged. This yielded an image where a green-shifted structure would imply high  $\text{Ca}^{2+}$  levels. Truly ratiometric images were created using the following procedure: maximum intensity projections of single channels were background corrected by using the thresholding tool on the channel with a higher signal-to-noise ratio. This ‘mask’ was then applied to both channels to exclude signal from background structures. By using the image calculator, the resulting, masked images of both channels (FRET/CFP) were divided to yield a greyscale, 32-bit float image also handling pixels divided by a custom look-up-table (LUT) derived from the “Fire LUT” (representing the highest ratios as yellow and lower ratios as violet to black) was applied. A ‘despeckle filter’ was applied to the original grey-scale image

projection from the FRET channel, and the intensity of the resultant image was then adjusted in Photoshop. The derived ratiometric RGB images were blended with the grey-scale image using the “Color” option to yield an image that represents the grey-scale as a function of intensity and the modified fire LUT as a function of FRET ratio.

To create large area timelapse videos, the single tile images were z-projected using the “maximum intensity projection” function in FIJI, stitched together via the semiautomatic merge tool in Photoshop and registered to the other timepoints by the “register virtual stack slices” plugin in FIJI.

## 4. Results

### 4.1 Characterization of GECI transgenic animals

To find out whether I would be able to detect calcium signals *in vivo*, I first studied the baseline fluorescent signal of the transgenic animals we received from the group of O. Griesbeck (s. chapters 1.3.2 and 3.2). Both lines, thy1-CerTN-L15 as well as thy1-TN-XXL, contain a blue and a yellow fluorescent protein variant and could be excited with a wavelength 840 nm of a femto-second pulsed laser beam. The dissimilarities in the fluorophores attached to the sensor backbone of the two sensor proteins (s. Table 1) and/or the expression levels yielded a difference in baseline brightness as seen in Figure 7.

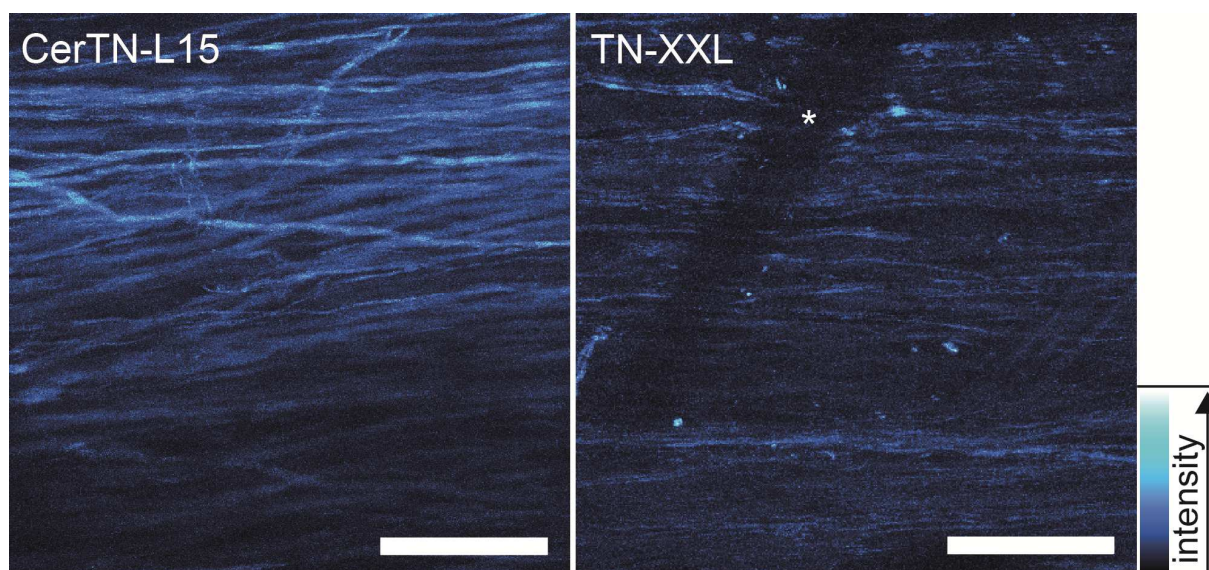
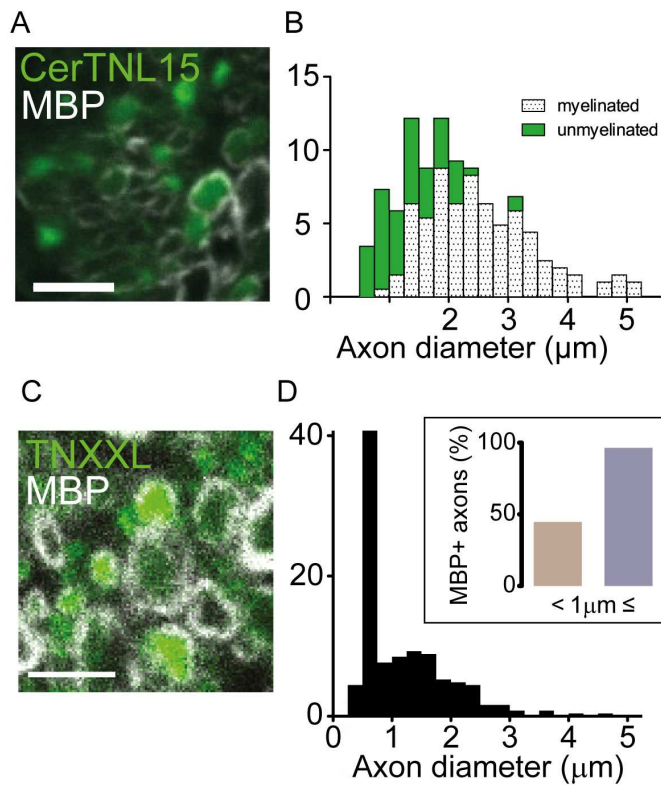


Figure 7 *In vivo* signal of thy1-CerTN-L15 and thy1-TN-XXL

Projection images showing the *in vivo* CFP signal of both GECI lines in the lumbar spinal cord, imaged under the 2-photon microscope. Axonal signal differs in brightness, here color-coded by the “cyan-hot” look-up-table shown in the scale on the right. Asterisk (right) highlights a blood vessel. Both images were scanned with the same detector settings and AOTF transmission of 5% (left) and 6% (right). Scale bar: 50  $\mu\text{m}$ .

As depicted in Figure 7, both lines provide a dense labelling pattern of axons with the GECIs. However, identification of a single axon and tracing it over up to hundreds of micrometres remains possible.



**Figure 8** Analysis of axon populations of the GECI lines.

(A)(C) Single plane confocal image showing a transverse section of the lumbar spinal cord of a thy1-CerTN-L15 and thy1-TN-XXL transgenic immunostained for myelin basic protein (MBP, white). Scale bars = 5 μm. (B) (D) Axon diameter distribution plotted as frequencies in 0.25 μm bins. Analysed in-situ on MBP immunostained spinal cord transverse sections for CerTN and *in vivo* for TNXXL. Box: Quantification of MBP ensheathement in thin (<1 μm) and thick (≥1 μm) caliber axons in TNXXL (179 axons, 2 mice). (C) and (D) taken and modified from Williams et al., 2014.

There is a visible and measurable difference in the size of the axons labelled in the lumbar spinal cord. Whereas thy1-TN-XXL labels mostly axons that are below 1 μm in diameter, the normal distribution of labelled axon diameters in thy1-CerTN-L15 centres around a mean of 2.16 μm (SD: 0.98 μm). I decided to do all experiments with the thy1-CerTN-L15 mouse strain

because of two reasons: First, the wider distribution of axon sizes. This allows the morphological assessment of small calibre as well as intermediate and larger calibre axons. Second, the brighter presentation of the fluorescent sensor proteins. All of the following experiments were thus done on thy1-CerTN-L15 animals, which I will refer to as “CerTN” in the following chapters.

## **4.2 Interpretation of ratiometric calcium indicator signals**

### **4.2.1 Imaging settings and bleedthrough correction**

As the ratiometric signal is interpreted as a direct correlate of intracellular calcium concentration (see chapter 1.3.2), I aimed to improve my imaging approach so that I can detect the FRET changes as close as possible to their full extent. The two main factors to influence this are 1.) an optimized signal-to-noise ratio and 2.) correction for spectral overlap of the channels, also known as “bleedthrough” or “crosstalk”. First, I measured signal-to-noise (S/N) for different excitation and detection settings, to yield optimized imaging parameters that I could use for the rest of the experiments. In Figure 9, S/N values are plotted separately for both the CFP and the YFP channel, with different PMT detector voltages on the abscissa and using incremental laser power (shown by symbols). The best compromise of decent S/N, while using “as-little-as-possible” laser intensities turned out to be the settings shown in Table 4. I established these imaging settings as the optimized setup for all experiments.

One major confounder in the detection of simultaneous fluorescent channels is spectral overlap. This phenomenon describes the imperfect separation of fluorophores with overlapping spectra in the recorded channels of a fluorescent microscope. The means to correct for this, spectral unmixing, is described in the literature (Zal and Gascoigne, 2004). In my experiments, I imaged transgenic animals expressing CFP only (thy1-CFP-23 line) and YFP only (thy1-YFP16), sequentially under the same conditions and settings like CerTN. I saw no channel crosstalk appearing in the CFP channel when exciting YFP. When imaging the CFP sample, I detected signal in the YFP channel that yielded 22 % of the signal in the CFP

channel. The calculated bleedthrough factor (BF) of 0.22 was from then on applied to all grey values measured in the YFP channel (see formula p. 35).

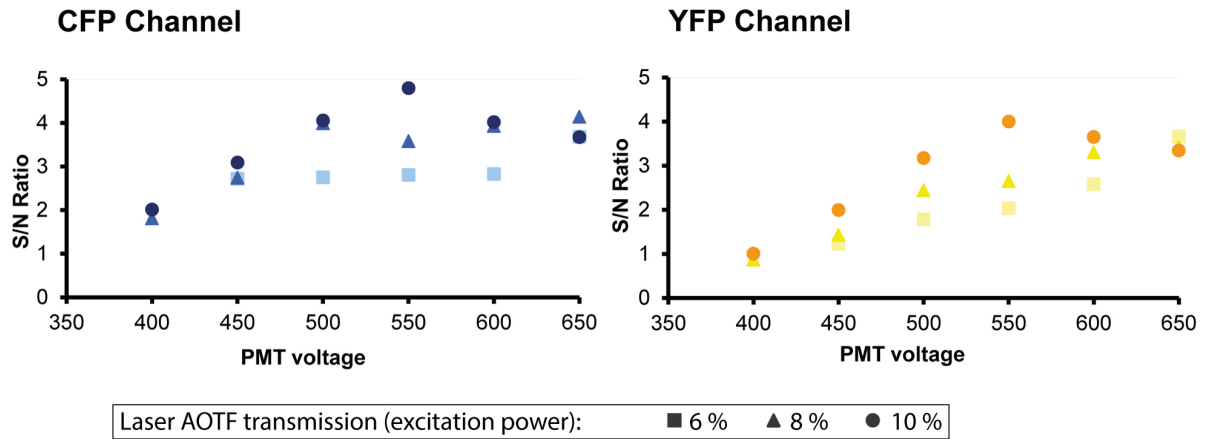


Figure 9 Signal-to-noise plot for different excitation detection parameters

Parameter	Value
Objective	25x / 1.05w
Zoom / Pixel number	3 / 512x512
Laser power out / AOTF Transmission	≈2.5 W / 5-8 %
Barrier filters	Channel 1: 460 - 510 nm Channel 2: 515 - 560 nm
PMT voltage	Channel 1: 600 V Channel 2: 600 V
PMT gain	Channel 1: 1 Channel 2: 1
PMT offset	Channel 1: 4 Channel 2: 4

Table 4 Determined optimal imaging settings for constant application

All parameters defined in this table were kept constant to make measured FRET ratios reliable and consistent. Laser power transmission had to be adapted according to preparation quality but did not change overall ratio.

#### 4.2.2 Baseline ratiometric signal and positive controls

To get a thorough understanding of the baseline ratios that spinal axons show in control animals, I imaged healthy CerTN transgenic mice and evaluated a total of 173 axons (3

---

animals) as described in chapter 3.3.6. The baseline YFP/CFP ratios are shown in Figure 10. Ratios are normally distributed with a mean value of 0.193 (SD = 0.028). To rule out any correlation with axon calibre (e.g. due to differences in sensor concentration and buffering capacities), values are plotted over the diameter of the measured axons. The even distribution does not suggest any correlation (Pearson  $r = -0.02$ ). I also could not detect a correlation of YFP/CFP ratio and labelling intensity as shown by the graph in Figure 10.

Extracellular  $\text{Ca}^{2+}$  is known to enter axons when they are transected. I used this principle as a positive control to assess if I can detect a ratio change in axons that had been mechanically transected in a spinal cord injury paradigm. On 2 days and 4 days post injury, I detected elevated YFP/CFP ratios in axons with different morphology, but mostly in axon fragments. Measured ratios are shown in Figure 10 and turned out to show an almost 3-fold increase of the mean control value (maximum value: 0.55, mean control: 0.19). This strongly suggests a clear readout of elevated calcium levels. These findings presented preliminary data for ongoing studies in two different disease paradigms. First, in the setting of EAE as presented in this work here. Second, in a model of spinal cord contusion, as shown in our corresponding publication (Williams et al., 2014).

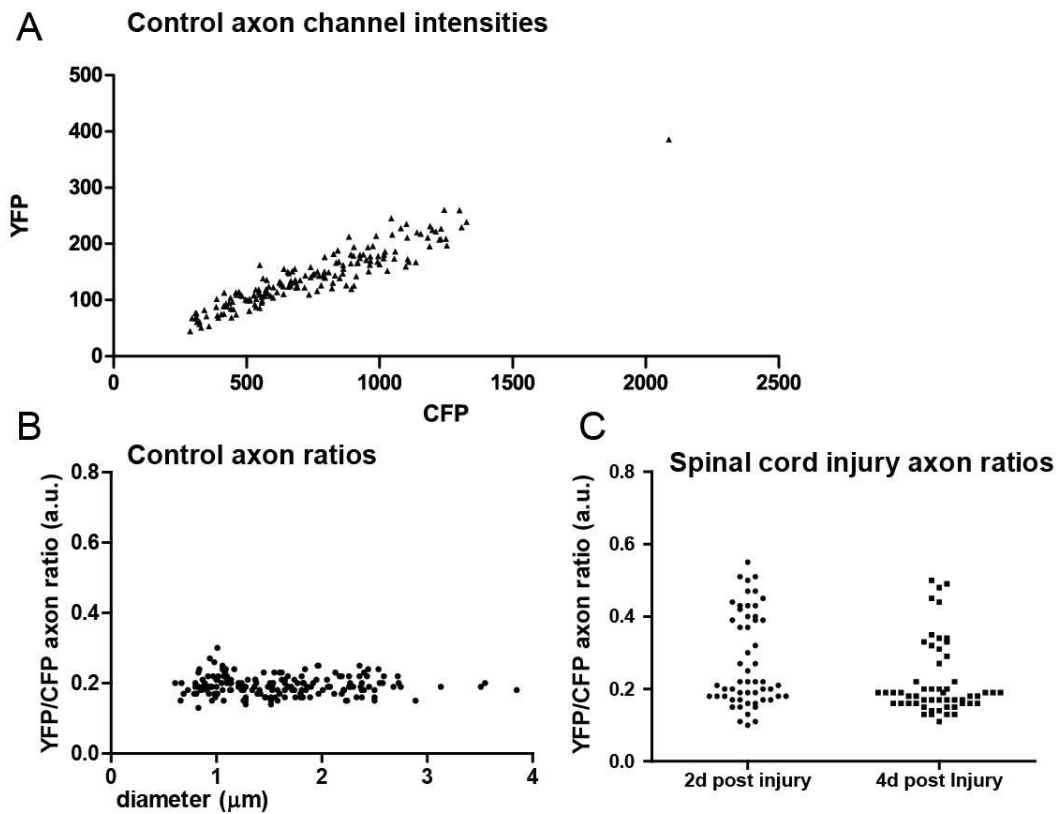


Figure 10 Baseline signal and ratios in healthy animals and positive control after spinal cord cut.

(A) YFP and CFP channel intensity scatter plot of single axons. The values are evenly distributed and signal intensities do not correlate with YFP/CFP ratio (B) Axonal calcium levels, as represented by YFP/CFP ratios are strongly regulated in control animals and show no correlation with axon diameters. (B) In a spinal cord injury paradigm, elevated calcium levels can be detected in a subset of axons 2d and 4d post injury.

### 4.3 Axonal calcium levels in acute EAE

My next step was to look at the lumbar spinal cord of a mouse in the acute phase of EAE. Using our *in vivo* imaging approach I could detect axons that showed increased YFP/CFP ratios and therefore elevated axonal calcium. Figure 11 shows the appearance of an inflamed spinal cord in EAE. Infiltrating immune cells appear in such lesion sites. Such sites can be identified *in vivo* based on the presence of morphologically altered axons in different stages of focal axonal degeneration (Nikić et al., 2011). I quantified the changes in axonal calcium and morphology, using the three different stages that our laboratory has shown to be sequential steps of a partly reversible degeneration process. For a robust readout of the calcium sensor, I

---

defined the control mean +3 SD as the cut-off value for YFP/CFP ratios that indicate elevated axonal calcium. As seen in the spinal cord cut paradigm (see chapter 4.2.2), many axonal fragments tend to show high calcium. Notably, in EAE I could detect that roughly half of the *stage 1* axons (axonal swellings without fragmentation) and 16 % of the “normal” appearing *stage 0* axons have increased  $\text{Ca}^{2+}$  levels. The ratio changes appear to be up to 4-fold and vary in their extent. The calculated ratios (normalized to the control population) were  $1.25 \pm 0.05$  in stage 0,  $1.81 \pm 0.11$  in stage1 and  $2.15 \pm 0.09$  in stage 2 axons (mean  $\pm$  SEM).

I observed the calcium elevations to affect the whole stretch of the axon length that I was able to detect in my imaging approach. These changes are consistent with the idea that  $\text{Ca}^{2+}$  is a mediator of axonal degeneration under neuroinflammatory conditions. To rule out any influence of acidosis or pH in general on the relative fluorescence of the two fluorophores incorporated in the sensor protein, I crossed thy1-CFP23 with thy1-YFP16 animals. The crossing of two lines with almost full labelling patterns would provide a majority of axons that show double labelling with a blue and a yellow fluorescent protein as integrated in the FRET sensor of CerTN. Differential pH effects on these two XFP variants could explain a ratio change, especially as there is evidence for tissue acidosis in the EAE spinal cord (Frieese et al., 2007). However, in our experiments we could not observe any change in axon ratio that would resemble the strong signal we see in axons with a functional FRET-based calcium sensor, as shown in Figure 12. Axon ratios presented with values centering around the control mean (stage 0:  $0.99 \pm 0.02$ , stage 1:  $1.01 \pm 0.05$ , stage 2:  $1.27 \pm 0.13$ , mean  $\pm$  SEM).

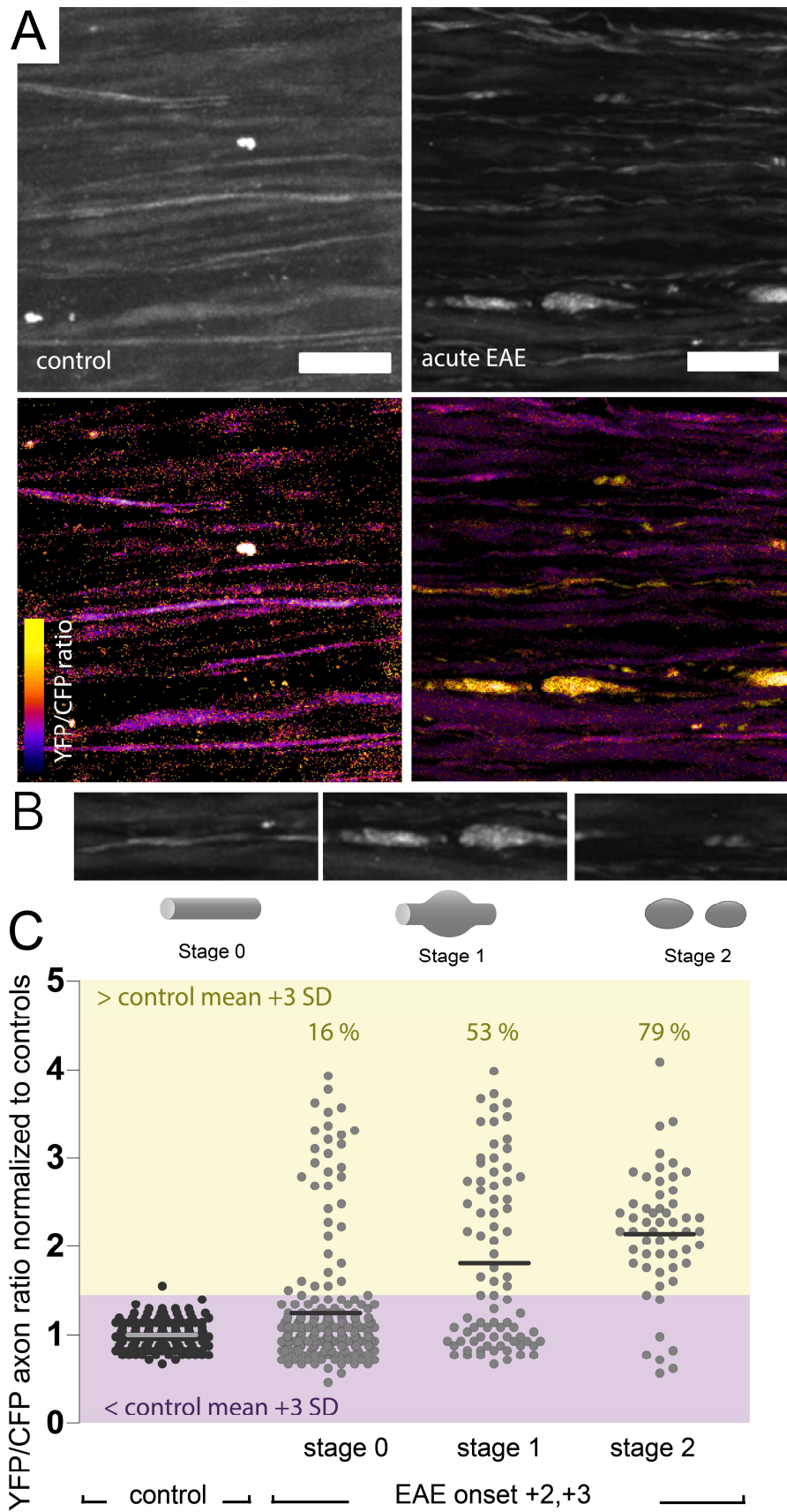


Figure 11 Axonal calcium levels in acute EAE

(A) 2-Photon *in vivo* image of the lumbar spinal cord of a control animal and an animal suffering EAE (onset +2d). Greyscale images show CerTN YFP channel in maximum intensity projection. Ratiometric images depict color-coded calcium levels, ranging from low (blue/violet) to high calcium (yellow), as shown in look-up table scale. Scale bar 20  $\mu\text{m}$ . (B) Stages of focal axonal degeneration taken from images in (A) showing a normal appearing (0), swollen (1) and fragmented (2) axons. (C) Axonal calcium levels in acute EAE lesions, shown by YFP/CFP ratios normalized to control group. Color-coded cut-off marks an increase of +3 SD above the control mean, defined in this study as elevated calcium. Percentages represent the number of axons that show elevated calcium, grouped in the different stages of degeneration. Control: n=3 animals, EAE n=5 animals.

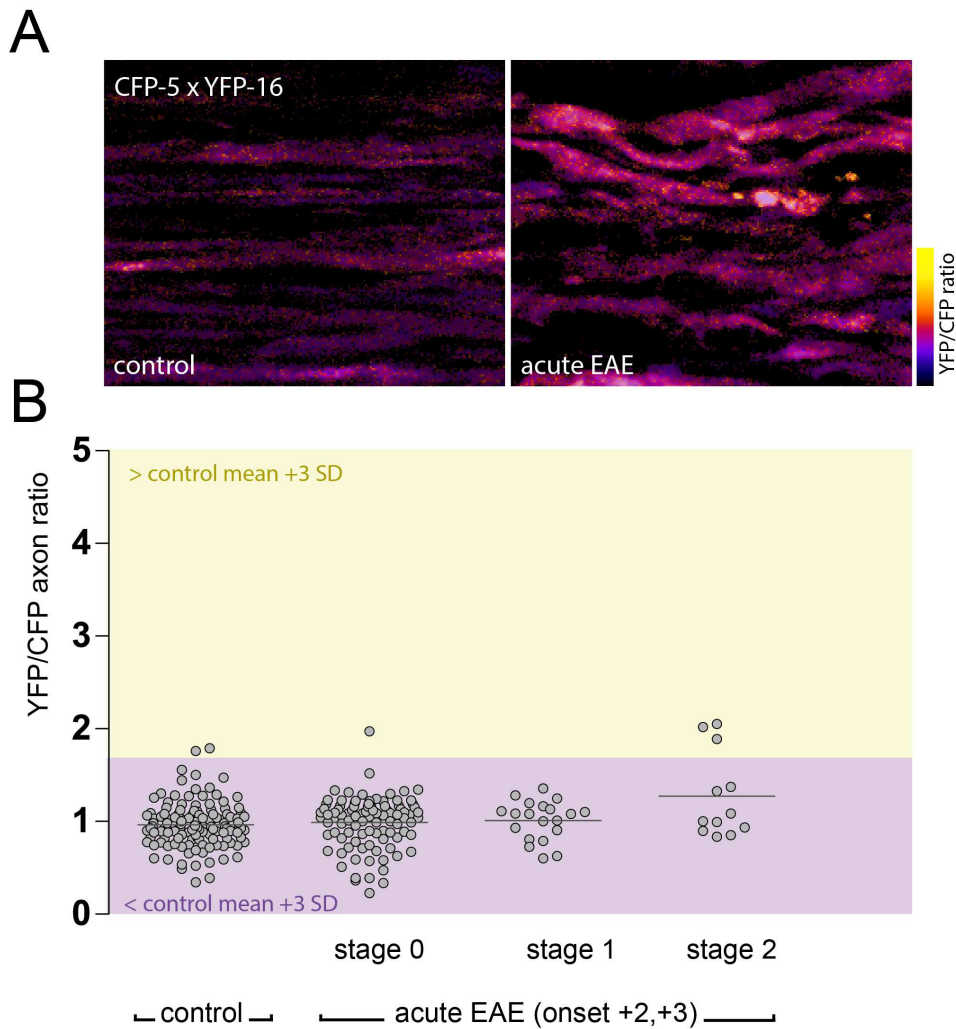


Figure 12 Effects of pH on fluorophores in acute EAE

(A) Representative ratiometric images showing spinal cord axons in CFP23xYFP16 control mice and animals suffering acute EAE. No effect is seen mimicking the measured change in ratio as observed in CerTN mice.

#### 4.4 Axonal calcium levels in EAE remission

To correlate these findings with lesion activity, I imaged animals which presented themselves in the remission phase of EAE (onset+10 d, onset +12 d) as shown in Figure 13. Similar to the acute lesions, I could detect morphological changes of axon populations and elevated intra-axonal calcium. However, the changes were shifted to the later phase of degeneration (stage 2,  $1.81 \pm 0.09$ ) and less of the morphologically intact (stage 0:  $0.92 \pm 0.03$ ) axons affected. Swollen axons (stage 1) showed also a lower mean ratio than in the acute situation ( $1.37 \pm 0.25$ , mean  $\pm$  SEM). This points towards the presentation of a “burnt-out” lesion with less activity.

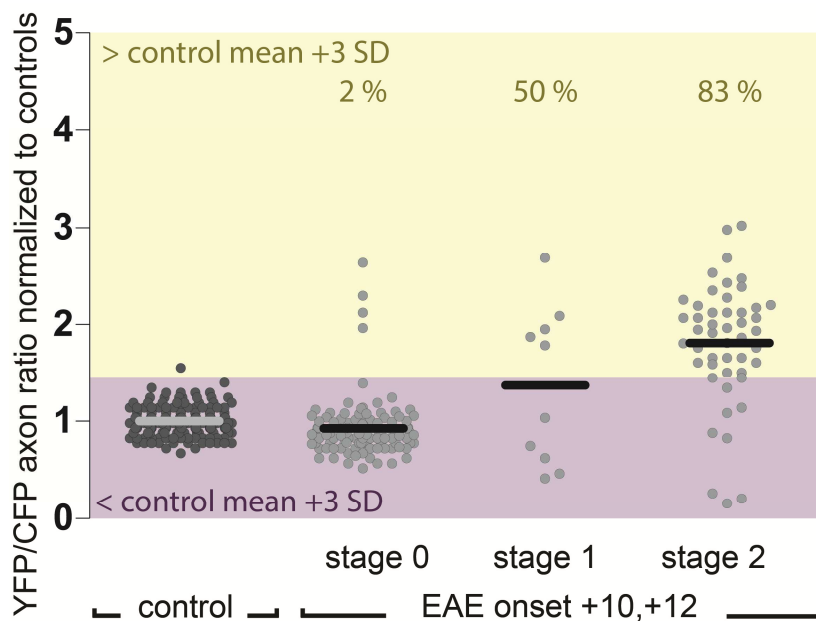


Figure 13 Axonal calcium levels in EAE remission

Axonal calcium levels in remitting EAE lesions (onset +10d, +12d), shown by YFP/CFP ratios normalized to the control group. Percentages represent the number of axons that show elevated calcium per stage of degeneration. Control: n=3 animals, EAE n=3 animals.

#### 4.5 Fate mapping of affected axonal populations over time

Since I discovered that elevated calcium levels appear in intact looking axons and this could be observed more frequently in the setting of acute EAE compared to the remission phase (see Figure 11 and Figure 13), I became interested in the timecourse of calcium influx and the correlated appearance of morphological changes. To follow axonal calcium dynamics *in vivo*, I imaged animals for 3-5 h in 30-45 min intervals. To exclude that changes seen in imaged axons are due to surgery-induced trauma and/or phototoxicity, I imaged control animals over the same timecourse and did not detect any changes in axonal calcium or morphology, as shown in Figure 14.

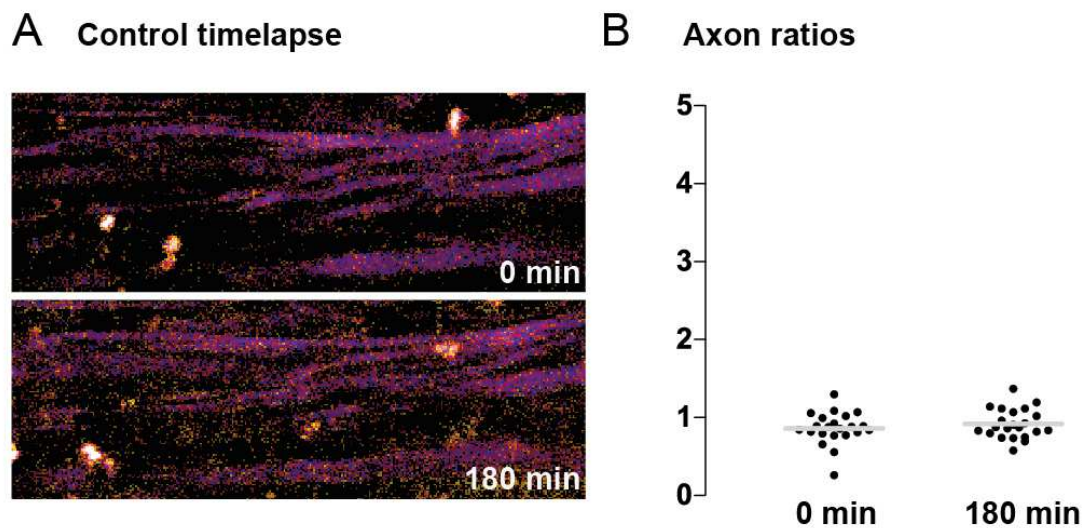


Figure 14 Control timelapse imaging

(A) Ratiometric projection images of representative region in a healthy control animal at t=0 and t=180 min. Minor variation due to breathing artefacts. (B) Quantification of YFP/CFP axon ratios of a cohort of axons at t=0 and t=180 min. Values normalized to t=0.

---

I then classified axonal morphology changes over time into the different stages of FAD. As plotted in Figure 15 (A), I could detect an overall constant rate of fragmenting axons (stage 2, red) between the different timepoints that did not occur in a time-locked manner as one would expect e.g. in trauma-induced degeneration. When specifying which transitions occur among morphological stages and between the states of  $\text{Ca}^{2+}$  high and  $\text{Ca}^{2+}$  low, all types could be detected. To evaluate the frequencies of the observed transitions I followed a cohort of 277 axons over time. I plotted the pooled transition probabilities averaged over time in the diagram shown in Figure 15 (C). As depicted in the transition diagram, the per hour probability for an axon to undergo subsequent degeneration is higher for entities with elevated  $\text{Ca}^{2+}$  than for neighboring axons without an intracellular calcium increase. This applies both to morphologically intact as well as swollen axons. Interestingly, axons can also recover high  $\text{Ca}^{2+}$  and morphological swellings. The chances to do the latter are higher for low intra-axonal  $\text{Ca}^{2+}$ .

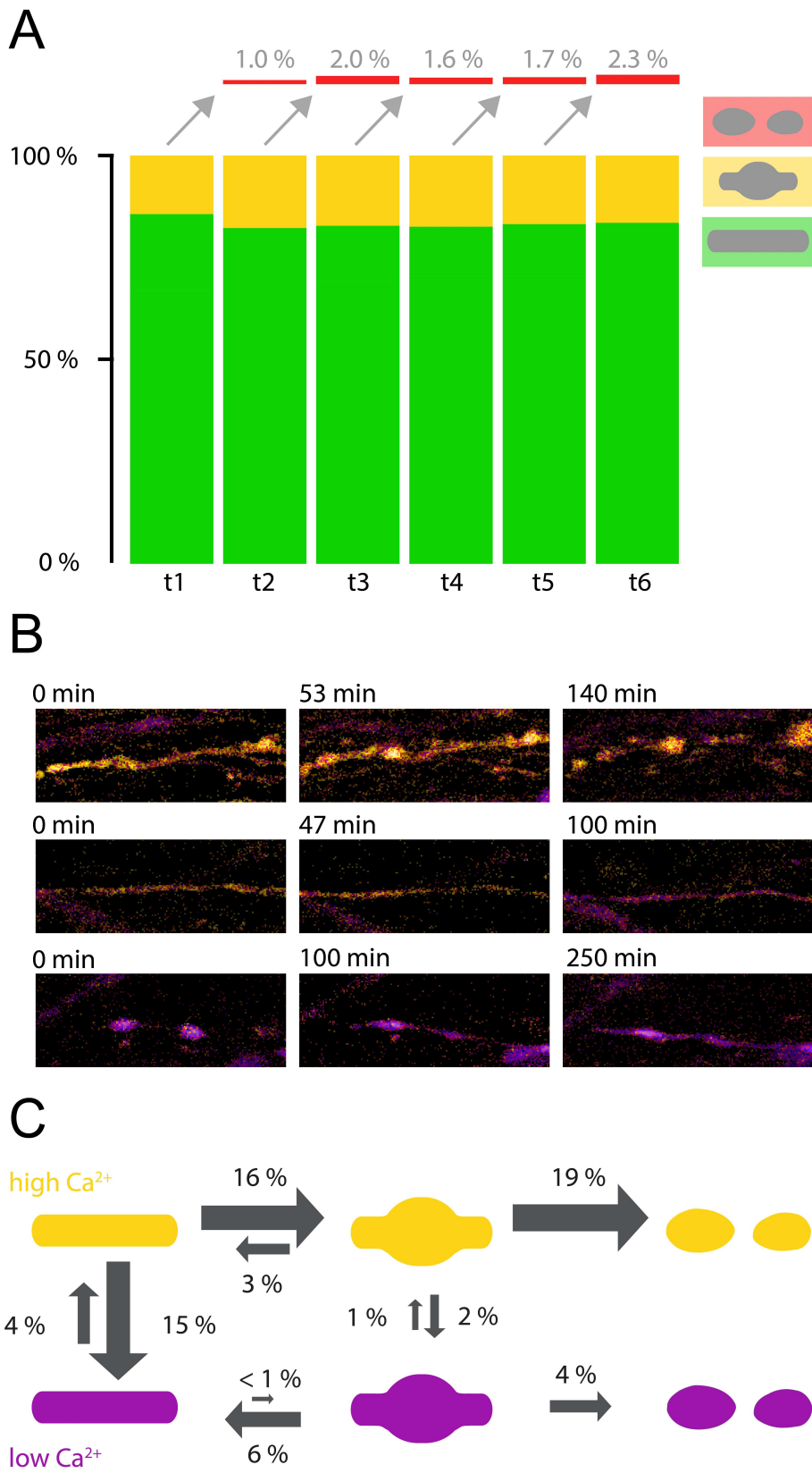


Figure 15 Assessment of axonal cohort over time

---

(A) Distribution of FAD stages 0 (green), 1 (yellow) and 2 (red) in a population of axons followed over the course of 6 timepoints (t1 - t6, intervals 30-45 min). Irreversible stage 2 are presented as drop-out fractions. (B) Pseudocolored ratiometric images of single axons showing axonal morphology and calcium at different timepoints: Axon 1 (top) degenerates to a fragmented stage while showing high calcium throughout all images. Axon 2 (middle) recovers low calcium levels without shape changes. Axon 3 (bottom) shows low calcium levels and recovers from stage 1. (C) Diagram showing probabilities (per hour and axon) of a transition to occur. Symbols reflect FAD stages 0, 1 and 2 as shown in Figure 11. n=277 axons in 8 animals.

#### ***4.6. Additional Figures***

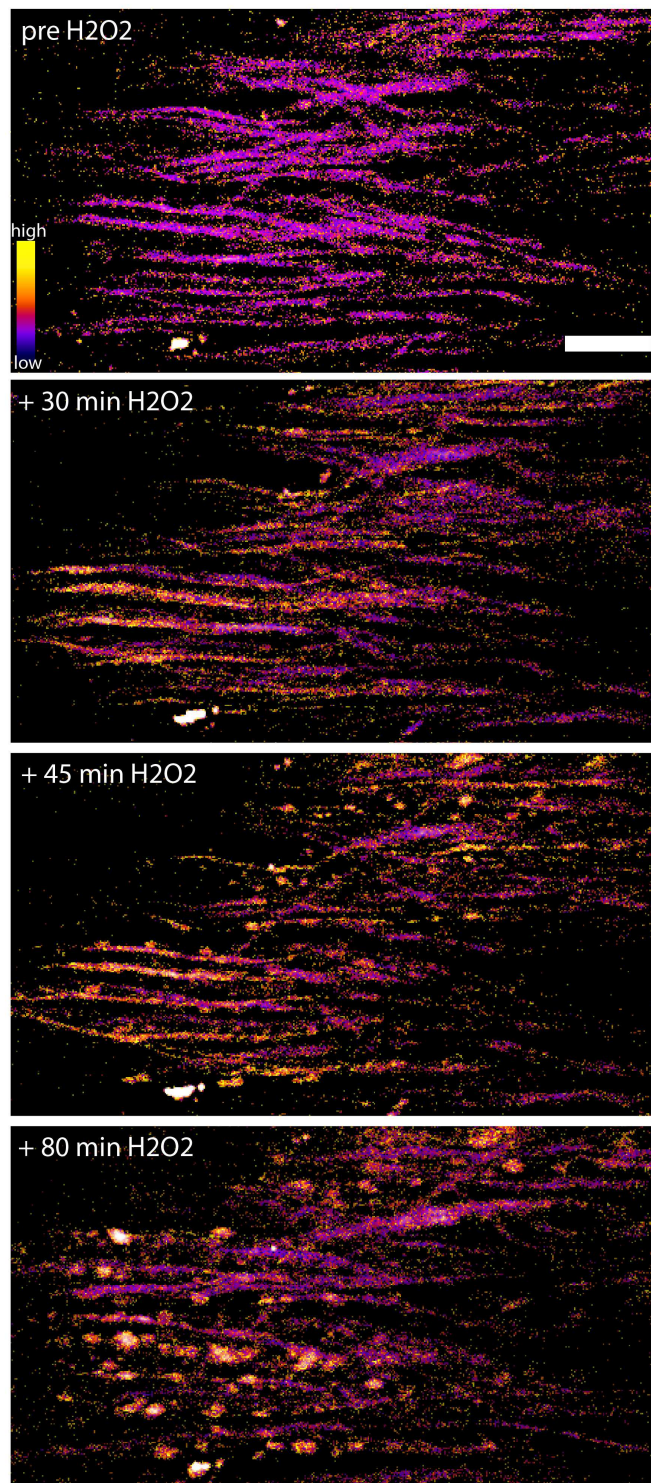


Figure 16 Effects of  $\text{H}_2\text{O}_2$  on healthy spinal cord axons

Ratiometric projection images of axons before and after incubation with 100mM  $\text{H}_2\text{O}_2$  (30, 45 and 80 min. respectively, incubation stopped for imaging periods). A clear rise of  $\text{Ca}^{2+}$  can be detected in a majority of axons with subsequent degeneration. Scale bar: 10  $\mu\text{m}$ .

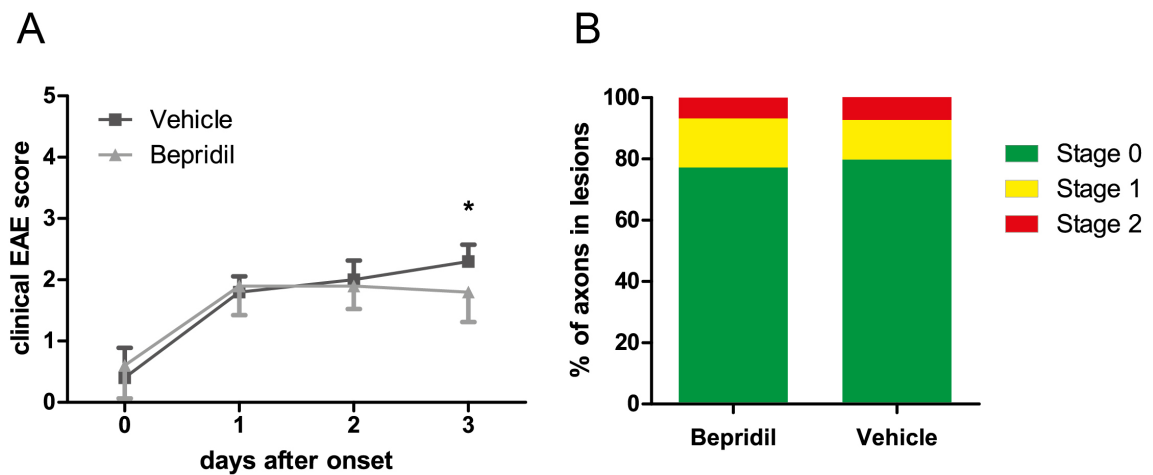


Figure 17 Effects of intrathecal treatment with bepridil in EAE

Animals (thy1-YFP16xMitoP) showing weight loss just before the onset of clinical symptoms were implanted an osmotic mini pump containing 0.4 mM bepridil (n=7) or vehicle (n=6) in aCSF. (A) Clinical scores of treated animals over the acute disease phase. Unpaired t-test (p=0.048) (B) Axon stages in inflammatory lesions were evaluated in fixed tissue sections. Lesions were classified by cellular infiltration (NeuroTrace staining).

## **5. Discussion**

### **5.1 *In vivo* calcium imaging: pitfalls and potentials**

#### **5.1.1 *Detection of calcium signals***

In this study I imaged axonal calcium levels *in vivo* in the murine spinal cord. The signal was collected by two-photon laser scanning microscopy of neurons expressing genetically encoded calcium indicator proteins. I was able to detect an increase in FRET ratios in diseased animals compared to a determined control baseline. The valid interpretation of this signal is of chief concern. For this we need to understand the functional principles and the correct readout of the received signals, as well as possible confounders.

The underlying  $\text{Ca}^{2+}$ -sensing mechanism of the CerTN protein is the FRET principle and the correct readout a change in the YFP/CFP channel ratio (see chapter 1.3.2). To calculate this ratio and optimize the signal strength, I corrected for background and bleedthrough (see chapters 3.3.6, 4.2.1). This led to a very confined normal distribution of axon ratios when measured in healthy control animals, as seen in chapter 4.2.2.

In the original description of the CerTNL15 sensor protein, Heim et al. used cortical and hippocampal slice preparations and *in-vivo* imaging in the murine cortex to assess the sensor protein's behaviour upon stimulation. Slice cultures were incubated in a depolarizing solution (10 mM  $\text{Ca}^{2+}$  and 80 mM  $\text{K}^+$ ) to provoke a rise of FRET ratios. Single patch-clamped cells were stimulated with current injections or iontophoretic glutamate application. The subsequent membrane depolarization, verified by electrophysiology techniques, could be linked to an increase in FRET ratio and therefore calcium influx. *In vivo* measurements on spiny dendrites showed the same effect (Heim et al., 2007).

In my positive control, transected axons in the traumatically injured spinal cord, I could detect FRET ratios that were up to 3-fold higher than the mean of the controls, but also intermediate stages could be seen. In the neuroinflammatory paradigm of EAE, I could detect

---

comparably high ratio changes in a population of the axons, with a majority of them showing morphological changes. Other groups have successfully measured  $\text{Ca}^{2+}$  elevations with a genetically encoded calcium indicator *in vivo* in different scenarios, e.g. in models of Alzheimer disease in the murine cortex (Kuchibhotla et al., 2008) and also in the inflamed brainstem of mice suffering a passive EAE variant (Siffrin et al., 2010).

As the signal is highly probable to arise from calcium fluctuations, there still can be major confounders. First, for the healthy axon population, we confirmed that the ratiometric signal did not correlate with the size of the axon or the signal intensity and thus the expression level of the sensor protein (see Figure 10). Second, in the setting of neuroinflammatory lesions tissue acidosis has been described (Friese et al., 2007), which could disturb the function of the sensor protein. Yellow fluorescent proteins are known to be more affected by acid/base imbalances and will change their fluorescent properties accordingly. To rule out an effect due to differential pH effects on the fluorescent reporter proteins forming the calcium sensor, we expressed both fluorescent proteins at the same time under neuronal promoters, however without any linking  $\text{Ca}^{2+}$  binding unit. This thy1-YFP16xCFP-23 transgenic line did not show any significant ratio changes in the setting of EAE (see Figure 12). Third, oxidative tissue damage has been described as a pronounced feature in EAE and MS (Fischer et al., 2012; Lassmann et al., 2012; Nikić et al., 2011). A direct effect of ROS/RNS on the sensor protein could be a potential confounder of  $\text{Ca}^{2+}$  measurements. In our experiments, the application of ROS/RNS on the spinal cord yielded a strong FRET increase (see Figure 16). At the same time, the parallel application of ROS/RNS and bepridil lead to diminished or almost no increase of axon FRET ratios (experiment series by C. Mahler, not shown). It is highly unlikely that a direct redox-mediated effect on the sensor protein could be diminished by a specific channel blocker (in this case bepridil). Therefore, we assumed no direct effect of ROS/RNS on our  $\text{Ca}^{2+}$  sensing proteins.

### 5.1.2 Interpretation of the measured signals

As we are confident to have measured actual intra-axonal calcium signals in our paradigm, a key interest appears to be the interpretation of the measurements. A first important question is, what actual amount of  $\text{Ca}^{2+}$  correlates with the FRET ratios measured in the experiments. The empirical measure of the indicator affinity gives a sensible approximation to this problem: As calcium indicators differ largely in their affinities for calcium, the dissociation constant ( $K_d$ ) is an important variable that reflects the likelihood that a complex of indicator and calcium ion will separate. In fact, it has a molar unit that equals the concentration of  $\text{Ca}^{2+}$  where half of the sensor proteins are  $\text{Ca}^{2+}$  bound (Grienberger and Konnerth, 2012). The  $K_d$  for CerTN-L15, the sensor protein mainly used in this study, is 1.2  $\mu\text{M}$  (Heim et al., 2007). The other sensor that I tested, TN-XXL, has a described value of 800 nM (Mank et al., 2008). Both calcium indicators showed strong (up to 3-fold) FRET changes in the experimental paradigms of this study. Based on the dose response characteristics of the sensor this would correspond to calcium concentrations of  $>10^{-6}$  M.

A precise calibration of the sensor readout with different calcium concentration e.g. in cell culture would not directly correlate with the actual *in vivo* data, since the  $K_d$  value can be changed by many parameters. These include pH, presence of  $\text{Mg}^{2+}$  and temperature – most of which are potentially changed in the setting of EAE (Grienberger and Konnerth, 2012). Therefore, we decided on a binary system to distinguish axons with largely elevated  $\text{Ca}^{2+}$  from others with baseline  $\text{Ca}^{2+}$  concentrations. Our criterium for “ $\text{Ca}^{2+}$  high” axons was a FRET ratio greater than a threshold of 3 SD over the mean control values. All values below this threshold we considered “ $\text{Ca}^{2+}$  low”. This approach likely gives a robust readout of actual and large-scale calcium increases compared to the control state in healthy animals. However, it might overlook many intermediate stages that could potentially present, as there was as well a variety amongst the group of “ $\text{Ca}^{2+}$  high” axons in our experiments. To get a better idea of the exact  $\Delta\text{Ca}^{2+}$  measured, one would have to correlate different sensor readouts, including also synthetic calcium dyes like Oregon-Green-BAPTA-1 (OGB-1) and relate it to measured response curves in literature (Hendel et al., 2008).

One major confounder is the intrinsic buffer capacity that all sensors exhibit. There is a constant equilibrium of calcium ions that are either free or bound to calcium buffers. GECIs expressed in the measured cell add their buffering capacity to the total capacity of the endogenous buffers that include parvalbumin, calbindin-D28k and calretinin (Baimbridge et al., 1992). The intracellular calcium dynamics are therefore strongly dependent on the amount of indicator in the cell. However, this is more a feature relevant when looking at rise and decay times, giving low-affinity indicators (such as CerTN-L15 in this study) some better signal kinetics because of their smaller buffer capacity (Neher and Augustine, 1992). In our study, we could not detect a higher probability for axons with a strong expression pattern (and therefore higher signal intensity) to show different FRET ratio readouts (see Figure 10A).

In the work of Dierenberger et al., a broad assessment of different organs in mice expressing the sensor protein TN-XXL was done to check for any effects of the  $\text{Ca}^{2+}$  indicator on the physiology of the host organism. The study includes microarray expression profiling, anatomical analysis, behavioural testing and recording of basic physiological parameters. According to the authors, the vast majority of parameters tested did not differ between TN-XXL transgenic mice and their littermates that were not transgenic (Dierenberger et al., 2012).

### **5.1.3 Potential improvements in signal detection**

In this work I showed calcium dynamics in a large population of degenerating axons. These signals appeared largely stable over space and time and only in very rare occasions, I was able to detect gradients of increased calcium that spread over the observed length of an axon (not shown). Whether or not this phenomenon was an imaging artefact still has to be ruled out. The spatial resolution in xy and z allowed for single axon detection in the dense population. However, it was not precise enough to resolve subcellular structures of the axon like nodes of Ranvier and check for spatially confined  $\text{Ca}^{2+}$  changes that might occur. These might also include interactions with subcellular structures like mitochondria or the ER. Diffusion of sensor protein within the axon might also complicate measurement of localized  $\text{Ca}^{2+}$  transients.

---

I frequently measured changes of axonal  $\text{Ca}^{2+}$  over time, as presented in chapter 4.5. However, these occurred over the time course of 2-4 hours, sampled in 20-40 min intervals. With the imaging equipment used, a much higher sampling speed would in principle be possible. The trade-off is a much smaller sampling area and, as a chief concern, potential phototoxicity. We therefore focused on the robust and slow  $\text{Ca}^{2+}$  dynamics of large populations.

Calcium signals in neurons can in principal undergo rapid changes. In models of degenerative diseases like Alzheimer, neuronal hyperexcitability has been detected by imaging calcium transients, and this altered activity has been attributed to morphological alterations in dendrites (Busche et al., 2008; Palop et al., 2007; Sišková et al., 2014). The hyperactivity patterns occurred in a fast-paced manner of up to 0.25 Hz. Since the calcium transients in principal correlate with the action potential firing of neurons (Kerr et al., 2005; Wallace et al., 2008), the sampling speed and the rise and decay time of the sensor must be able to reflect the measured dynamics. The low imaging frequency and the low affinity of our sensor did likely not reveal fast-paced  $\text{Ca}^{2+}$  alterations that take place in healthy and inert appearing axons, or even fluctuations in axons we addressed as “ $\text{Ca}^{2+}$  high”. A very different approach would implement low power but high frequency sampling (Chen et al., 2012) and possibly two different calcium sensors that work in a low-affinity and high-affinity range, respectively. Since the spectral variety of sensors has improved in the last few years (Walker et al., 2013), measuring a different  $\text{Ca}^{2+}$  signal in two spectral bands would in principle be possible. Our collaborators that provided the  $\text{Ca}^{2+}$  sensor transgenic mice have in the meantime bioengineered their GECIs and developed a variant with higher fluorescent change, improved signal kinetics and created a potpourri of different affinity sensors (Thestrup et al., 2014). Using several variants of the “Twitch” family of sensors could potentially give a deeper insight to the  $\text{Ca}^{2+}$  dynamics seen in the neuroinflammatory paradigm.

## **5.2 Calcium predicts the fate of degenerating axons in inflammatory lesions**

In a related *in vivo* study in a model of contusion spinal cord injury, we showed the role of  $\text{Ca}^{2+}$  dynamics for the fate of axons to degenerate. At the first observation time point, few minutes after injury, over half of the axons showed elevated intra-axonal calcium levels. Interestingly, over time, elevated  $\text{Ca}^{2+}$  levels recovered to normal in some axons, while they persisted in others. Axons with persisting  $\text{Ca}^{2+}$  elevations were more prone to degenerate (Williams et al., 2014). We undertook a similar approach in the setting of neuroinflammation, as shown in this work.

### **5.2.1 Calcium in focal axonal degeneration**

In this work I assessed axonal  $\text{Ca}^{2+}$  levels in the setting of acute lesions in the lumbar spinal cord of mice suffering EAE. One to three days after clinical disease onset, I could detect altered  $\text{Ca}^{2+}$  concentrations in a subset of the observed axon population. I was also able to reproduce the presence of focal axonal degeneration (FAD) stages as described by Nikic et al. The distribution of the observed axon population in the FAD stages (0: morphologically intact, 1: swollen and 2: fragmented axons) appeared comparable to the original study (Nikić et al., 2011). In a putative lesion, I attributed each axon a FAD stage and measured its  $\text{Ca}^{2+}$  level. A majority of almost 80 % of fragmented axons and approximately half of the swollen axons presented with high  $\text{Ca}^{2+}$ . Among the normal appearing axons I could show that roughly 20% exhibit increased  $\text{Ca}^{2+}$  levels.

The concept of *focal* axonal degeneration implies that it is a process that occurs at one or more discrete sites along the axon, synchronously and results in spreading fragmentation. Therefore, two major points are of interest when looking at axonal  $\text{Ca}^{2+}$  in EAE. Firstly, where in relation to inflammatory infiltration can one detect elevated  $\text{Ca}^{2+}$ . Secondly, how is the  $\text{Ca}^{2+}$  distributed within the axon. To address this, we stained for cell nuclei *in vivo* to get an imaging correlate of the infiltrating immune cells and therefore label a putative lesion site. Well in line with prior studies, dense patches of infiltrating cells appear in the lumbar spinal

---

cord of EAE mice (Nikić et al., 2011; et al., 2013). Advanced stages of FAD and axons with elevated  $\text{Ca}^{2+}$  appear in these lesions. The stretch of an axon that could be analysed varied considerably, due to a dense labelling pattern that limits identification of an axon among its neighbours. In some instances I was able to track an axon over a length of  $\pm 1$  mm. Nearly all detected  $\text{Ca}^{2+}$  elevations expanded over the entire stretch of axon observed (not shown). Thus,  $\text{Ca}^{2+}$  elevations in EAE most likely correlate with inflammatory foci and affect a long stretch of an axon. However, it remains open whether an axon will still exhibit elevated  $\text{Ca}^{2+}$  in a more remote segment of the spinal cord cranial or caudal to the lesion site, and whether a gradient appears in relation to lesion sites. To address this question, a transgenic strain with a very sparse GECI labelling pattern would have to be studied, similar to the thy1-GFP-S mouse line (Feng et al., 2000).

### ***5.2.2 Assessing the predictive value of increased calcium***

In our experiments, the distribution of FAD stages appeared shifted towards fragmented axons (stage 2) in EAE remission (10-12 days after clinical onset) compared to the acute phase. At the same time, there were only few morphologically intact axons (stage 0) that exhibited elevated  $\text{Ca}^{2+}$ . This implies that the population of stage 0/high  $\text{Ca}^{2+}$  axons are a feature of an acute lesion and either recover their  $\text{Ca}^{2+}$  towards the remission phase or degenerate and eventually fragment.

The dynamic analysis of large axon populations (see chapter 4.5) allowed us to get an unprecedented view into the patterns and timecourse of  $\text{Ca}^{2+}$  and morphological changes in EAE lesions. As reflected in the diagram (Figure 15), we saw a large variety of transitions of the observed axons. Therefore we calculated the probability of an axon to undergo a certain change (per hour of observation) in order to get a clue about which of the changes happen more frequently than others. I drew three main conclusions on the basis of this diagram: First, both axonal swelling and fragmentation are more likely to happen with elevated intra-axonal  $\text{Ca}^{2+}$ . Second, recovery of swellings appears more frequently in low- $\text{Ca}^{2+}$  axons. Third, intact looking axons can change between states of increased and normal  $\text{Ca}^{2+}$ . Taken together, this

implicates a predictive value of elevated  $\text{Ca}^{2+}$  levels in axons, indicating a high risk of subsequent degeneration when present. Nikic et al. assessed the transition probabilities in a comparable approach. The rates appeared to be in a similar range, with some variability. This is likely to be due to the different axon population imaged in the used transgenic lines and the pooling of the acute phase (onset+1 to onset+3) in this study.

### **5.3 Sources and mechanisms of calcium overload**

Several mechanisms have been proposed to be involved in inflammatory axon degeneration, among these mitochondrial dysfunction and energy failure, as well as exposition to reactive oxygen and nitrogen species (ROS/RNS). These players could potentially all be linked to imbalances in intra-axonal  $\text{Ca}^{2+}$  levels. Mitochondrial dysfunction and the resulting energy depletion, together with the inflammatory demyelination, are presumed to lead to activation, dysfunction and altered distribution of ion channels (Friese et al., 2014). ROS/RNS could have both indirect effects on ion homeostasis by either acting on mitochondrial energy production or else by directly interfering with ion channel function or membrane integrity. Below, I will discuss these potential mediators of inflammatory axon degeneration and how they might be mechanistically linked to calcium dysregulation.

#### **5.3.1 Correlation with other mediators of inflammatory axon degeneration**

##### **5.3.1.1 Mitochondrial damage**

Mitochondrial dysfunction and damage has been proposed to be a major cause of inflammatory axon degeneration (Dutta et al., 2006; Trapp and Stys, 2009). Damage to mitochondria can be detected both in chronically demyelinated axons of inactive lesions and in active inflammatory lesions, where infiltrating macrophages and activated microglia are present. It is possible that there may be distinct mechanisms of mitochondrial damage that can induce axon degeneration depending on the stage of the disease (Witte et al., 2014). The obvious, presumed effects of mitochondrial damage include energy failure and ion channel dysfunction, e.g. leading to overload of the

cytoplasm with  $\text{Ca}^{2+}$ . A release of mitochondrial  $\text{Ca}^{2+}$  into the cytosolic compartment could also be possible.

In the setting of *acute* inflammatory lesions in EAE, our group has shown that mitochondrial alterations are an early ultrastructural sign of focal axonal degeneration. When quantifying the mitochondrial shape through a ratio of mitochondrial length and width, about 30 % of normal appearing axons (stage 0) already show signs of mitochondrial swelling and shortening. Interestingly, the demyelination of these axons was not a necessary prerequisite for these mitochondrial alterations. In addition, when the mitochondrial membrane potential was measured, it showed that concomitant functional changes occurred with altered shape. In brain biopsies from multiple sclerosis patients, altered mitochondrial shapes could be also seen, appearing both in morphologically intact and in swollen axons (Nikić et al., 2011). Moreover, our lab has detected widespread transport deficits in EAE, which even precede structural alterations of axons, cargos, or microtubules (Sorbara et al., 2014). Taken together, this data proposes that there could both be problems with function and distribution of mitochondria.

*Chronic* lesions contain a large population of axons that have survived the acute inflammatory attack but stay demyelinated. However, a certain percentage of these axons will eventually degenerate. Mahad and colleagues showed deficiency of complex IV of the respiratory chain in injured axons in MS. These changes were accompanied by accumulations of APP and non-phosphorylated neurofilament-SMI-32, which are markers of transport failure and degeneration of axons (Mahad et al., 2009). Interestingly, in some axons in chronic MS lesions that did not show accumulations of these markers there was also evidence of compensatory upregulation of complex II and complex IV activities. Another study showed an increase of mitochondrial size and respiratory chain enzyme activity in demyelinated but uninjured axons (Witte et al., 2009).

This impairment of mitochondrial function could contribute to axonal degeneration as proposed by the “virtual-hypoxia” hypothesis: One important function of axonal

mitochondria is the synthesis of ATP by oxidative phosphorylation. Chronic challenge with ROS/RNS can lead to an impairment of energy production by accumulating mutations in the mitochondrial DNA (Lin and Beal, 2006). However, axons have a large energy demand and need the majority of their available ATP to maintain ionic equilibrium during information processing (Howarth et al., 2012). At the same time, evidence speaks for an even increased energy demand in demyelinated lesions: Lack of myelin in otherwise intact axons changes ion channel distribution, in particular sodium channels (Craner et al., 2004a), leading to increased energy consumption to keep up conductivity of the affected axon. Taken together, the imbalance of chronic failure in ATP production, increased exposition to ROS/RNS and higher energy demand would induce a state of “virtual hypoxia” in demyelinated CNS lesions. The occurrence of tissue acidosis and the induction of hypoxia-inducible factor-1 $\alpha$  (HIF-1 $\alpha$ ) shown in neuroinflammatory lesions are consistent with such a process (Friese et al., 2014; Trapp and Stys, 2009). This is highly relevant for this study, since these mechanisms could lead to an overload of the axon with Na<sup>+</sup> and Ca<sup>2+</sup> through various pathways that will be discussed in chapter 5.3.2.

### **5.3.1.2 Reactive oxygen and nitrogen species**

The changes in mitochondrial transport, shape and function in intact, myelinated axons make it likely that soluble factors are inducing these alterations. Reactive oxygen and nitrogen species have been widely suggested to be involved in MS pathogenesis. *In vitro* data suggests ROS/RNS as strong candidates for inflammatory axon degeneration (Higgins et al., 2010; Witte et al., 2010). In the work of Nikic et al., *in vivo* exposure of the spinal cord of healthy animals to ROS/RNS induced degenerative changes that were strikingly similar to those seen in focal axonal degeneration. I was able to reproduce this in our Ca<sup>2+</sup> imaging paradigm. Interestingly, I could detect an increase in axonal Ca<sup>2+</sup> in a majority of axons shortly after application of H<sub>2</sub>O<sub>2</sub> to the spinal cord. The Ca<sup>2+</sup> high axons were more prone to degenerate in a fashion similar to FAD (see Figure 16). A similar effect could be evoked by the addition of the NO donor spermine NONOate to a healthy spinal cord (experiments performed by Christoph Mahler, data not shown).

Both mitochondrial changes and intra-axonal  $\text{Ca}^{2+}$  elevation induced by ROS/RNS-application were thus similar to the axonal changes observed by our group in EAE. Furthermore, *in vivo* measurements in EAE have shown increased levels of  $\text{H}_2\text{O}_2$  in spinal cords. When using ROS/RNS scavengers for treatment in the acute phase of the disease, the likelihood of axons undergoing FAD could be influenced by shifting them towards recovery (Nikić et al., 2011). This is well in line with the findings in MS, where strong evidence points to increased ROS/RNS production in inflamed areas (Haider et al., 2011; Smith and Lassmann, 2002).

To better understand the effects of reactive species, it is worthwhile to take a closer look on the different molecules that are subsumed in these groups, their reactive potential and their possible sources. Therefore I will now discuss first the family of ROS, and afterwards RNS.

Various forms of ROS exist: The most frequent types are superoxide ( $\text{O}_2^-$ ) and its derivatives hydroxyl radical ( $\text{OH}\cdot$ ) as well as hydrogen peroxide ( $\text{H}_2\text{O}_2$ ). They vary in stability and their interactions with iron or copper in cells (Haider et al., 2011; van Horssen et al., 2011). Mononuclear phagocytes in MS lesions are able to produce ROS through enzymes including myeloperoxidase, xanthine and NADPH oxidases (NOX) (Fischer et al., 2012). ROS is capable of inducing damage to biological structures such as polyunsaturated fatty acids (PUFA) found in membrane lipids, functional proteins, and DNA/RNA. As the CNS exhibits high oxygen turnover and is rich in PUFA, it is particularly vulnerable to lipid peroxidation. In addition, oxidative damage to cellular membrane lipids generates 4-hydroxy-2-nonenal (4-HNE). This reactive aldehyde also appears toxic to CNS cells (van Horssen et al., 2011).

The effects of RNS, specifically NO, can be manifold (Smith and Lassmann, 2002). *In vitro* studies suggest that high levels of NO can lead to the induction of conduction block and therefore axonal injury. Conduction appears to be especially blocked in demyelinated and early remyelinated axons that are exposed to NO (Redford et al., 1997; Smith et al., 2001).

Additionally, NO affects the components of the mitochondrial respiratory chain (Gonsette, 2008). When NO reacts with superoxide, it produces an especially potent toxic metabolite: peroxynitrate. Its strong oxidising and nitration activity affects proteins, lipids, DNA and carbohydrates. Peroxynitrite reacts also with tyrosine residues, resulting in nitrotyrosine (NT). The presence of the latter in MS lesions could be shown by immunohistochemistry (Gonsette, 2008; Liu et al., 2001; Oleszak et al., 1998). Substantial levels of one major known producer of NO, iNOS, could be detected in MS lesions and co-localized with macrophage/microglia markers (Hill et al., 2004).

### **5.3.2 Mediators of calcium influx**

Intracellularly,  $\text{Ca}^{2+}$  is a tightly regulated ion. The concentration gradient across the plasma membrane spans from  $10^{-3}$  M  $\text{Ca}^{2+}$  outside to  $10^{-7}$  M  $\text{Ca}^{2+}$  inside the cell. Endoplasmic or axoplasmic reticulum and mitochondria are known to be important intracellular reservoirs of  $\text{Ca}^{2+}$  that can release or buffer the ion and even cycle it between them, for example during apoptosis. There are a multitude of channels and transporters that carefully regulate both the in- and efflux of  $\text{Ca}^{2+}$  through the plasma membrane and the organelles, as shown in Figure 18. Pathological activation and/or deactivation of these mechanisms leads to aberrant  $\text{Ca}^{2+}$  levels within the axon, however, factors released by infiltrating immune cells might also be able to directly compromise axonal membrane integrity and lead to direct influx of  $\text{Ca}^{2+}$  from the extracellular space.

In this study, I could show that  $\text{Ca}^{2+}$  levels are increased in a subset of degenerating axons in the spinal cord of animals during EAE. In addition, I could show that such increased  $\text{Ca}^{2+}$  levels can rapidly be induced by the application of either ROS or RNS, leading to subsequent degeneration. This suggests that the model of ROS/RNS mediated axonal degeneration is a valuable paradigm to assess the effect of these mediators on  $\text{Ca}^{2+}$  influx. There are at least three possible mechanisms how ROS/RNS could induce such a  $\text{Ca}^{2+}$  influx: (i) a direct attack on the axonal membrane, (ii) the direct activation/deactivation of  $\text{Ca}^{2+}$  conducting channels and transporters (iii) an indirect effect through the activation of

the “virtual hypoxia” pathway that ultimately results in  $\text{Ca}^{2+}$  overload. I will discuss the three mechanisms and how they could be addressed experimentally in the following paragraphs.

### **5.3.2.1 Membrane disruption**

In chapter 5.3.1.2 the different species that are subsumed under the term ROS/RNS were introduced. Metabolites like peroxynitrate are aggressive enough to affect all kinds of biological matter, including membrane lipids. Also, the specific tendency of ROS to attack poly-unsaturated fatty acids (PUFA) points towards a potential effect on the axolemma through lipid peroxidation. This mechanism has drawn attention in MS, however mainly concerning oligodendrocyte pathology (Juurlink et al., 1998). The formation of membrane disruptions stable enough to allow for large-scale  $\text{Ca}^{2+}$  influx in axons has been shown *in vivo* by our group in a model of spinal cord contusion (I contributed to this study as a collaborator). In these experiments, a strong  $\text{Ca}^{2+}$  increase after contusion could be suppressed by chelating extracellular  $\text{Ca}^{2+}$  with EGTA. To check for pore formation, fluorescently conjugated macromolecules (0.8 kD cadaverine or 10 kD dextran) were loaded into the subdural space before contusion. These molecules remained excluded from axons in the healthy spinal cord but got taken up after contusion by a large number of axons. Around 75% of the  $\text{Ca}^{2+}$  elevated axons appeared to have taken up the dye when loaded 15 minutes after contusion, suggesting the existence of axonal pores that permit the entry of  $\text{Ca}^{2+}$  and even the comparatively much larger dye molecules, and that persist at least for some time after the initial injury. The fate of the axons was positively influenced when the pores spontaneously resealed during the observed period (Williams et al., 2014). Although spinal cord contusion is a different model with a mechanical impact preceding pore formation, the existence of membrane pores could also be a plausible explanation for  $\text{Ca}^{2+}$  entry into axons passing through EAE lesions. One putative mechanism for the formation of pores in the axolemma is lipid peroxidation, nitration or related effects by ROS/RNS.

### 5.3.2.2 Direct effects on $\text{Ca}^{2+}$ channels

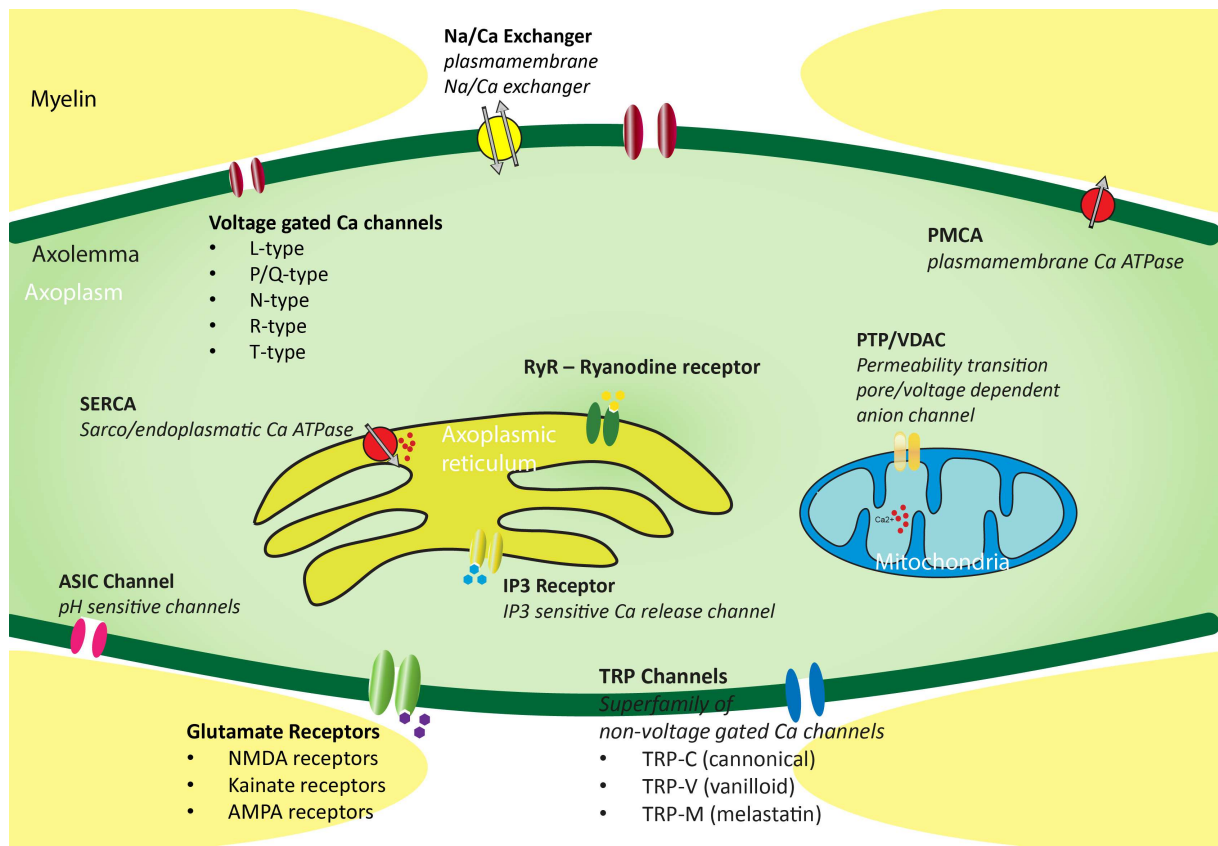


Figure 18  $\text{Ca}^{2+}$  conducting structures of the axonal and organelle membranes

A variety of channels and transporters have been described to be existent in an axon and its organelles. A majority of them could potentially react to ROS/RNS exposition or energy failure.

ROS/RNS could also act directly on  $\text{Ca}^{2+}$  conducting channels and transporters.  $\text{Ca}^{2+}$  flux through both the outer membrane and the release from intracellular stores is tightly regulated in cells. It has become increasingly clear that many  $\text{Ca}^{2+}$  channels are modulated by ROS/RNS, which in fact perform a broad range of physiological, regulatory functions in cells. Among the channels that have been described to be influenced by redox changes are the ryanodine receptor,  $\text{IP}_3$  receptor,  $\text{Ca}^{2+}$  ATPases in the sarcoplasmic reticulum (SERCA) or plasma membrane (PMCA and NCX), voltage gated calcium channels (VGCC), members of the TRP family, glutamate receptors as well as the permeability transition pore (PTP) in mitochondria (Waring, 2005). In a series of experiments done by my colleague Christoph Mahler, we aimed to pharmacologically block a selection of the

channels mentioned above *in vivo*, in the experimental paradigms of ROS or RNS-mediated axon damage in the spinal cord. We observed the strongest effect both on calcium rise and subsequent degeneration when blocking the reverse action of the sodium-calcium exchanger (NCX) of the plasma membrane with Bepridil and KB-R7943. The effect was more pronounced in the setting of NO mediated degeneration, suggesting a direct effect of NO on the NCX (C. Mahler, personal communication). However, the described effects could also be attributed to the virtual hypoxia hypothesis, as explained in the next paragraph.

### **5.3.2.3 Energy failure and virtual hypoxia pathway**

The third possible mechanism of redox-mediated  $\text{Ca}^{2+}$  influx is an indirect path: The reduction or halt of oxidative phosphorylation in mitochondria due to elevated levels of endogenous and/or exogenous ROS/RNS can lead to the lack of ATP. The resulting failure of energy-dependent pumps like the  $\text{Na}^+/\text{K}^+$  ATPase leads to accumulation of intra-axonal  $\text{Na}^+$ . To extrude  $\text{Na}^+$  from the cytosol, the NCX would start operating in reverse mode and ultimately increase the concentration of cytosolic  $\text{Ca}^{2+}$ . Interfering with these mechanisms as the final pathway of “virtual hypoxia”, in particular sodium blockade with phenytoin or flecainide, have partly been shown to alleviate symptoms in EAE and EAN (Bechtold et al., 2004; 2005; Black et al., 2006; Morsali et al., 2013). Another possibility would be the specific blockage of the reversely operating NCX, as described in the last paragraph. The strong protective effect we saw in our experiments when inhibiting the reversely operating NCX in redox mediated axon damage with bepridil could therefore be due to this indirect pathway and not, as discussed above, through a direct activation by ROS/RNS. The idea of linked  $\text{Ca}^{2+}$  and  $\text{Na}^+$  overload in NO mediated degeneration is supported by *in vivo* electrophysiological experiments showing conduction block after application of NO on spinal root axons. In an *in vitro* preparation, these researchers were also able to diminish degeneration of these axons by the application of lidocaine, flecainide or bepridil (Kapoor et al., 2003). As bepridil is also an inhibitor of L-type voltage gated calcium channels, the protective effect is even stronger, since VGCC are

capable of amplifying  $\text{Ca}^{2+}$  influx by opening in response to depolarization. However, in the more complex case of EAE the effect of targeting this pathway is less clear. Interestingly, there is evidence that  $\alpha 1\text{B}$ , the pore-forming subunit of the N-type calcium channel, is accumulated within axons and axonal spheroids within demyelinating lesions in MS (Kornek et al., 2001). As N-type VGCC are presumed to have their site of action at nerve terminals rather than at the internodal axolemma, this would point towards an effect of pathologically altered expression patterns of VGCCs in neuroinflammatory lesions that could contribute to increased intra-axonal  $\text{Ca}^{2+}$ .

To test the therapeutic effect of bepridil in EAE in a preliminary experiment, we implanted osmotic mini pumps containing a solution of bepridil or vehicle dissolved in aCSF in thy1-YFP16xMitoP mice showing weight loss just before the onset of clinical symptoms. Both groups received a continuous intrathecal delivery of solution over the timecourse of 2 days. In a blinded, fixed tissue analysis I looked at inflammatory foci (revealed by staining for infiltrating cell nuclei) for axonal pathology. Even though the clinical scores might show a barely significant treatment effect on day 3, I was not able to detect a significant difference in the distribution of FAD stages between the Bepridil and vehicle group. Therefore, we were not able to link the strong effects observed in ROS/RNS mediated axon damage with a reduced level of inflammatory axon damage. However, further assessment is needed at this point to determine, for example, whether in this delivery paradigm sufficiently high concentrations of drug reach the inflammatory lesions within the spinal cord. In this regard, measuring axonal  $\text{Ca}^{2+}$  dynamics in EAE mice implanted with either saline or bepridil pumps could provide useful information.

#### **5.3.2.4 Glutamate excitotoxicity**

However, it is not only ROS/RNS that likely challenges axons in EAE and MS. Exceeding levels of glutamate are seen as a potent mediator of neuronal death, through a mechanism referred to as excitotoxicity. The term stands for excess stimulation of neurons by neurotransmitters like glutamate or related molecules, leading to massive activation of

glutamate receptors such as AMPA and NMDA that it turn can lead to substantial influx of  $\text{Ca}^{2+}$  ions. This pathway is somewhat coupled with the situation in virtual hypoxia and redox-mediated damage: impaired mitochondria will neither be able to produce the energy needed to stop the overload of the cell with  $\text{Ca}^{2+}$ , nor buffer it sufficiently, but rather release more  $\text{Ca}^{2+}$ . Glutamate excitotoxicity and oxidative stress are thought to have a final common pathway and appear as the “evil twins” in many neurodegenerative diseases. In MS, studies implicate higher levels of glutamate or aspartate in the cerebrospinal fluid of patients, not just in acute relapses but also during clinically stable phases (Sarchielli et al., 2003; Stover et al., 1997). MR spectroscopy showed evidence of higher glutamate levels even in normal appearing white matter of MS patients (Srinivasan et al., 2005). The amount of glutamate has been correlated with oligodendrocyte and axon damage in MS (Werner et al., 2001). In EAE, application of the AMPA/kainate antagonist NBQX yielded increased oligodendrocyte survival and reduced dephosphorylation of neurofilament H, indicating less axon damage. According to the authors, effects on lesion size and the degree of central nervous system inflammation were not observed (Pitt et al., 2000).

However these results remain open to interpretation, as it is unlikely that the systemic blockade of a widely distributed receptor like AMPA/kainate can specifically repress neuro-axonal overstimulation to prevent damage without effects on other CNS cells that might be involved in the phenomenon. In another interesting study using an adoptive transfer EAE model and *in vivo* imaging, Siffrin and colleagues observed direct interaction of MOG-specific  $\text{Th}_{17}$  cells and neuronal cells in demyelinating lesions that was associated with extensive axonal damage and intra-axonal calcium fluctuations (Siffrin et al., 2010). Their assessment showed the formation of immune synapses (‘kinapses’) at the point of interaction. By blocking NMDA receptors with MK-801, they were able to partially reverse the  $\text{Ca}^{2+}$  transients *in vivo*, supporting their hypothesis that it is T-cell derived glutamate which leads to overstimulation of neurons (Siffrin et al., 2010). The presence of receptors for excitatory molecules is assumed to be upregulated on neurons and/or

oligodendrocytes in MS, rendering these cells more vulnerable to excitotoxicity (Newcombe et al., 2008). One group has suggested expression of ionotropic glutamate receptors even in the membrane of axons in the spinal cord that could become harmful under pathological conditions (Ouardouz et al., 2009a; 2009b), which would make glutamate excitotoxicity a strong candidate for inducing the focal axonal degeneration observed in our paradigm.

### **5.3.2.5 Other mechanisms**

Two other putative mechanisms of  $\text{Ca}^{2+}$  overload in degenerating axons of neuroinflammatory lesions appear somewhat linked but downstream to the combined effects of excitotoxicity and redox mediated energy depletion: the role of the mitochondrial permeability transition pore (MPTP) and acid-sensing ion channel-1 (ASIC1). Forte et al. observed an improved recovery of EAE in mice lacking cyclophilin D (CypD), a key regulator of the MPTP (Forte et al., 2007). Evidence presented a strong preservation of axons in the spinal cords of CypD knockout mice and an increased resistance to ROS/RNS of cultured CypD<sup>-/-</sup> neurons, probably due to an enhanced  $\text{Ca}^{2+}$  buffering capacity of mitochondria. By immunohistochemical staining they demonstrated that the effect was not due to reduced infiltration of inflammatory immune cells. This would imply that challenged mitochondria are taking part in axonal  $\text{Ca}^{2+}$  overload via the opening of the MPTP.

A strong treatment effect has also been observed when knocking out, or pharmacologically blocking, ASIC1. This is a neuronally expressed, proton-gated channel that is permeable to  $\text{Na}^+$  and  $\text{Ca}^{2+}$ . Friese and colleagues assessed pH levels in the spinal cord and were able to show tissue acidosis in the inflamed spinal cord ( $\text{pH } 6.60 \pm 0.23$ ) compared to controls ( $\text{pH } 7.41 \pm 0.06$ ). As this low pH is compatible with the activation of ASIC1, they proposed that the markedly reduced clinical deficit and reduced axonal degeneration of *Asic1*<sup>-/-</sup> mice compared to wild-type mice suffering EAE is due to less ion influx through

this channel. A tantalising aspect of this study is the use of amiloride, a blocker of ASIC and broadly used cardiovascular pharmaceutical, to mimic the effects seen in *Asic1<sup>-/-</sup>* mice. Again, as ASIC1 is known to be expressed on immune cells, the hypothesis that the protective effect is due to direct blockade of ASIC1 on neurons cannot be conclusively proven. However, adoptive transfer showed that ASIC mediated mechanisms of T-cells were not an important factor for the clinical effect seen in this study (Friese et al., 2007).

### **5.3.3 Effects of Ca<sup>2+</sup> overload**

Another important question that arises from our study is whether the Ca<sup>2+</sup> elevations in EAE are capable of triggering degenerative processes in axons, and if so, how they lead to the eventual disintegration of axonal structures. As Ca<sup>2+</sup> overload is often seen as one common step in a multitude of degeneration pathways, the factors that would appear “downstream” are highly interesting and maybe relevant for our understanding of neurodegeneration in MS and beyond. Importantly, additional targets for therapy could be identified in these downstream mechanisms.

One possible downstream mechanisms of Ca<sup>2+</sup> influx is the activation of Calpains, a protease family, which have been suggested to be key players in cytoskeletal degradation, for example, during Wallerian degeneration (George et al., 1995; Yang et al., 2013; Zhai et al., 2003). *In vivo*, application of calpain inhibitors was able to completely block acute axonal degeneration after the mechanic transection of spinal axons (Kerschensteiner et al., 2005). In our work in the spinal cord contusion paradigm, calpain inhibitors likewise could protect axons for long periods of time (*in vivo* observation of up to 8 h) and were able to positively influence the fate of axons with increased Ca<sup>2+</sup> levels (Williams et al., 2014). These proteases could therefore be a key component that links Ca<sup>2+</sup> influx to axonal dismantling in EAE and MS. In EAE, one study showed calpain to be upregulated in the optic nerve at the onset of the disease. These changes were attenuated following treatment

with calpeptin, a calpain inhibitor. However, inflammation, microgliosis and astrogliosis were also altered with the calpeptin treatment, and the aim of the study was not to study specifically axon degeneration (Das et al., 2013). Another group used the calpain inhibitor CYLA to treat EAE in mice. In their study, they were able to see a reduction of clinical signs, tissue calpain content, demyelination and inflammatory infiltration (Hassen et al., 2008).

Another element of the axonal injury cascade in neuroinflammation has been suggested recently in a study (Schattling et al., 2012), in which the transient receptor potential melastatin 4 (TRPM4) cation channel was proposed to be crucial in the process of axon degeneration and the accumulation of irreversible neurological disability. Either knockout of the TRPM4 protein or pharmacological inhibition using glibenclamide, an antidiabetic drug, resulted in reduced axonal and neuronal degeneration and ameliorated clinical disease scores in EAE. The channel's expression was shown to be increased on axons in the inflamed spinal cord in mice and in the CNS of MS patients. The authors put great effort into excluding immune-related effects of TRPM4 deficiency: In one central experiment they established bone marrow–chimeric mice by reconstituting lethally irradiated *Trpm4*<sup>-/-</sup> or WT mice with either *Trpm4*<sup>-/-</sup> or WT bone marrow, showing that immune cells deficient for *Trpm4* were not responsible for the reduced disease severity that they reported (Schattling et al., 2012). As the TRPM4 channel is known to be activated by intracellular Ca<sup>2+</sup> rises (Launay et al., 2002) and deactivated by ATP, it becomes highly relevant in respect to our study as a potential amplifier of Ca<sup>2+</sup> induced degeneration. Also, the authors point out the osmotic effect of large-scale Na<sup>+</sup> influx through this channel, which could be one explanation to the swellings seen in axons undergoing FAD.

#### **5.4 Future therapeutic strategies**

During the last few decades, MS research and clinical management have made great progress regarding the acute inflammatory components of MS. Reducing both the clinical

severity and the frequency of relapses has become possible – a big relief for patients suffering from RR-MS. However, the underlying mechanisms of neurodegeneration as the cause of irreversible disability are still far from being understood. Finding a drug to reduce, halt or ideally even prevent progressive worsening of neurological deficits in long-time MS patients would be an immense success that would benefit all patients.

A strategy to develop such new therapeutic approaches has to first focus on the system where the pharmacological interventions are being tested in: In this case, one has to consider whether EAE is a suitable animal model that resembles MS closely enough concerning the aspects of the disease that one wants to characterize. EAE models have been proven vital for studying general concepts as well as specific processes of autoimmunity and a lot of our knowledge about MS is derived from this rodent model. However, as with many other rodent models of a human disease, many of the preclinical, experimental studies showing strong therapeutic success in EAE actually have failed to show the same efficacy in MS. When critically reviewing the weaknesses of EAE, the following aspects are in focus: First, most of the models' variants are no spontaneous disease. They therefore do not reproduce the likely quite heterogeneous mechanisms that induce MS but rather produce a prominent  $T_{H1}$ -cell or  $T_{H17}$  response promoted by the combination of mycobacteria and complete freuds adjuvant. Second, the timecourse in classical acute EAE appears to be rather that of a post-infectious demyelinating disease than of actual relapsing-remitting and secondary progressive MS. Third, general differences between human versus laboratory animal populations provide further complications: inbred, pathogen-free mice with a fixed diet are compared with all sorts of human ethnicities, dietary habits and environmental factors from different parts of the world (Friese et al., 2006). However, many of the listed differences between MS and EAE focus on the aetiology and immunopathogenesis of the diseases. In this and related studies, we assess the fundamental principles of axonal damage in a neuroinflammatory setting. The aetiology of the disease becomes secondary in this kind of paradigm. It has been shown that in terms of the principle constitution of CNS inflammatory lesions, the

---

mouse model and the human disease share many common aspects. As our approach is a mechanistic one, which looks at the *effects* of immune cells and their released molecules on axonal structures, I believe that EAE and its spinal cord lesions is a suitable model. A drug that could specifically target one of these mechanisms would be an ideal candidate for a translational approach and a new treatment strategy that aims at neuroprotection rather than immunomodulation.

On the basis of the evidence presented in this and other studies, ion dysregulation (specifically  $\text{Ca}^{2+}$ ) appears to be one of the important drivers of neuronal and axonal demise during EAE and MS. Some ion channels show adaptive changes to the inflammatory milieu by altering their relative distribution on the neuronal and axonal membrane, potentially even relocalizing from the soma to the axon. Amongst these are the  $\text{Na}_v$ , VGCC, TRPM4 and ASIC1a ion channels. Although these channels have been shown to take part in axonal degeneration, one could hypothesize that their axonal re-distribution could have some initial benefits in keeping the axon intact and preserving its proper functioning. If one aims to intervene in this system, it remains crucial to understand these different expression patterns and solve what relative contribution the different channels make in allowing pathological ion flux and therefore degeneration of the axons (Friese et al., 2014). In the following paragraphs, I will briefly discuss some translational approaches that have been undertaken so far:

Significant, likely neuroprotective effects of voltage-gated sodium channel blockade have been shown in EAE (Bechtold et al., 2004; Kapoor et al., 2003). This clinical efficacy could however not be translated to patients as shown recently in a randomised, double-blind, placebo-controlled, parallel-group trial of lamotrigine (a widely used anticonvulsive drug) in patients with secondary progressive MS. The effect of lamotrigine on cerebral volume of patients with SP-MS did not differ from that of placebo over 24 months. It even seemed to cause early volume loss that reversed partially on discontinuation of treatment (Kapoor et al., 2010).

---

Backed by strong effects both on the clinical score of mice, and on the reduction of axonal and myelin damage seen in histopathological analysis, preclinical efficacy of amiloride has been well documented in the EAE model. The fact that it did not exhibit strong modulation of tissue inflammation, and targets the ASIC channel that is overexpressed on CNS axons, makes chances high that its effects are mainly neuroprotective (see chapter 5.3.2). As the drug has been in use for many years for the treatment of hypertension and congestive cardiac failure, a group of researchers led by L. Fugger and J. Palace initiated a translational study and started treating a cohort of 14 PP-MS patients with amiloride. It will be highly interesting to see the outcome of this pilot study and a potential randomized, controlled trial assessing the effects of this novel treatment strategy (Arun et al., 2013).

The critical role of the NMDA receptor in glutamate-mediated excitotoxicity has driven the quest to find suitable antagonists as neuroprotective agents. This therapeutic strategy has been especially pursued in conditions of ischemia like stroke or brain injury. Even though a lot of resources have been spent to find treatment strategies that tackle NMDA-mediated neuronal damage, large clinical studies have failed so far. Furthermore NMDA antagonists have several adverse CNS effects, including hallucinations, a centrally mediated increase in blood pressure and, at high doses, catatonia and anesthesia (Kemp and McKernan, 2002). Therefore it remains hard to predict whether a specific and effective targeting of glutamate-mediated axon damage will at some point prove to be an applicable treatment for MS.

In work previous to my study, my colleagues could effectively halt degeneration of axons and mitochondrial changes in the inflamed spinal cord with scavengers of ROS/RNS. This strategy yielded robust results and potentially interferes with the interaction of immune cells and the neuro-axonal compartment (Nikić et al., 2011; Sorbara et al., 2014). Two recent studies reported protective properties in different EAE models of a synthetic antioxidant called “MitoQ”. It specifically accumulates in mitochondria, and did not seem

to alter levels of inflammation. Ideally, this agent would protect mitochondria against ROS and therefore reduce axonal damage (Mao et al., 2013). There is also evidence that activation of the Nrf2/ARE pathway might play a protective role in the pathogenesis of MS, however not just by neuroprotection. Hence, further activation of the Nrf2/ARE system via monofunctional inducers could prove an effective strategy. Notably, dimethyl-fumarate (DMF) and its primary metabolite monomethyl fumarate (MMF) are potent activators of this pathway (van Horssen et al., 2011). As DMF (BG-12, Tecfidera®) has been just introduced as a new, oral drug to treat RR-MS, this mechanism will be of special interest, especially when assessing the long-term effects of the treatment. In principle, antioxidant treatment to tackle neuro-axonal degeneration in MS seems to be a promising candidate. However, many issues, mainly concerning pharmacokinetics but also target specificity, still have to be solved.

### **5.5 Concluding remarks**

Multiple sclerosis, with its enigmatic etiology and complex pathophysiology has been baffling researches for many years now. In recent years the focus of investigation has broadened, and neurobiological aspects such as the immune-mediated damage of neurons and their axons are being explored. These aspects are of substantial clinical importance as the gradually increasing disability appears to be a clinical correlate of progressive loss of axonal connections. The interactions of immune cells with axons are potentially responsible for this demise. However the exact mechanisms of the degeneration process remain elusive. As the detailed analysis of pathological mechanisms in animal models provides a solid basis for translational approaches, investigating the molecular mediators of axonal degeneration in MS models remains a promising approach to find future neuroprotective therapies for MS and related diseases.

---

In this work I established an imaging approach to monitor changes in intra-axonal calcium concentrations with single axon resolution in the spinal cord of living animals. In actively induced EAE, the most common mouse model of MS, I showed that  $\text{Ca}^{2+}$  is a critical factor mediating axon degeneration in inflammatory lesions. With elevated  $\text{Ca}^{2+}$  concentrations, the probability increases that an axon will first swell and afterwards fragment, although there also appears to be chances for an axon to recover - both in terms of returning to normal  $\text{Ca}^{2+}$  levels and in the fact that swellings can subsequently disappear. This renders the process very interesting, as it suggests that it might be accessible for intervention. Therefore one has to discover, how the rise in  $\text{Ca}^{2+}$  is induced and which molecular players mediate it.

I have discussed a broad range of potential mechanisms of  $\text{Ca}^{2+}$  entry into the intra-axonal compartment. I have emphasized the effects of ROS/RNS, which can have a large spectrum of possible indirect and direct effects on structures that can mediate  $\text{Ca}^{2+}$  elevation in an axon. As preceding work in our group has drawn a link between immune-released ROS/RNS and focal axonal degeneration, the mechanistic details including the  $\text{Ca}^{2+}$  rise remain highly interesting and have to be further assessed. The related mechanisms of the “virtual hypoxia” pathway also need to be re-evaluated in the context of this work. Additionally, the relevance of glutamate excitotoxicity for the described processes remains a key interest in the field and is also directly linked to intra-axonal  $\text{Ca}^{2+}$ . Even though it is technically challenging to assess the individual contribution of these pathways to axonal demise in a complex neuroinflammatory environment, it stays a highly promising field for pharmacological intervention.

While the first clinical studies of potentially neuroprotective agents in MS have been performed in the last decade, the results of these (largely failed) studies suggest that there is still a long way to go. However, in the large variety of compounds that are approved and in daily use in modern medicine, there might be many hidden pearls to be tested for their neuroprotective potential in EAE and MS – which would bypass at least one phase of clinical testing and therefore save some years in development. As I cited the MS patient M. Lemelle in

the beginning of this thesis, patients are in constant anxiety to accept and adapt to the new challenges brought by disease progression. Research must move forward in understanding the complex processes of MS and how they are linked. It must translate this into treatment strategies that allow patients to maintain a “normal” daily life and thus fundamentally improve its quality.

---

## 6. References

- Abdul-Majid, K.B., Jirholt, J., Stadelmann, C., Stefferl, A., Kjellén, P., Wallström, E., Holmdahl, R., Lassmann, H., Olsson, T., and Harris, R.A. (2000). Screening of several H-2 congenic mouse strains identified H-2(q) mice as highly susceptible to MOG-induced EAE with minimal adjuvant requirement. *Journal of Neuroimmunology* 111, 23–33.
- Arun, T., Tomassini, V., Sbardella, E., Rüter, M. de, Matthews, L., Leite, M., Gelineau-Morel, R., Cavey, A., Vergo, S., Craner, M., et al. (2013). Targeting ASIC1 in primary progressive multiple sclerosis: evidence of neuroprotection with amiloride. *Brain* 136, 106–15.
- Babetto, E., Beirowski, B., Russler, E., Milbrandt, J., and DiAntonio, A. (2013). The Phr1 ubiquitin ligase promotes injury-induced axon self-destruction. *Cell Reports* 3, 1422–9.
- Baimbridge, Celio, and Rogers (1992). Calcium-binding proteins in the nervous system. *Trends in Neurosciences* 15, 303–8.
- Barkhof, F., Calabresi, P., Miller, D., and Reingold, S. (2009). Imaging outcomes for neuroprotection and repair in multiple sclerosis trials. *Nature Reviews. Neurology* 5, 256–66.
- Bechtold, D., Kapoor, R., and Smith, K. (2004). Axonal protection using flecainide in experimental autoimmune encephalomyelitis. *Annals of Neurology* 55, 607–16.
- Bechtold, D., Yue, X., Evans, R., Davies, M., Gregson, N., and Smith, K. (2005). Axonal protection in experimental autoimmune neuritis by the sodium channel blocking agent flecainide. *Brain* 128, 18–28.
- Berg, J., Hung, Y., and Yellen, G. (2009). A genetically encoded fluorescent reporter of ATP:ADP ratio. *Nature Methods* 6, 161–6.
- Bitsch, A., Schuchardt, J., Bunkowski, S., Kuhlmann, T., and Brück, W. (2000). Acute axonal injury in multiple sclerosis. Correlation with demyelination and inflammation. *Brain* 123, 1174–83.
- Bjartmar, C., Kidd, G., Mörk, S., Rudick, R., and Trapp, B. (2000). Neurological disability correlates with spinal cord axonal loss and reduced N-acetyl aspartate in chronic multiple sclerosis patients. *Annals of Neurology* 48, 893–901.
- Black, J., Liu, S., Hains, B., Saab, C., and Waxman, S. (2006). Long-term protection of central axons with phenytoin in monophasic and chronic-relapsing EAE. *Brain* 129, 3196–208.
- Breckwoldt, M., Pfister, F., Bradley, P., Marinković, P., Williams, P., Brill, M., Plomer, B., Schmalz, A., Clair, D., Naumann, R., Griesbeck, O., Schwarzländer, M., Godinho, L., Bareyre, F., Dick T., Kerschensteiner, M., and Misgeld, T. (2014). Multiparametric optical analysis of mitochondrial redox signals during neuronal physiology and pathology in vivo. *Nature Medicine* 20, 555–60.
- Brown, A.M., and McFarlin, D.E. (1981). Relapsing experimental allergic encephalomyelitis in the SJL/J mouse. *Laboratory Investigation; a Journal of Technical Methods and Pathology* 45, 278–84.

- 
- Busche, M., Eichhoff, G., Adelsberger, H., Abramowski, D., Wiederhold, K.-H., Haass, C., Staufenbiel, M., Konnerth, A., and Garaschuk, O. (2008). Clusters of hyperactive neurons near amyloid plaques in a mouse model of Alzheimer's disease. *Science* 321, 1686–9.
- Chard, Griffin, Parker, Kapoor, Thompson, and Miller (2002). Brain atrophy in clinically early relapsing-remitting multiple sclerosis. *Brain* 125, 327–37.
- Chen, X., Leischner, U., Varga, Z., Jia, H., Deca, D., Rochefort, N., and Konnerth, A. (2012). LOTOS-based two-photon calcium imaging of dendritic spines in vivo. *Nature Protocols* 7, 1818–29.
- Compston, A., and Coles, A. (2008). Multiple sclerosis. *Lancet* 372, 1502–17.
- Compston, A., Confavreux, C., Lassmann, H., McDonald, I., Miller, D., Noseworthy, Smith, K., and Wekerle, H. (2005). McAlpine's multiple sclerosis.
- Confavreux, C., and Vukusic, S. (2006). Age at disability milestones in multiple sclerosis. *Brain* 129, 595–605.
- Conforti, L., Gilley, J., and Coleman, M. (2014). Wallerian degeneration: an emerging axon death pathway linking injury and disease. *Nature Reviews Neuroscience* 15, 394–409.
- Court, F., and Coleman, M. (2012). Mitochondria as a central sensor for axonal degenerative stimuli. *Trends in Neurosciences* 35, 364–72.
- Craner, M., Newcombe, J., Black, J., Hartle, C., Cuzner, and Waxman, S. (2004a). Molecular changes in neurons in multiple sclerosis: altered axonal expression of Nav1.2 and Nav1.6 sodium channels and Na<sup>+</sup>/Ca<sup>2+</sup> exchanger. *Proceedings of the National Academy of Sciences* 101, 8168–73.
- Craner, M., Hains, B., Lo, A., Black, J., and Waxman, S. (2004b). Co-localization of sodium channel Nav1.6 and the sodium-calcium exchanger at sites of axonal injury in the spinal cord in EAE. *Brain* 127, 294–303.
- Das, A., Guyton, Smith, A., Wallace, G., McDowell, M., Matzelle, D., Ray, S., and Banik, N. (2013). Calpain inhibitor attenuated optic nerve damage in acute optic neuritis in rats. *Journal of Neurochemistry* 124, 133–46.
- Denk, W., and Svoboda, K. (1997). Photon upmanship: why multiphoton imaging is more than a gimmick. *Neuron* 18, 351–7.
- Denk, W., Strickler, J.H., and Webb, W.W. (1990). Two-photon laser scanning fluorescence microscopy. *Science* 248, 73–6.
- De Stefano, N., Matthews, P.M., Fu, L., Narayanan, S., Stanley, J., Francis, G.S., Antel, J.P., and Arnold, D.L. (1998). Axonal damage correlates with disability in patients with relapsing-remitting multiple sclerosis. Results of a longitudinal magnetic resonance spectroscopy study. *Brain* 121, 1469–77.
- De Stefano, N., Bartolozzi, M.L., and Guidi, L. (2005). Magnetic resonance spectroscopy as a measure of brain damage in multiple sclerosis. *Journal of the Neurological Sciences* 233, 203–208.
- Direnberger, S., Mues, M., Micale, V., Wotjak, C., Dietzel, S., Schubert, M., Scharr, A., Hassan, S., Wahl-Schott, C., Biel, M., Krishnamoorthy G., and Griesbeck, O. (2012). Biocompatibility of a genetically encoded calcium indicator in a transgenic mouse model. *Nature Communications* 3, 1031.

- 
- Dutta, R., McDonough, J., Yin, X., Peterson, J., Chang, A., Torres, T., Gudz, T., Macklin, W., Lewis, D., Fox, R., Rudick, R., Mirnics, K., and Trapp B. (2006). Mitochondrial dysfunction as a cause of axonal degeneration in multiple sclerosis patients. *Annals of Neurology* 59, 478–89.
- Feng, G., Mellor, R.H., Bernstein, M., Keller-Peck, C., Nguyen, Q.T., Wallace, M., Nerbonne, J.M., Lichtman, J.W., and Sanes, J.R. (2000). Imaging neuronal subsets in transgenic mice expressing multiple spectral variants of GFP. *Neuron* 28, 41–51.
- Ferguson, B., Matyszak, M.K., Esiri, M.M., and Perry, V.H. (1997). Axonal damage in acute multiple sclerosis lesions. *Brain* 120, 393–99.
- Fischer, M., Sharma, R., Lim, J., Haider, L., Frischer, J., Drexhage, J., Mahad, D., Bradl, M., Horssen, J. van, and Lassmann, H. (2012). NADPH oxidase expression in active multiple sclerosis lesions in relation to oxidative tissue damage and mitochondrial injury. *Brain* 135, 886–99.
- Forte, M., Gold, B., Marracci, G., Chaudhary, P., Basso, E., Johnsen, D., Yu, X., Fowlkes, J., Rahder, M., Stem, K., Bernardi, P., and Bourdette D. (2007). Cyclophilin D inactivation protects axons in experimental autoimmune encephalomyelitis, an animal model of multiple sclerosis. *Proceedings of the National Academy of Sciences* 104, 7558–63.
- Friese, M., Montalban, X., Willcox, N., Bell, J., Martin, R., and Fugger, L. (2006). The value of animal models for drug development in multiple sclerosis. *Brain* 129, 1940–52.
- Friese, M., Craner, M., Ezensperger, R., Vergo, S., Wemmie, J., Welsh, M., Vincent, A., and Fugger, L. (2007). Acid-sensing ion channel-1 contributes to axonal degeneration in autoimmune inflammation of the central nervous system. *Nature Medicine* 13, 1483–9.
- Friese, M., Schattling, B., and Fugger, L. (2014). Mechanisms of neurodegeneration and axonal dysfunction in multiple sclerosis. *Nature Reviews Neurology* 10, 225–238.
- Gadjanski, I., Boretius, S., Williams, S., Lingor, P., Knöferle, J., Sättler, M., Fairless, R., Hochmeister, S., Sühs, K.-W., Michaelis, T., et al. (2009). Role of n-type voltage-dependent calcium channels in autoimmune optic neuritis. *Annals of Neurology* 66, 81–93.
- Garaschuk, O., Griesbeck, O., and Konnerth, A. (2007). Troponin C-based biosensors: a new family of genetically encoded indicators for in vivo calcium imaging in the nervous system. *Cell Calcium* 42, 351–61.
- George, E.B., Glass, J.D., and Griffin, J.W. (1995). Axotomy-induced axonal degeneration is mediated by calcium influx through ion-specific channels. *The Journal of Neuroscience* : 15, 6445–52.
- Gonsette, R.E. (2008). Review: Oxidative stress and excitotoxicity: a therapeutic issue in multiple sclerosis? *Multiple Sclerosis* 14, 22–34.
- Gregersen, J.W., Holmes, S., and Fugger, L. (2004). Humanized animal models for autoimmune diseases. *Tissue Antigens* 63, 383–94.
- Grienberger, C., and Konnerth, A. (2012). Imaging calcium in neurons. *Neuron* 73, 862–85.
- Griesbeck, O. (2004). Fluorescent proteins as sensors for cellular functions. *Current Opinion in Neurobiology* 14, 636–41.

- 
- Gutscher, M., Pauleau, A.-L., Marty, L., Brach, T., Wabnitz, G., Samstag, Y., Meyer, A., and Dick, T. (2008). Real-time imaging of the intracellular glutathione redox potential. *Nature Methods* 5, 553–9.
- Haider, L., Fischer, M., Frischer, J., Bauer, J., Höftberger, R., Botond, G., Esterbauer, H., Binder, C., Witztum, J., and Lassmann, H. (2011). Oxidative damage in multiple sclerosis lesions. *Brain* 134, 1914–24.
- Haider, L., Simeonidou, C., Steinberger, G., Hametner, S., Grigoriadis, N., Deretzi, G., Kovacs, G., Kutzelnigg, A., Lassmann, H., and Frischer, J. (2014). Multiple sclerosis deep grey matter: the relation between demyelination, neurodegeneration, inflammation and iron. *Journal of Neurology, Neurosurgery & Psychiatry*.
- Hassen, G., Feliberti, J., Kesner, L., Stracher, A., and Mokhtarian, F. (2008). Prevention of axonal injury using calpain inhibitor in chronic progressive experimental autoimmune encephalomyelitis. *Brain Research* 1236, 206–15.
- Heim, N., and Griesbeck, O. (2004). Genetically encoded indicators of cellular calcium dynamics based on troponin C and green fluorescent protein. *The Journal of Biological Chemistry* 279, 14280–6.
- Heim, N., Garaschuk, O., Friedrich, M., Mank, M., Milos, R., Kovalchuk, Y., Konnerth, A., and Griesbeck, O. (2007). Improved calcium imaging in transgenic mice expressing a troponin C-based biosensor. *Nature Methods* 4, 127–9.
- Helmchen, F., and Denk, W. (2005). Deep tissue two-photon microscopy. *Nature Methods* 2, 932–40.
- Hendel, T., Mank, M., Schnell, B., Griesbeck, O., Borst, A., and Reiff, D. (2008). Fluorescence changes of genetic calcium indicators and OGB-1 correlated with neural activity and calcium in vivo and in vitro. *The Journal of Neuroscience* 28, 7399–411.
- Higgins, G., Beart, P., Shin, Y., Chen, M., Cheung, N., and Nagley, P. (2010). Oxidative stress: emerging mitochondrial and cellular themes and variations in neuronal injury. *Journal of Alzheimer's Disease* 20, 453–473.
- Hill, K., Zollinger, L., Watt, H., Carlson, N., and Rose, J. (2004). Inducible nitric oxide synthase in chronic active multiple sclerosis plaques: distribution, cellular expression and association with myelin damage. *Journal of Neuroimmunology* 151, 171–9.
- Horszen, J. van, Witte, M., Schreibelt, G., and Vries, H. de (2011). Radical changes in multiple sclerosis pathogenesis. *Biochimica et Biophysica Acta* 1812, 141–50.
- Howarth, C., Gleeson, P., and Attwell, D. (2012). Updated energy budgets for neural computation in the neocortex and cerebellum. *Journal of Cerebral Blood Flow and Metabolism* 32, 1222–32.
- Jares-Erijman, E.A., and Jovin, T.M. (2003). FRET imaging. *Nature Biotechnology* 21, 1387–95.
- Juurlink, B.H., Thorburne, S.K., and Hertz, L. (1998). Peroxide-scavenging deficit underlies oligodendrocyte susceptibility to oxidative stress. *Glia* 22, 371–8.
- Kabat, E.A., Wolf, A., and Bezer, A.E. (1947). The rapid production of acute disseminated encephalomyelitis in rhesus monkeys by injection of heterologous and homologous brain tissue with adjuvants. *The Journal of Experimental Medicine* 85, 117–30.

- 
- Kaneko, S., Wang, J., Kaneko, M., Yiu, G., Hurrell, J., Chitnis, T., Khoury, S., and He, Z. (2006). Protecting axonal degeneration by increasing nicotinamide adenine dinucleotide levels in experimental autoimmune encephalomyelitis models. *The Journal of Neuroscience* 26, 9794–804.
- Kapoor, R., Davies, M., Blaker, P., Hall, S., and Smith, K. (2003). Blockers of sodium and calcium entry protect axons from nitric oxide-mediated degeneration. *Annals of Neurology* 53, 174–80.
- Kapoor, R., Furby, J., Hayton, T., Smith, K., Altmann, D., Brenner, R., Chataway, J., Hughes, R., and Miller, D. (2010). Lamotrigine for neuroprotection in secondary progressive multiple sclerosis: a randomised, double-blind, placebo-controlled, parallel-group trial. *The Lancet. Neurology* 9, 681–8.
- Kemp, J., and McKernan, R. (2002). NMDA receptor pathways as drug targets. *Nature Neuroscience* 5, 1039–1042.
- Kerr, J., Greenberg, D., and Helmchen, F. (2005). Imaging input and output of neocortical networks in vivo. *Proceedings of the National Academy of Sciences* 102, 14063–8.
- Kerschensteiner, M., Schwab, M., Lichtman, J., and Misgeld, T. (2005). In vivo imaging of axonal degeneration and regeneration in the injured spinal cord. *Nature Medicine* 11, 572–7.
- Kleele, T., Marinković, P., Williams, P., Stern, S., Weigand, E., Engerer, P., Naumann, R., Hartmann, J., Karl, R., Bradke, F., Bishop, D., Herms, J., Konnerth, A., Kerschensteiner, M., Godinho, L., and Misgeld, T. (2014). An assay to image neuronal microtubule dynamics in mice. *Nature Communications* 5, 4827.
- Kornek, B., Storch, M.K., Weissert, R., Wallstroem, E., Stefferl, A., Olsson, T., Linington, C., Schmidbauer, M., and Lassmann, H. (2000). Multiple sclerosis and chronic autoimmune encephalomyelitis: a comparative quantitative study of axonal injury in active, inactive, and remyelinated lesions. *The American Journal of Pathology* 157, 267–76.
- Kornek, B., Storch, M., Bauer, J., Djamshidian, A., Weissert, R., Wallstroem, E., Stefferl, A., Zimprich, F., Olsson, T., Linington, C., Schmidbauer, M., and Lassmann, H. (2001). Distribution of a calcium channel subunit in dystrophic axons in multiple sclerosis and experimental autoimmune encephalomyelitis. *Brain* 124, 1114–24.
- Krishnamoorthy, G., and Wekerle, H. (2009). EAE: an immunologist's magic eye. *European Journal of Immunology* 39, 2031–2035.
- Krishnamoorthy, G., Holz, A., and Wekerle, H. (2007). Experimental models of spontaneous autoimmune disease in the central nervous system. *Journal of Molecular Medicine* 85, 1161–73.
- Kuchibhotla, K.V., Goldman, S.T., Lattarulo, C.R., and Wu, H.Y. (2008). A $\beta$  plaques lead to aberrant regulation of calcium homeostasis in vivo resulting in structural and functional disruption of neuronal networks. *Neuron* 59, 214–225.
- Kuhlmann, T., Lingfeld, G., Bitsch, A., Schuchardt, J., and Brück, W. (2002). Acute axonal damage in multiple sclerosis is most extensive in early disease stages and decreases over time. *Brain* 125, 2202–12.

- 
- Lassmann, H. (2003). Axonal injury in multiple sclerosis. *Journal of Neurology, Neurosurgery, and Psychiatry* 74, 695–697.
- Lassmann, H., Brück, W., and Lucchinetti, C. (2001). Heterogeneity of multiple sclerosis pathogenesis: implications for diagnosis and therapy. *Trends in Molecular Medicine* 7, 115–21.
- Lassmann, H., Horssen, J. van, and Mahad, D. (2012). Progressive multiple sclerosis: pathology and pathogenesis. *Nature Reviews. Neurology* 8, 647–56.
- Launay, P., Fleig, A., Perraud, A., Scharenberg, A., Penner, R., and Kinet, J. (2002). TRPM4 is a Ca<sup>2+</sup>-activated nonselective cation channel mediating cell membrane depolarization. *Cell* 109, 397–407.
- Lemelle, N. (2011). My New Normals - Living with Multiple Sclerosis. 10 Aug. 2014. <<http://www.mynewnormals.com/short-story/im-ready-part-4>>
- Lennon, V., Kryzer, T., Pittock, S., Verkman, and Hinson, S. (2005). IgG marker of optic-spinal multiple sclerosis binds to the aquaporin-4 water channel. *The Journal of Experimental Medicine* 202, 473–477.
- Lin, M., and Beal (2006). Mitochondrial dysfunction and oxidative stress in neurodegenerative diseases. *Nature* 443, 787–95.
- Liu, Zhao, Brosnan, and Lee (2001). Expression of inducible nitric oxide synthase and nitrotyrosine in multiple sclerosis lesions. *The American Journal of Pathology* 158, 2057–66.
- Lublin, Maurer, Berry, and Tippett (1981). Delayed, relapsing experimental allergic encephalomyelitis in mice. *Journal of Immunology (Baltimore, Md. : 1950)* 126, 819–22.
- Lunn, Perry, Brown, Rosen, and Gordon (1989). Absence of Wallerian Degeneration does not Hinder Regeneration in Peripheral Nerve. *The European Journal of Neuroscience* 1, 27–33.
- Mack, T., Reiner, M., Beirowski, B., Mi, W., Emanuelli, M., Wagner, D., Thomson, D., Gillingwater, T., Court, F., Conforti, L., et al. (2001). Wallerian degeneration of injured axons and synapses is delayed by a Ube4b/Nmnat chimeric gene. *Nature Neuroscience* 4, 1199–1206
- Magliozzi, R., Howell, O., Vora, A., Serafini, B., Nicholas, R., Puopolo, M., Reynolds, R., and Aloisi, F. (2007). Meningeal B-cell follicles in secondary progressive multiple sclerosis associate with early onset of disease and severe cortical pathology. *Brain* 130, 1089–1104.
- Mahad, D., Ziabreva, I., Campbell, G., Lax, N., White, K., Hanson, P., Lassmann, H., and Turnbull, D. (2009). Mitochondrial changes within axons in multiple sclerosis. *Brain* 132, 1161–74.
- Mank, M., and Griesbeck, O. (2008). Genetically encoded calcium indicators. *Chemical Reviews* 108, 1550–64.
- Mank, M., Reiff, D., Heim, N., Friedrich, M., Borst, A., and Griesbeck, O. (2006). A FRET-based calcium biosensor with fast signal kinetics and high fluorescence change. *Biophysical Journal* 90, 1790–6.

- 
- Mank, M., Santos, A., Drenth, S., Mrcic-Flogel, T., Hofer, S., Stein, V., Hendel, T., Reiff, D., Levelt, C., Borst, A., et al. (2008). A genetically encoded calcium indicator for chronic in vivo two-photon imaging. *Nature Methods* 5, 805–11.
- Mao, P., Manczak, M., Shirendeb, U., and Reddy (2013). MitoQ, a mitochondria-targeted antioxidant, delays disease progression and alleviates pathogenesis in an experimental autoimmune encephalomyelitis mouse model of multiple sclerosis. *Biochimica et Biophysica Acta* 1832, 2322–31.
- McDonald, I., Compston, A., Edan, G., Goodkin, D., Hartung, H., Lublin, F., McFarland, H., Paty, D., Polman, C., Reingold, S., et al. (2001). Recommended diagnostic criteria for multiple sclerosis: Guidelines from the international panel on the diagnosis of multiple sclerosis. *Annals of Neurology* 50, 121–27.
- Misgeld, T., and Kerschensteiner, M. (2006). In vivo imaging of the diseased nervous system. *Nature Reviews. Neuroscience* 7, 449–63.
- Misgeld, T., Nikic, I., and Kerschensteiner, M. (2007a). In vivo imaging of single axons in the mouse spinal cord. *Nature Protocols* 2, 263–8.
- Misgeld, T., Kerschensteiner, M., Bareyre, F., Burgess, R., and Lichtman, J. (2007b). Imaging axonal transport of mitochondria in vivo. *Nature Methods* 4, 559–61.
- Miyawaki, Llopis, Heim, McCaffery, Adams, Ikura, and Tsien (1997). Fluorescent indicators for Ca<sup>2+</sup> based on green fluorescent proteins and calmodulin. *Nature* 388, 882–7.
- Morsali, D., Bechtold, D., Lee, W., Chauhdry, S., Palchaudhuri, U., Hassoon, P., Snell, D., Malpass, K., Piers, T., Pocock, J., et al. (2013). Safinamide and flecainide protect axons and reduce microglial activation in models of multiple sclerosis. *Brain* 136, 1067–82.
- Neher, and Augustine (1992). Calcium gradients and buffers in bovine chromaffin cells. *The Journal of Physiology* 450, 273–301.
- Newcombe, J., Uddin, A., Dove, R., Patel, B., Turski, L., Nishizawa, Y., and Smith, T. (2008). Glutamate Receptor Expression in Multiple Sclerosis Lesions. *Brain Pathology* 18, 52–61.
- Nikić, I., Merkler, D., Sorbara, C., Brinkoetter, M., Kreutzfeldt, M., Bareyre, F., Brück, W., Bishop, D., Misgeld, T., and Kerschensteiner, M. (2011). A reversible form of axon damage in experimental autoimmune encephalomyelitis and multiple sclerosis. *Nature Medicine* 17, 495–9.
- Noseworthy, J., Lucchinetti, C., Rodriguez, M., and Weinshenker, B. (2000). Multiple Sclerosis. *New England Journal of Medicine* 343, 938–52.
- Oleszak, E.L., Zaczynska, E., Bhattacharjee, M., Butunoi, C., Legido, A., and Katsetos, C.D. (1998). Inducible nitric oxide synthase and nitrotyrosine are found in monocytes/macrophages and/or astrocytes in acute, but not in chronic, multiple sclerosis. *Clinical and Diagnostic Laboratory Immunology* 5, 438–45.
- Osterloh, J., Yang, J., Rooney, T., Fox, Adalbert, R., Powell, E., Sheehan, A., Avery, M., Hackett, R., Logan, M., et al. (2012). dSarm/Sarm1 is required for activation of an injury-induced axon death pathway. *Science* 337, 481–4.
- Ouardouz, M., Coderre, E., Zamponi, G., Hameed, S., Yin, X., Trapp, B., and Stys, P. (2009a). Glutamate receptors on myelinated spinal cord axons: II. AMPA and GluR5 receptors. *Annals Neurology* 65, 160–6.

- 
- Ouardouz, M., Coderre, E., Basak, A., Chen, A., Zamponi, G., Hameed, S., Rehak, R., Yin, X., Trapp, B., and Stys, P. (2009b). Glutamate receptors on myelinated spinal cord axons: I. GluR6 kainate receptors. *Annals Neurology* 65, 151–9.
- O’Riordan, J.O., Thompson, A.J., Kingsley, D.P., MacManus, D.G., Kendall, B.E., Rudge, P., McDonald, W.I., and Miller, D.H. (1998). The prognostic value of brain MRI in clinically isolated syndromes of the CNS. A 10-year follow-up. *Brain* 121, 495–503.
- Palop, J., Chin, J., Roberson, E., Wang, J., Thwin, M., Bien-Ly, N., Yoo, J., Ho, K., Yu, G.-Q., Kreitzer, A., et al. (2007). Aberrant excitatory neuronal activity and compensatory remodeling of inhibitory hippocampal circuits in mouse models of Alzheimer’s disease. *Neuron* 55, 697–711.
- Pawley, J., Denk, W., Piston, D., and Webb, W. (1995). *Handbook of Biological Confocal Microscopy*. 445–458.
- Perry, V.H., Lunn, E.R., Brown, M.C., Cahusac, S., and Gordon, S. (1990). Evidence that the Rate of Wallerian Degeneration is Controlled by a Single Autosomal Dominant Gene. *The European Journal of Neuroscience* 2, 408–13.
- Petzold, A., Boer, J. de, Schippling, S., Vermersch, P., Kardon, R., Green, A., Calabresi, P., and Polman, C. (2010). Optical coherence tomography in multiple sclerosis: a systematic review and meta-analysis. *The Lancet. Neurology* 9, 921–32.
- Pfriefer, F., and Slezak, M. (2012). Genetic approaches to study glial cells in the rodent brain. *Glia* 60, 681-701
- Pitt, D., Werner, P., and Raine, C. (2000). Glutamate excitotoxicity in a model of multiple sclerosis. *Nature Medicine* 6, 67–70.
- Polman, C., Reingold, S., Edan, G., Filippi, M., Hartung, H., Kappos, L., Lublin, F., Metz, L., MCFarland, H., O’Connor, P., et al. (2005). Diagnostic criteria for multiple sclerosis: 2005 revisions to the “McDonald Criteria.” *Annals of Neurology* 58, 840-46.
- Polman, C., Reingold, S., Banwell, B., Clanet, M., Cohen, J., Filippi, M., Fujihara, K., Havrdova, E., Hutchinson, M., Kappos, L., et al. (2011). Diagnostic criteria for multiple sclerosis: 2010 Revisions to the McDonald criteria. *Annals of Neurology* 69, 292-302.
- Redford, E.J., Kapoor, R., and Smith, K.J. (1997). Nitric oxide donors reversibly block axonal conduction: demyelinated axons are especially susceptible. *Brain* 120, 2149-57.
- Rivers, T.M., and Schwentker, F.F. (1935). Encephalomyelitis accompanied by myelin destruction experimentally produced in monkeys. *The Journal of Experimental Medicine* 61, 689–702.
- Rivers, T.M., Sprunt, D.H., and Berry, G.P. (1933). Observations on attempts to produce acute disseminated encephalomyelitis in monkeys. *The Journal of Experimental Medicine* 58, 39–53.
- Romanelli, E., Sorbara, C., Nikić, I., Dagkalis, A., Misgeld, T., and Kerschensteiner, M. (2013). Cellular, subcellular and functional in vivo labeling of the spinal cord using vital dyes. *Nature Protocols* 8, 481–90.
- Rossi, S., Chiara, V., Furlan, R., Musella, A., Cavasinni, F., Muzio, L., Bernardi, G., Martino, G., and Centonze, D. (2010). Abnormal activity of the Na/Ca exchanger enhances

- 
- glutamate transmission in experimental autoimmune encephalomyelitis. *Brain, Behavior, and Immunity* 24, 1379–85.
- Sadovnick, Eisen, Ebers, and Paty (1991). Cause of death in patients attending multiple sclerosis clinics. *Neurology* 41, 1193–6.
- Sarchielli, P., Greco, L., Floridi, A., Floridi, A., and Gallai, V. (2003). Excitatory amino acids and multiple sclerosis: evidence from cerebrospinal fluid. *Archives of Neurology* 60, 1082–8.
- Schattling, B., Steinbach, K., Thies, E., Kruse, M., Menigoz, A., Ufer, F., Flockerzi, V., Brück, W., Pongs, O., Vennekens, R., et al. (2012). TRPM4 cation channel mediates axonal and neuronal degeneration in experimental autoimmune encephalomyelitis and multiple sclerosis. *Nature Medicine* 18, 1805–11.
- Schlaepfer (1974). Calcium-induced degeneration of axoplasm in isolated segments of rat peripheral nerve. *Brain Research* 69, 203–15.
- Shi, Y., Feng, Y., Kang, J., Liu, C., Li, Z., Li, D., Cao, W., Qiu, J., Guo, Z., Bi, E., et al. (2007). Critical regulation of CD4+ T cell survival and autoimmunity by  $\beta$ -arrestin 1. *Nature Immunology* 8, 817–24.
- Siffrin, V., Radbruch, H., Glumm, R., Niesner, R., Paterka, M., Herz, J., Leuenberger, T., Lehmann, S., Luenstedt, S., Rinnenthal, J., et al. (2010). In vivo imaging of partially reversible th17 cell-induced neuronal dysfunction in the course of encephalomyelitis. *Immunity* 33, 424–36.
- Sišková, Z., Justus, D., Kaneko, H., Friedrichs, D., Henneberg, N., Beutel, T., Pitsch, J., Schoch, S., Becker, A., Kammer, H. von der, et al. (2014). Dendritic structural degeneration is functionally linked to cellular hyperexcitability in a mouse model of Alzheimer's disease. *Neuron* 84, 1023–33.
- Smith, K., and Lassmann, H. (2002). The role of nitric oxide in multiple sclerosis. *The Lancet. Neurology* 1, 232–41.
- Smith, K.J., Kapoor, R., Hall, S.M., and Davies, M. (2001). Electrically active axons degenerate when exposed to nitric oxide. *Annals of Neurology* 49, 470–6.
- Sorbara, C., Wagner, N., Ladwig, A., Nikić, I., Merkler, D., Kleele, T., Marinković, P., Naumann, R., Godinho, L., Bareyre, F., et al. (2014). Pervasive axonal transport deficits in multiple sclerosis models. *Neuron* 84, 1183–90.
- Sospedra, M., and Martin, R. (2005). Immunology of multiple sclerosis. *Annual Review of Immunology* 23, 683–747.
- Sospedra, M., and Martin, R. (2006). Molecular mimicry in multiple sclerosis. *Autoimmunity* 39, 3–8.
- Srinivasan, R., Sailasuta, N., Hurd, R., Nelson, S., and Pelletier, D. (2005). Evidence of elevated glutamate in multiple sclerosis using magnetic resonance spectroscopy at 3 T. *Brain* 128, 1016–25.
- Steinman (1999). Assessment of animal models for MS and demyelinating disease in the design of rational therapy. *Neuron* 24, 511–4.

- 
- Steinman, L. (2003). Optic neuritis, a new variant of experimental encephalomyelitis, a durable model for all seasons, now in its seventieth year. *The Journal of Experimental Medicine* 197, 1065–71.
- Steinman, L., Martin, R., Bernard, C., Conlon, P., and Oksenberg, J. (2002). Multiple sclerosis: deeper understanding of its pathogenesis reveals new targets for therapy. *Annual Review of Neuroscience* 25, 491–505.
- Stover, Pleines, Morganti-Kossmann, Kossmann, Lowitzsch, and Kempinski (1997). Neurotransmitters in cerebrospinal fluid reflect pathological activity. *European Journal of Clinical Investigation* 27, 1038–43.
- Tantama, M., Hung, Y., and Yellen, G. (2011). Imaging Intracellular pH in Live Cells with a Genetically Encoded Red Fluorescent Protein Sensor. *Journal of the American Chemical Society* 133, 10034–7.
- Thestrup, T., Litzlbauer, J., Bartholomäus, I., Mues, M., Russo, L., Dana, H., Kovalchuk, Y., Liang, Y., Kalamakis, G., Laukat, Y., et al. (2014). Optimized ratiometric calcium sensors for functional in vivo imaging of neurons and T lymphocytes. *Nature Methods* 11, 175–82.
- Trapp, B., and Stys, P. (2009). Virtual hypoxia and chronic necrosis of demyelinated axons in multiple sclerosis. *The Lancet. Neurology* 8, 280–91.
- Trapp, B., Peterson, J., Ransohoff, R., Rudick, R., Mörk, S., and Bö, L. (1998). Axonal Transection in the Lesions of Multiple Sclerosis. *N. Engl. J. Med.* 338, 278–85.
- Viglietta, V., Baecher-Allan, C., Weiner, H., and Hafler, D. (2004). Loss of Functional Suppression by CD4+CD25+ Regulatory T Cells in Patients with Multiple Sclerosis. *The Journal of Experimental Medicine* 199(7), 971–9.
- Walker, A., Burrone, J., and Meyer, M. (2013). Functional imaging in the zebrafish retinotectal system using RGECO. *Frontiers in Neural Circuits* 7, 34.
- Wallace, D., Borgloh, S. zum, Astori, S., Yang, Y., Bausen, M., Kügler, S., Palmer, A., Tsien, R., Sprengel, R., Kerr, J., et al. (2008). Single-spike detection in vitro and in vivo with a genetic Ca<sup>2+</sup> sensor. *Nature Methods* 5, 797–804.
- Waring, P. (2005). Redox active calcium ion channels and cell death. *Archives of Biochemistry and Biophysics* 434, 33–42.
- Weinshenker, B.G., Bass, B., Rice, G.P., Noseworthy, J., Carriere, W., Baskerville, J., and Ebers, G.C. (1989). The natural history of multiple sclerosis: a geographically based study. I. Clinical course and disability. *Brain* 112 ( Pt 1), 133–46.
- Werner, P., Pitt, D., and Raine, C. (2001). Multiple sclerosis: altered glutamate homeostasis in lesions correlates with oligodendrocyte and axonal damage. *Annals of Neurology* 50, 169–180.
- Williams, P., Marincu, B.-N., Sorbara, C., Mahler, C., Schumacher, A.-M., Griesbeck, O., Kerschensteiner, M., and Misgeld, T. (2014). A recoverable state of axon injury persists for hours after spinal cord contusion in vivo. *Nature Communications* 5, 5683.
- Witte, M., Bø, L., Rodenburg, R., Belien, J., Musters, R., Hazes, T., Wintjes, L., Smeitink, J., Geurts, J., Vries, H., et al. (2009). Enhanced number and activity of mitochondria in multiple sclerosis lesions. *The Journal of Pathology* 219, 193–204.

- 
- Witte, M., Geurts, J., Vries, H. de, Valk, P. van der, and Horssen, J. van (2010). Mitochondrial dysfunction: a potential link between neuroinflammation and neurodegeneration? *Mitochondrion* 10, 411–8.
- Witte, M., Mahad, D., Lassmann, H., and Horssen, J. van (2014). Mitochondrial dysfunction contributes to neurodegeneration in multiple sclerosis. *Trends in Molecular Medicine* 20, 179–87.
- Yang, J., Weimer, R., Kallop, D., Olsen, O., Wu, Z., Renier, N., Uryu, K., and Tessier-Lavigne, M. (2013). Regulation of Axon Degeneration after Injury and in Development by the Endogenous Calpain Inhibitor Calpastatin. *Neuron* 80, 1175–89.
- Zal, T., and Gascoigne, N. (2004). Photobleaching-corrected FRET efficiency imaging of live cells. *Biophysical Journal* 86, 3923–39.
- Zhai, Q., Wang, J., Kim, A., Liu, Q., Watts, R., Hoopfer, E., Mitchison, T., Luo, L., and He, Z. (2003). Involvement of the ubiquitin-proteasome system in the early stages of wallerian degeneration. *Neuron* 39, 217–25.
- Zhao, Y., and Yang, Y. (2014). Profiling metabolic states with genetically encoded fluorescent biosensors for NADH. *Current Opinion in Biotechnology* 31C, 86–92.
- Zipfel, W., Williams, R., and Webb, W. (2003). Nonlinear magic: multiphoton microscopy in the biosciences. *Nature Biotechnology* 21, 1369–77.

---

## **7. Acknowledgements**

This work was made possible by the “Promotionsstudium des Förderprogramms für Forschung und Lehre” (FöFoLe), a programme that enables medical students to do intensive experimental research at the LMU. I am grateful that I have been given the opportunity to pursue an ambitious research topic while being well supervised and supported by all people involved.

I would like to thank all members of the unit of therapy research of the Institute of Clinical Neuroimmunology (INIM). I owe a lot of my interest and knowledge for this to my supervisor, Martin Kerschensteiner, who did an excellent job in supporting the whole project, giving accurate and well-considered advice and evoking the enthusiasm needed to persevere the work. I was lucky to get a lot of additional input, outstanding technical knowledge and advice from Thomas Misgeld (TUM), who co-supervised this project and enabled me to also use his facilities for the experiments. Ivana Nikic carefully introduced me to all methods she had established in the lab and was therefore a great help. Peter Bradley kindly proofread the manuscript. All other lab members gave me important “benchwork” advice on a daily basis that I am also very thankful for.

Of course, the grand support from my parents and my sisters was a prerequisite for me to reach the point where I could even start this work. I am very happy that I did have such an exceptional home. I would like to thank all my dear friends that showed a great amount of support.

---

# ***Eidesstattliche Versicherung***

***Schumacher, Adrian Minh***

---

Name, Vorname

Ich erkläre hiermit an Eides statt,  
dass ich die vorliegende Dissertation mit dem Thema

***Die Rolle von Kalzium bei der axonalen Schädigung im Tiermodell der Multiplen Sklerose.***

selbständig verfasst, mich außer der angegebenen keiner weiteren Hilfsmittel bedient und alle Erkenntnisse, die aus dem Schrifttum ganz oder annähernd übernommen sind, als solche kenntlich gemacht und nach ihrer Herkunft unter Bezeichnung der Fundstelle einzeln nachgewiesen habe.

Ich erkläre des Weiteren, dass die hier vorgelegte Dissertation nicht in gleicher oder in ähnlicher Form bei einer anderen Stelle zur Erlangung eines akademischen Grades eingereicht wurde.

---

Ort, Datum

---

Unterschrift Doktorand